

2012

Exploring Synaptic Vesicle Exocytosis

Pablo Ariel

Follow this and additional works at: http://digitalcommons.rockefeller.edu/student_theses_and_dissertations

 Part of the [Life Sciences Commons](#)

Recommended Citation

Ariel, Pablo, "Exploring Synaptic Vesicle Exocytosis" (2012). *Student Theses and Dissertations*. Paper 170.



EXPLORING SYNAPTIC VESICLE EXOCYTOSIS

A Thesis Presented to the Faculty of
The Rockefeller University
in Partial Fulfillment of the Requirements for
the degree of Doctor of Philosophy

by

Pablo Ariel

June 2012

EXPLORING SYNAPTIC VESICLE EXOCYTOSIS

Pablo Ariel, Ph.D.

The Rockefeller University 2012

The strength of a synapse is an important variable that will affect the function of neural circuits. This thesis develops optical techniques to study determinants of presynaptic efficiency. Our methods are largely based on a chimera of a pH-sensitive variant of the green fluorescent protein and the vesicular glutamate transporter. This reporter is incorporated into synaptic vesicles and increases its fluorescence when those vesicles fuse with the presynaptic membrane. Using this reporter, we measure the size of the primed pool of vesicles (\mathbf{n}), a privileged subset of synaptic vesicles which are docked at the active zone and can immediately fuse with the membrane, thereby releasing neurotransmitter in response to an action potential. We also estimate the probability that a vesicle within that pool will fuse upon arrival of a stimulus to the presynaptic terminal (\mathbf{P}_v). Our studies show that at each bouton in a cultured rat hippocampal neuron there are four primed vesicles per synapses, each of which has a 10% chance of fusing with the membrane in response to a stimulus. These values only represent averages; both \mathbf{P}_v and \mathbf{n} vary widely between neurons and between synapses made by those neurons.

Tomosyn, a molecule intimately involved with the fusion machinery of synaptic vesicles, exercises a negative control on exocytosis. Reducing the levels of this protein, without eliminating it completely from a synapse, leads to increases in \mathbf{P}_v , but does not affect \mathbf{n} .

In addition to measuring synaptic properties of individual neurons, our methods can be used to study P_v and n at the level of single synapses. There is considerable variability among synapses in these properties, even between synapses formed by the same axon. This variability is not correlated with the fraction of P/Q or N-type Ca^{2+} channel subtypes present at each presynaptic terminal. Furthermore, it cannot be explained by the variance in distances between these channels and primed vesicles. Synapses differ not only in their basic properties, but also in the degree to which their strength can be modulated. In particular, activation of the cAMP pathway leads synapses with lower P_v to potentiate more than synapses with high P_v .

In conclusion, the methods developed herein represent a powerful approach to study the molecular determinants of synaptic vesicle exocytosis at the level of individual synapses.

a Vicky, Papá, Mamá y Caro

ACKNOWLEDGEMENTS

First and foremost, I would like to thank Tim Ryan. His enthusiasm for science, logical rigor, and creativity have made my time in his lab a great learning experience. It has been an intellectually challenging and fun adventure. I also appreciate his encouragement and empathy when things were not going so well. I am fortunate to have had the opportunity to learn from an expert craftsman in science.

It has been a privilege to work with J. Balaji, Meera Mani, Gabor Brasnjo, Moritz Armbruster, Sung Hyun Kim, Ping-Yue Pan, Vidhya Rangaraju, Mike Hoppa, Nat Calloway, Yogesh Gera and Ricky Kwan. I appreciate the countless hours we have shared discussing results, building microscopes and dissecting papers. I would particularly like to thank Ricky, who made all the cells I used in Chapter 3 of this thesis, Balaji, who gave me valuable lessons in applied optics, Sung, for doing the same in molecular biology, Mike, for our many discussions of Ca^{2+} channels, and Moritz for being my go-to guy for electronics and analysis questions. Moritz in particular pointed out the issue of statistical fluctuations expected in single synapse experiments, a key insight for the design of the protocol in Chapter 5. In addition to the science, I have had a great time getting to know everyone in the lab on a personal level, in conversations that ranged from traditional lunch delivery systems in India to military service in Korea, and everything in between.

Jeremy Dittman has been a great source of advice and ideas. Conversations with him always made me think more deeply about my experiments. It was his idea to use 4-

aminopyridine to increase Ca^{2+} influx and empty the primed pool of vesicles with a single action potential, an important experiment in Chapter 3.

I am grateful to Jim Hudspeth, Cori Bargmann and Marcelo Magnasco for their encouragement and feedback in our yearly committee rendezvous. The meetings always left me fired up and excited to do new experiments.

The Dean's Office at Rockefeller and the Biochemistry Department office at Cornell Medical College eliminated most administrative concerns from my life, a fact for which I am very thankful. In particular, Edith Perryman at Cornell and Cristian Rosario at Rockefeller cheerfully kept me insulated from the need to deal with almost all bureaucratic issues.

My friends have made my weekends memorable over the past 6 years, be it searching for the perfect brunch or soup dumpling, building snowmen in Central Park or apple-picking in upstate New York. I also appreciate the long conversations spent commiserating about the travails of graduate school. To Diego, Ani, Mer, Marcos, Gus, Dan, Molly, Tuolumne and Warren, a heartfelt thanks.

My parents and sister have been behind me ever since I declared one night over dinner in Buenos Aires that I hoped to come to the US for graduate school. I would not have made it here without them.

Final thanks go to my wife, Vicky, whose love and support are the foundation for everything I have done since we embarked on this adventure and came to the US together.

TABLE OF CONTENTS

1. INTRODUCTION	1
1.1 The basics of synaptic transmission	1
1.2 A framework to study neurotransmitter release	3
1.3 Model systems and methods to study synaptic transmission	13
1.4 Tomosyn – a negative regulator of synaptic transmission	16
1.5 Variability between synapses	24
2. MATERIALS and METHODS.....	29
2.1 Cell culture and optical setup	29
2.2 Image and data analysis of vG-pH.....	31
2.3 Error analysis.....	34
2.4 Ca ²⁺ indicator measurements and analysis.....	38
2.5 shRNA and tomosyn plasmids	39
2.6 Immunostaining analysis of tomosyn levels	40
2.7 Statistical analysis and data presentation	41
3. OPTICAL MAPPING OF RELEASE PROPERTIES IN SYNAPSES	43
3.1 Exocytosis measured at high time resolution with vG-pH.....	43
3.2 A single AP that causes a large increase in intracellular Ca ²⁺ can release the entire RRP	45
3.3 High frequency action potential bursts deplete the RRP.....	51
3.4 Comparison of methods	55
3.5 Estimation of P _v	56
3.6 Discussion	57
4. TOMOSYN.....	62
4.1 Knockdown of tomosyn in hippocampal neurons.....	62
4.2 Effects of tomosyn knockdown on synaptic efficacy.....	65
4.3 Does PKA phosphorylation of tomosyn play a role in synaptic transmission?	69
4.4 Unsuccessful attempt to rescue effects of shRNA	71
4.5 Discussion	75

5. EXOCYTOSIS PROPERTIES OF SINGLE SYNAPSES.....	80
5.1 General measurement considerations.....	80
5.2 Data quality and filtering.....	83
5.3 Individual synapses vary considerably in P_v and n	87
5.4 An exploration of molecular determinants of variability in P_v and n	92
5.5 Malleability of synapses – the cAMP pathway.....	104
5.6 Discussion.....	113
6. FINAL DISCUSSION.....	122
A. APPENDIX.....	125
A.1 Derivation of equation 5.1.....	125
A.2 Models of forskolin effects on P_v and n	126
A.3 Model of random distribution of Ca^{2+} channels in the active zone.....	130
REFERENCES.....	132

LIST OF FIGURES

1. INTRODUCTION	
1.1 Models of priming with possible mechanisms to control the number of primed vesicles (n).....	6
1.2 Determinants of vesicle fusion probability (P_v).....	9
1.3 Possible presynaptic mechanisms controlling the amount of neurotransmitter released per vesicle.....	12
1.4 Tomosyn domain structure.....	17
3. OPTICAL MAPPING OF RELEASE PROPERTIES IN SYNAPSES	
3.1 Exocytosis in response to 1 AP measured at 10 ms time resolution with vG-pH.....	45
3.2 Single APs cause exocytosis of the entire RRP in conditions with large intracellular Ca ²⁺ increases.....	50
3.3 Bursts of action potentials at 100 Hz in 4mM external Ca ²⁺ deplete the RRP after exocytosis of approximately 7% of the TRP.....	54
3.4 Different estimates of RRP size are consistent.....	56
3.5 P_v varies over a wide range across cells.....	57
3.6 Synapses are in range very responsive to changes in Ca ²⁺	60
4. TOMOSYN	
4.1 shRNA targeting tomosyn-1 leads to partial reduction of tomosyn levels in hippocampal neurons.....	64
4.2 Reduction in tomosyn concentration increased P_v and modified short term plasticity.....	67
4.3 Reduction in tomosyn concentration had no effect on exocytosis in response to strong stimuli.....	69
4.4 The effect of forskolin on responses to single APs was not altered in the presence of tomosyn-1 shRNA.....	70
4.5 Rescue of tomosyn levels with HA-tagged tomosyn-1 did not revert the effects of tomosyn-1 knockdown.....	74
5. EXOCYTOSIS PROPERTIES OF SINGLE SYNAPSES	
5.1 P_v and RRP size can be measured precisely at many individual boutons in parallel.....	85
5.2 Large variation in P_v and RRP size between individual synapses.....	91

5.3 P/Q and N-type Ca ²⁺ channels do not differ in their coupling to primed synaptic vesicles.....	94
5.4 Block of P/Q-type Ca ²⁺ channels leads to weaker and more variable decrease of exocytosis than block of N type Ca ²⁺ channels.....	96
5.5 P/Q-type Ca ²⁺ channel distribution is independent of P_v and n	98
5.6 N-type Ca ²⁺ channel distribution is independent of P_v and n	100
5.7 Vesicle to channel distance is not a major determinant of P_v in our experiments.....	103
5.8 The effect of forskolin on exocytosis in response to a single action potential is negatively correlated with P_v	107
5.9 Two scenarios that could account for different P_v between synapses.....	108
5.10 Synapses with low initial P_v will potentiate more in the presence of forskolin.....	110
5.11 Forskolin effects are more variable than expected from model.....	112
5.12 Modeling the effects of Ca ²⁺ channel numbers.....	116

LIST OF ABBREVIATIONS

AP: action potential

Baf: bafilomycin, a proton pump inhibitor

cAMP: cyclic adenosine monophosphate

CV: coefficient of variation

DIC: differential interference contrast

EGTA-AM: acetoxymethyl ester of ethylene glycol tetraacetic acid

GFP: green fluorescent protein

n: size of the primed pool of vesicles

NSF: *N*-ethylmaleimide-sensitive factor

PKA: protein kinase A

P_r: probability of neurotransmitter release in response to a single action potential

P_v: probability of fusion of a primed vesicle in response to a single action potential

ROI: region of interest

RRP: readily releasable pool of vesicles, also known as primed pool of vesicles

SE: standard error of the mean

shRNA: short hairpin ribonucleic acid

SNARE: soluble NSF attachment protein receptor

SUMO: small ubiquitin-like modifier protein

TIRF: total internal reflection

TP: total pool of vesicles inside a synapse

TRP: total pool of releasable vesicles inside a synapse

vG-pH: pHluorin fused to a luminal loop in the vesicular glutamate transporter

1. INTRODUCTION

1.1 The basics of synaptic transmission

Most neurons in the mammalian central nervous system are connected by chemical synapses. These specialized structures do not simply transmit a sequence of action potentials (APs) from one cell to the next, but can act as filters to modify the signal (Abbott and Regehr, 2004). For example, connections that are strong (like the climbing fiber synapse of the cerebellum) reliably transmit individual, isolated APs yet depress in response to trains where the same stimuli are delivered at high frequency. On the other hand, synapses that are initially weak (like the parallel fiber of the cerebellum) tend to facilitate, giving a larger response per stimulus if APs are delivered in bursts. These examples illustrate how strong synapses can function as low pass filters and weak synapses can operate as high pass filters, influencing how information flows through neural circuits (Abbott and Regehr, 2004). In addition to these relatively rapid effects (on the order of seconds), activity dependent presynaptic changes can occur on longer timescales (hours or longer) and lead to enduring modifications of network properties (McBain and Kauer, 2009). Thus, what determines a synapse's strength at the molecular level is a key question that has important implications for circuit function.

Before addressing neurotransmitter release, it is worth briefly reviewing the anatomy of the structure involved, as determined from three-dimensional reconstructions based on electron microscopy. While there is considerable variety among synapses, small (around 1 μm diameter) synapses of the central nervous system typically have on the

order of a hundred vesicles, of which only a small subset (approximately 5%) are in direct contact with the presynaptic membrane (Schikorski and Stevens, 1997). This subset of vesicles, referred to as the docked pool, contacts the membrane in a region known as the active zone, in direct apposition across the synaptic cleft with a specialized area on the postsynaptic cell known as the postsynaptic density (Schoch and Gundelfinger, 2006).

When an AP arrives at a presynaptic terminal, the depolarization leads to opening of Ca^{2+} channels. Calcium ions rush into the terminal down their electrochemical gradient and bind to a Ca^{2+} sensor (Bennett, 1999) widely thought to be synaptotagmin (Sun et al., 2007; Burgalossi et al., 2010; Pang and Sudhof, 2010; Kochubey et al., 2011), on the synaptic vesicle membrane. Through a series of steps that take less than a millisecond and are not fully understood, this binding leads to SNARE-dependent membrane fusion of the vesicle with the membrane and release of neurotransmitter into the synaptic cleft (Chapman, 2008). Neurotransmitter quickly diffuses across the cleft and binds to postsynaptic ionotropic receptors that cause rapid conductance changes and/or metabotropic receptors that lead to slower effects mediated by G-protein coupled receptors in the postsynaptic cell.

1.2 A framework to study neurotransmitter release

A simple model used as a framework to study this process posits that as a result of a single AP in the presynaptic neuron, a response Q is elicited in the postsynaptic cell (Schneggenburger et al., 2002):

$$Q = n \cdot P_v \cdot q \quad (1.1)$$

where

- n = the number of primed vesicles, i.e. vesicles immediately available for fusion (also known as the readily releasable pool or RRP size). These vesicles have undergone all biochemical steps except for the final Ca^{2+} -dependent fusion step.
- P_v = the probability that each of those vesicles has of fusing with the membrane in response to one AP
- q = the size of the postsynaptic response to a single vesicle fusion event (also known as quantal size)

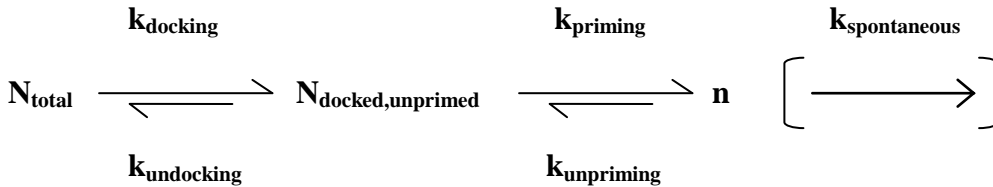
Two important assumptions implicit in this model are that all primed vesicles have the same fusion probability and that they behave independently. Even if these assumptions do not hold in every case, the model is still a very useful way to think about synaptic transmission. Note that the model makes no restrictions on the possibility of more than one vesicle fusing at once (multivesicular release) at a given synapse. For some time there was a debate regarding whether multivesicular release could take place at synapses of the mammalian central nervous system. However, there is now convincing evidence that this can happen (Abenavoli et al., 2002; Oertner et al., 2002; Balaji and Ryan, 2007; Ariel and Ryan, 2010) so it does not seem warranted to modify the model to restrict the possibility of multivesicular release occurring. Finally, a very important point

regards how this model connects to the typically measured parameter $\mathbf{P_r}$ (neurotransmitter release probability). $\mathbf{P_r}$ is the probability that a synapse will not fail, that is, that a presynaptic AP will elicit a response in the postsynaptic cell. This will be equivalent to the probability that *at least* one vesicle fuses in response to one AP. Given the implicit binomial distribution underlying the model:

$$\mathbf{P_r} = 1 - (1 - \mathbf{P_v})^n \quad (1.2)$$

With this framework in mind, it is worth exploring how \mathbf{n} , $\mathbf{P_v}$, and \mathbf{q} can be influenced to determine synaptic strength.

Several factors can influence the number of primed vesicles. In a simplified model, \mathbf{n} will be set by the interplay of rates of docking (and undocking), priming (and unpriming) and possibly (see below) spontaneous fusion (Fig. 1.1A):



where

- $\mathbf{N_{total}}$ = the total number of synaptic vesicles in a nerve terminal
- $\mathbf{N_{docked,unprimed}}$ = the number of vesicles in contact with the presynaptic membrane that are not fusion competent
- $\mathbf{k_i}$ = rate constants for process \mathbf{i} , where \mathbf{i} can be: docking, undocking, priming, unpriming and spontaneous vesicle fusion

In this scenario, the rate constants of each step will influence \mathbf{n} but so will any change in the total number of vesicles in the terminal, merely due to mass action. For example, anything that increased $\mathbf{N_{total}}$ would raise \mathbf{n} without controlling docking or priming

processes *per se*. Additionally, even in the absence of stimulation there is a low rate of release of neurotransmitter due to spontaneous fusion of synaptic vesicles with the membrane. While there is some debate as to whether these vesicles are in the primed pool to begin with (Fredj and Burrone, 2009; Hua et al., 2010; Wilhelm et al., 2010), if they were, any change in the spontaneous fusion (or mini) rate could lead to a reduction in steady state n . An alternative proposal for the control of n posits that fusion can only take place at certain “slots” or “sites” (Neher, 2010). In this scenario, control of the number of the sites is key. Thus, the important variables would be the abundance of molecules that make up the slots, and the rate constants of assembly and destruction of the sites (Fig. 1.1B). These two scenarios are not incompatible, but rather should be considered extremes in a continuum of possibilities. The first implicitly assumes that the molecules necessary for fusion (presumably the site constituents) are in abundance and not rate limiting. Conversely, the second assumes that construction of sites is much slower than the docking and priming reactions such that once a site is formed, it captures a primed vesicle quickly. If the rates of the various processes outlined above are comparable, n will be set by a complex interplay between the number of vesicles, the number of sites and the rates of docking and priming within those sites. Which extreme of the model is a better representation of what actually occurs during priming is currently unknown. However, the fact that synaptic vesicle fusion and docking are localized to a specialized region of the plasma membrane (the active zone) supports the concept of slots, though what is rate-limiting in the process of docking and priming a vesicle at those sites is unclear.

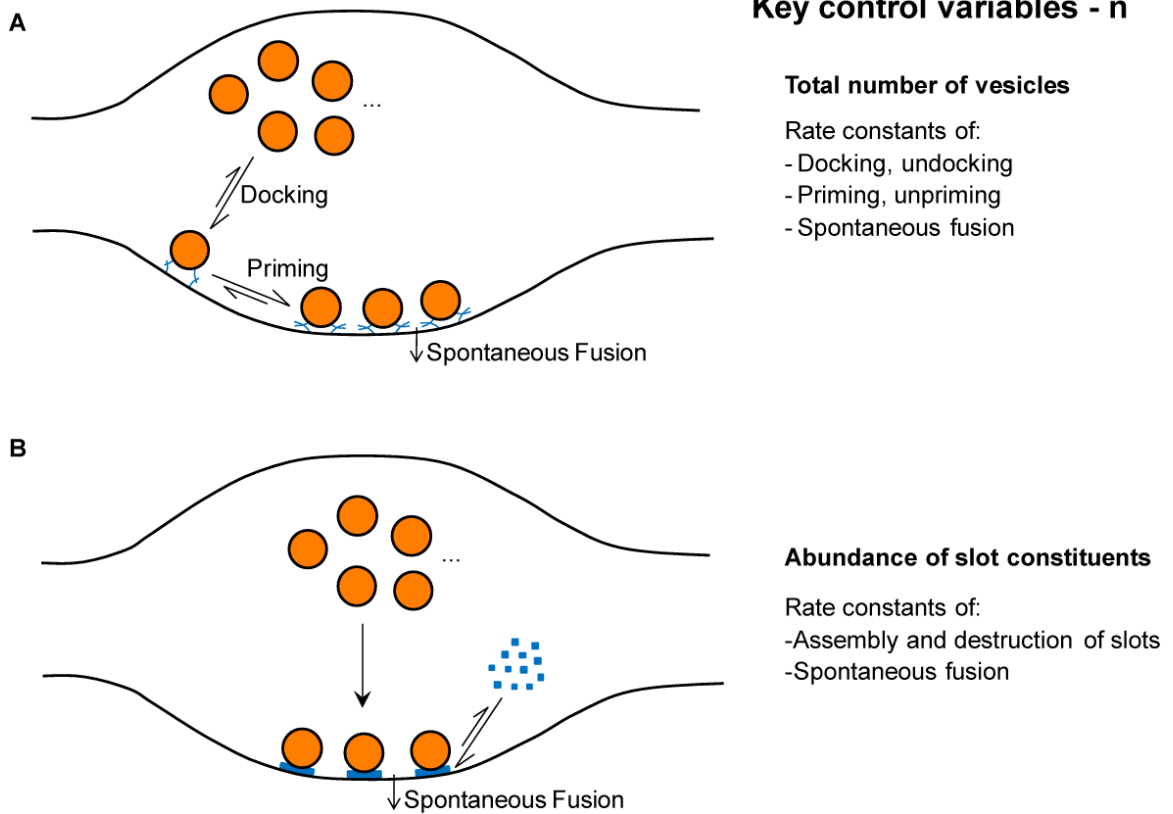


Figure 1.1. Models of priming with possible mechanisms to control the number of primed vesicles (n). **(A)** n is determined by the equilibrium between the rates of docking, undocking, priming, unpriming, and spontaneous fusion. SNARE complexes are symbolized by crossed blue lines and are shown in a loose configuration in the case of the docked, unprimed vesicle. **(B)** Model that assumes the construction of release slots is the rate limiting factor for control of n , whereas other processes are at saturation. Molecules that make up the slots are shown as blue squares that assemble to form release sites at the membrane.

An interesting question is whether docking is the morphological equivalent of priming or if any additional biochemical steps are needed to make a vesicle fusion competent. An illustrative example of how thinking on this point has evolved is munc13, the mammalian homolog of a *Caenorhabditis elegans* gene that causes severe paralysis when mutated (unc13), and contains domains that can bind phorbol esters and Ca^{2+}

(Brose et al., 1995). Knocking out both isoforms expressed at hippocampal synapses eliminated neurotransmitter release (Varoqueaux et al., 2002). However, there was no effect on the number of docked vesicles determined from electron microscopy using an aldehyde fixation method. This was taken as evidence that after a synaptic vesicle docked, additional priming steps needed to take place before achieving fusion competence. The issue was revisited in a recent study on hippocampal slice cultures using high-pressure freezing and electron tomography, circumventing potential aldehyde fixation artifacts (Siksou et al., 2009). Contrary to the previous findings, the docked vesicle pool was almost completely eliminated in the absence of munc13. This led the authors to propose that docking is the morphological correlate of priming in small synapses of the central nervous system. It is important to point out that exact definitions of what constituted a docked vesicle were slightly different in both studies (see Verhage and Sorensen, 2008, for further discussion of this issue), with the latter taking a stringent approach of only considering vesicles in contact with the plasma membrane and the former including vesicles within 6nm of the active zone. However, even applying the more inclusive criteria to the results using high-pressure freezing and electron tomography, the newer technique still shows a dramatic (~80%) reduction in the number of docked vesicles. Further study of additional mutants with high-pressure freezing and electron tomography will be needed to shed more light on this issue. If there are additional biochemical steps necessary for fusion competence after vesicle docking, eliminating molecules critical only for those steps would lead to smaller n - assayed physiologically (see below) -, yet no changes in the number of docked vesicles - assayed ultrastructurally -. On the contrary, if docking is equivalent to priming, we would expect

a tight correlation of effects on n and the number of docked vesicles over a wide variety of molecular interventions. Based on results from docking of synaptic vesicles in *C. elegans*, or of dense core vesicles in chromaffin cells, particularly interesting candidates to revisit in mammalian synapses with high-pressure freezing are syntaxin, SNAP-25, synaptotagmin and munc18 (Hammarlund et al., 2007; de Wit et al., 2009; de Wit, 2010).

When considering how the value of P_v can be modulated, the main points to examine are local Ca^{2+} (its concentration at the vesicle) and vesicle fusion willingness (Fig. 1.2). P_v is steeply dependent on the Ca^{2+} concentration at synaptotagmin molecules on primed synaptic vesicles (Bollmann et al., 2000; Schneggenburger and Neher, 2000; Sun et al., 2007; Burgalossi et al., 2010) so control of that local concentration will have a strong effect on synaptic strength (Schneggenburger and Neher, 2005). Local levels of Ca^{2+} will be influenced both by how much Ca^{2+} comes into the terminal in the first place and by how much the concentration decays between the source (Ca^{2+} channels on the presynaptic membrane) and the primed vesicles. The amount of Ca^{2+} influx will be set by the intrinsic characteristics and abundance of Ca^{2+} channels (Fig. 1.2A), the extra- to intracellular electrochemical Ca^{2+} gradient and the shape of the AP waveform. The concentration decay to the vesicle will depend on the average distance between vesicles and Ca^{2+} channels (referred to as the coupling between them, Fig. 1.2B) and will also be shaped by any molecules between the channels and vesicles that can bind Ca^{2+} (Fig. 1.2C). Depending on their concentrations, mobility, binding and unbinding rate constants, these Ca^{2+} buffers can potentially influence the local concentration of Ca^{2+} at primed vesicles (Schwaller, 2010).

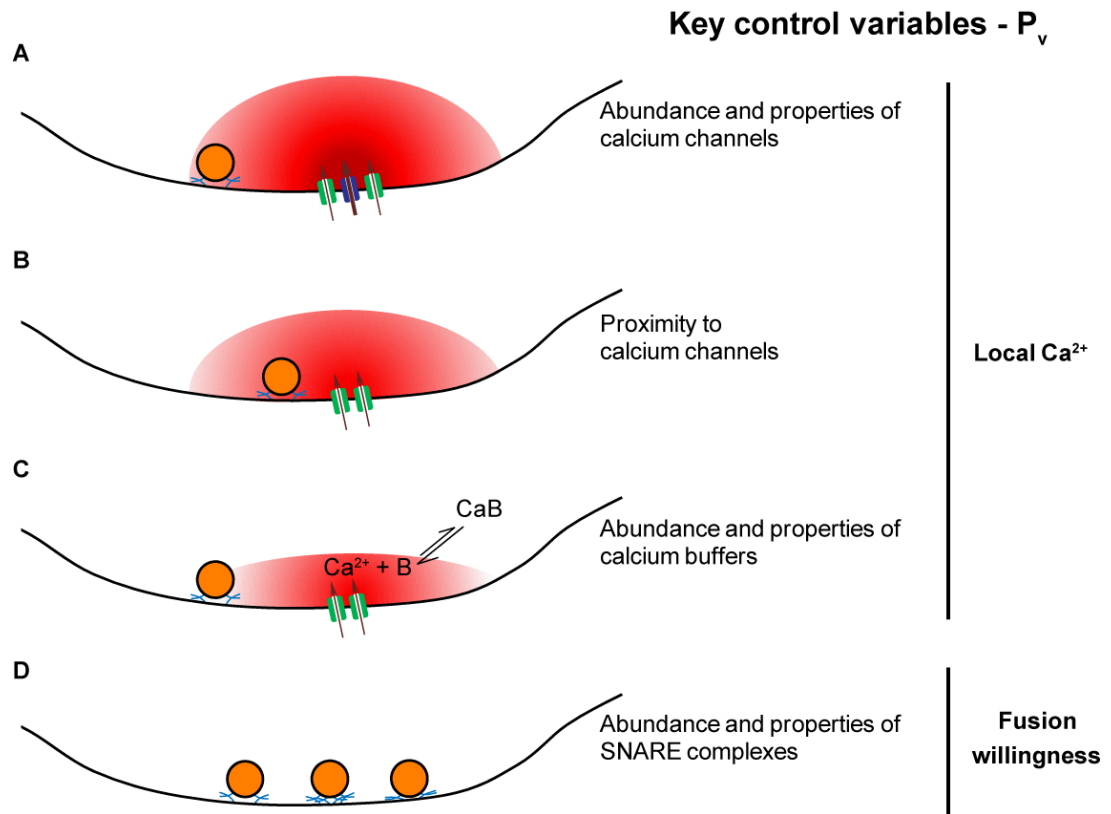


Figure 1.2. Determinants of vesicle fusion probability (P_v). (A) to (C) Factors that influence the local Ca^{2+} concentration at the vesicle. Ca^{2+} concentration is symbolized by the intensity of red. The higher the Ca^{2+} concentration at a vesicle, the higher its P_v . (D) Effects of abundance and properties of SNARE complexes. SNARE complexes are symbolized by crossed blue lines. Higher numbers of complexes per vesicle, or tighter complexes, are presumed to lead to higher fusion willingness, and therefore higher P_v .

The second major determinant of P_v is the fusion willingness (or fusogenicity) of a primed vesicle once calcium ions are bound to synaptotagmin (Fig. 1.2D). That is, once Ca^{2+} is bound to synaptotagmin molecules on a synaptic vesicle, how likely is that vesicle to fuse with the membrane? To consider this issue, we must first briefly discuss what is known about the fusion process itself (reviewed in Jahn and Scheller, 2006; Rizo and Rosenmund, 2008).

An indispensable requirement for fusion is the formation of a parallel four-helix bundle between the SNARE motifs of synaptobrevin, a protein on the synaptic vesicle, and SNAP-25 and syntaxin-1, two proteins on the presynaptic membrane. Synaptobrevin provides one helix, through its R-SNARE domain, while SNAP-25 and syntaxin-1 provide two and one helices respectively through their Q-SNARE domains. The resulting four-helix bundle is called a *trans*-SNARE complex because it bridges two membranes. This tightly wound complex brings the vesicle and plasma membrane into close proximity and is thought to provide the driving force behind membrane fusion. After vesicle fusion, synaptobrevin joins SNAP-25 and syntaxin-1 on the presynaptic membrane. In that state, the four helix bundle - still assembled - is known as a *cis*-SNARE complex because all its constituents are on the same membrane. The disassembly of the *cis*-SNARE complex is an ATP-dependent process mediated by NSF (*N*-ethylmaleimide-sensitive factor). This frees synaptobrevin so it can be taken up by endocytosis into synaptic vesicles and be available for further rounds of fusion. With these observations in mind, fusogenicity might depend on the exact state or abundance of *trans*-SNARE complexes on a primed vesicle (Mohrmann et al., 2010). Molecules such as complexin, tomosyn, or munc18 that can interact with the assembled SNARE complex or its constituents could potentially alter fusion willingness through either mechanism (Wojcik and Brose, 2007).

After considering the ways in which \mathbf{P}_v can be influenced, we can revisit the assumption of homogenous \mathbf{P}_v between vesicles in the primed pool. For example, is it reasonable to assume that all primed vesicles will be at the same distance from Ca^{2+} channels? Similarly, do we need to posit that all primed vesicles have the same number of

trans-SNARE complexes assembled? This uniformity seems unlikely, so our model must necessarily be taken as a first approximation that will only describe idealized, average primed vesicles on a per synapse basis. There might be considerable variability between vesicles in the same active zone lurking underneath this simplifying assumption. In fact, there have been claims in the literature of heterogeneity in \mathbf{P}_v between vesicles (Sakaba and Neher, 2001b; Moulder and Mennerick, 2005). However, neither of these studies offers measures of \mathbf{P}_v at the level of a single active zone, making it impossible to rule out that the variability results from vesicles in different active zones having different properties. Perhaps with increasingly precise techniques, the issue of within-synapse heterogeneity between primed vesicles will become tractable. For the moment, we are stuck with only a blurred picture that averages across the primed vesicles in a synapse.

For \mathbf{q} , there can be both pre- and postsynaptic influences. On the presynaptic side, the amount of neurotransmitter per vesicle might vary with the number or activity of neurotransmitter vesicular transporters present (Fig. 1.3A) and the vesicle size (Fig. 1.3B). Additionally, there is a controversy regarding “kiss and run”, i.e. events that do not lead to full fusion and collapse of the vesicle (He and Wu, 2007; Dittman and Ryan, 2009; Granseth et al., 2009; Zhang et al., 2009). If these events involve a small pore that opens only briefly or flickers, they could lead to less neurotransmitter release into the cleft (Fig. 1.3C). Finally, while this thesis focuses on presynaptic properties, it is worth keeping in mind that the abundance and specific properties of postsynaptic receptors, together with their orientation relative to release sites, can profoundly influence the size of the postsynaptic response.

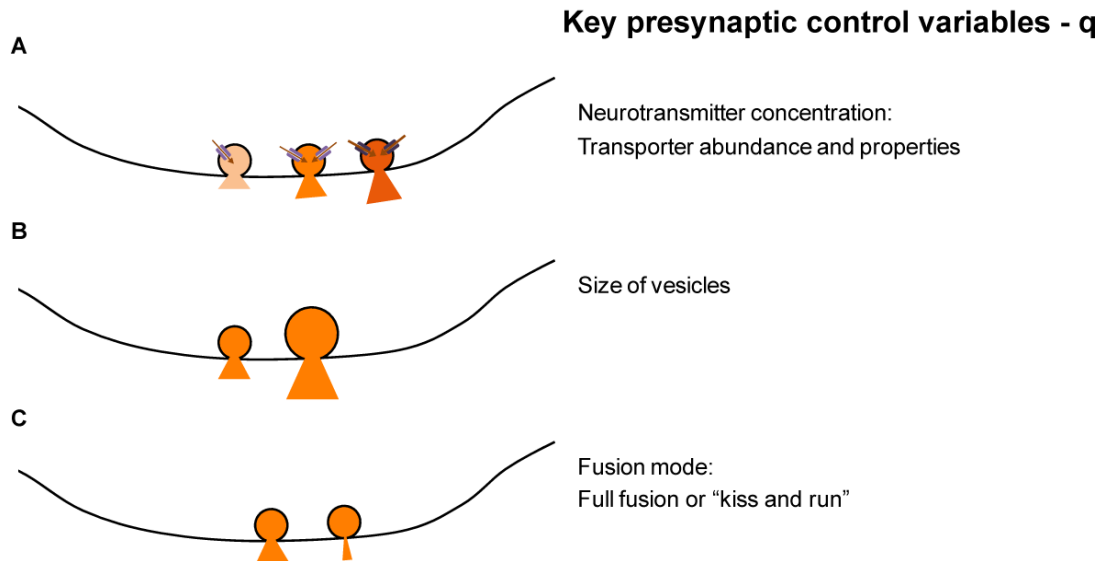


Figure 1.3. Possible presynaptic mechanisms controlling the amount of neurotransmitter released per vesicle. **(A)** The increasing intensity of orange symbolizes higher concentrations of neurotransmitter in each vesicle as a result of an increase in the number of transporters or their rates of transport. **(B)** Larger vesicles will release more molecules of neurotransmitter if the concentration is constant. **(C)** Small, flickering fusion pores might occur during “kiss and run” and lead to less neurotransmitter release per vesicle.

So far, we have discussed what happens when a *single* AP invades the nerve terminal. However, neurons can burst, firing many APs at frequencies up to 100 Hz and higher. Under those circumstances synaptic transmission will be influenced by factors beyond those considered above (Xu-Friedman and Regehr, 2004; Fioravante and Regehr, 2011). The size of the primed pool of vesicles at any given moment will be determined by the balance of vesicle fusion and priming rates. Under conditions of sustained activity, not only vesicle fusion, but also priming rates are Ca^{2+} dependent (Dittman and Regehr, 1998; Stevens and Wesseling, 1998; Wang and Kaczmarek, 1998; Neher and Sakaba, 2008). Therefore, Ca^{2+} channel inactivation (Xu and Wu, 2005) or facilitation (Ishikawa et al., 2005; Mochida et al., 2008), exhaustion of extracellular Ca^{2+} in the synaptic cleft

(Borst and Sakmann, 1999; Rusakov and Fine, 2003), saturation of intracellular Ca^{2+} buffers (Blatow et al., 2003), and the rates of Ca^{2+} clearance (Scullin et al., 2010) during a burst of APs can all shape the postsynaptic response. Additionally, if there are slots for release, these might require a clearance time before they become available once more (Hosoi et al., 2009; Neher, 2010). Finally, on the postsynaptic side receptors may saturate, desensitize (Xu-Friedman and Regehr, 2004) or even diffuse out of the postsynaptic density (Heine et al., 2008) during a burst. These effects can complicate attempts to use postsynaptic measurements as linear indicators of presynaptic activity.

1.3 Model systems and methods to study synaptic transmission

Given this panoply of potential influences on the neurotransmitter release process, to convincingly ascribe the functions of a molecule to any one of the processes mentioned above requires considerable effort. Typical experiments involve genetic manipulation of neurons to eliminate or replace certain molecules or increase their concentration. If there are pharmacological tools available to interfere with a molecule's function these can also be used, ideally coupled with experiments in the absence of the molecule to test for any off-target effects. There are many possible techniques and preparations to estimate \mathbf{n} , \mathbf{P}_v , and \mathbf{q} , with a few general considerations applicable to any of them. Methods to measure \mathbf{n} tend to rely on a strong, fast stimulus that causes exocytosis of all primed vesicles before there is time for significant replenishment of that pool of vesicles through priming processes. Under those conditions, the size of the response will be equivalent to \mathbf{n} . In cases where there is significant replenishment during the stimulus, a model of the vesicle priming process is needed to correct the estimate appropriately. To measure \mathbf{P}_v , the size

of the response to one AP is simply divided by n . This places a minimum requirement on the sensitivity of any method used to determine P_v , as it must be possible to measure the response to a single AP precisely. Finally, to estimate q , it is necessary to determine the postsynaptic response to a single vesicle fusion event or quanta. A usual approach is to use the average response to spontaneous, low frequency events that happen in the absence of stimulation and which are presumed to correspond to single vesicles fusing.

The best biophysical measurements of synaptic transmission currently available come from the calyx of Held, a large, cup-like excitatory synapse in the auditory pathway (Sakaba et al., 2002; Schneggenburger and Forsythe, 2006). This giant synapse has hundreds of active zones and effectively operates as a parallel array of small synapses. It has become a valuable model system to study synaptic transmission because its large size makes it amenable to both pre- and postsynaptic whole-cell recording and Ca^{2+} uncaging experiments. In this synapse n has been estimated as the size of the response to a step increase in Ca^{2+} concentration using uncaging, a constant current or a burst of APs. At the moment, Ca^{2+} uncaging is the only tool that allows unambiguous separation of effects on local Ca^{2+} and fusion willingness by bypassing Ca^{2+} channels entirely and elevating Ca^{2+} with spatial uniformity to cause neurotransmitter release. Historically, the main disadvantage of the calyx of Held preparation has been the difficulty in achieving molecular control of the system beyond non-lethal knockouts or peptide injections. However, recent developments promise this will no longer be the case (Young and Neher, 2009; Han et al., 2011; Kochubey and Schneggenburger, 2011).

Perhaps the most widely used system for molecular studies of presynaptic release in mammalian synapses is primary culture of cortical or hippocampal rodent neurons,

studied electrophysiologically. Cultures of neurons can be prepared easily from genetically modified mice and studied even in cases where the mutations are lethal beyond birth. Simple transfection protocols to knock down, overexpress or replace proteins of interest can be used for detailed studies of structure-function relationships. In these cultures, which can be dissociated or autaptic (where a single neuron is grown on a microisland of glia and synapses onto itself), n is usually estimated as the response to application of a hypertonic solution containing 500 mOsm of sucrose. This stimulus was shown to correlate with the size of the primed pool of vesicles as determined by depletion experiments using bursts of action potentials (Rosenmund and Stevens, 1996). However, the mechanism involved remains mysterious and its correspondence with primed vesicles accessed with physiological stimuli is under debate (Moulder and Mennerick, 2005; Stevens and Williams, 2007). Alternatively, bursts of 20-40 APs at 20-40 Hz have been used to deplete the pool. Unfortunately, there is typically substantial replenishment of primed vesicles during this stimulus and a large correction must be applied (Moulder and Mennerick, 2005; Stevens and Williams, 2007). A downside of the primary culture system was, until very recently (Burgalossi et al., 2010), the inability to perform Ca^{2+} uncaging experiments to directly probe the fusion willingness of synaptic vesicles. Additionally, any electrophysiological method will be affected by the complications inherent in using a postsynaptic measure to estimate presynaptic function.

In Chapter 3 of this thesis, we develop an alternative assay to estimate \mathbf{P}_v and n using a direct optical presynaptic readout based on the pH-sensitive GFP pHluorin (Miesenbock et al., 1998) tagged to the lumen of the vesicular glutamate transporter (Voglmaier et al., 2006).

1.4 Tomosyn – a negative regulator of synaptic transmission

Of the many molecules that regulate synaptic transmission, tomosyn is a particularly interesting example. It is a 130 kDa protein that was discovered as an interaction partner for syntaxin-1 in a pull-down assay from rat brain cytosol (Fujita et al., 1998). Since then, it has emerged as an important player in synaptic vesicle exocytosis, one of the few that exercises a negative control on synaptic efficacy (Ashery et al., 2009). However, the exact mechanisms by which it performs this function are not clear.

Tomosyn's domain structure contains a pair of N-terminal, seven-bladed WD40 β -propeller domains, and a C-terminal R-SNARE domain similar to synaptobrevin (Fig. 1.4). β -propellers are so named because the carbon backbone folds into several blades with a roughly radial symmetry and each of these blades is formed by several β -sheets. The C-terminal domain structure has been determined in conjunction with syntaxin-1a and SNAP25, forming a SNARE complex (Pobbati et al., 2004). Additionally, the structure of the N-terminal β -propellers of the yeast ortholog Sro7 has been solved (Hattendorf et al., 2007) and used as a basis for homology modeling of rat tomosyn (Williams et al., 2011). This analysis shows there are three unstructured loops emanating from between the blades of the second β -propeller. There is also a small tail domain between the second β -propeller and the R-SNARE domain, which folds back and binds to the bottom of the β -propellers in the yeast Sro7 structure.

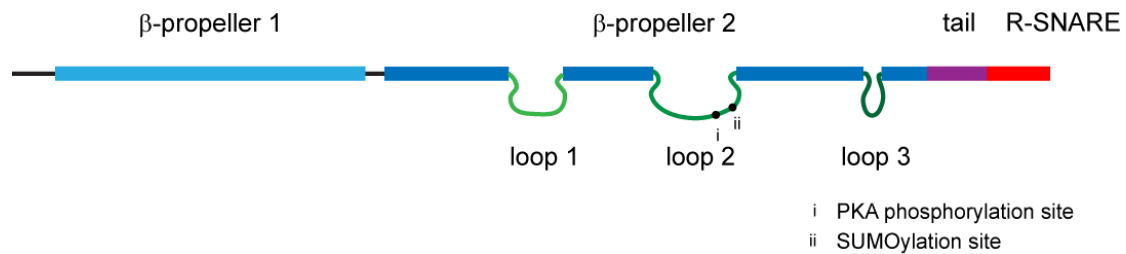


Figure 1.4. Tomosyn domain structure (based on Williams et al., 2011).

In rodents, there are two tomosyn genes (62% sequence identity) that are alternatively spliced to generate seven isoforms in total: -m, -b, -s for tomosyn-1 and -m, -b, -xb and -s for tomosyn-2 (Groffen et al., 2005). All isoforms retain the basic domain structure and alternative splicing events are concentrated in a hypervariable region in loop 2. The -m and -s isoforms are brain specific, whereas isoform -b is ubiquitous (Yokoyama et al., 1999). Tomosyn-1 and -2 have different, but partially overlapping mRNA expression patterns in the brain. Somatic, dendritic and presynaptic localizations have been reported for the protein in different brain regions (Fujita et al., 1998; Barak et al., 2011). While tomosyn's structure indicates it is a cytosolic protein, it has been found closely associated with synaptic vesicles, using mass spectrometry in purified preparations of this organelle (Takamori et al., 2006). Tomosyn-1 and -2 are differentially regulated during development with the expression levels of the latter rising more sharply (30 vs. 2.7-fold rise in mRNA levels between E10 and P12, Groffen et al., 2005). Most work has focused on tomosyn-1, which we will discuss in more depth in what follows. Preliminary reports on tomosyn-2 suggest it is functionally equivalent (Williams et al., 2011) but might execute its function in a postsynaptic compartment (Barak et al., 2011).

The idea that tomosyn might inhibit exocytosis was present in the original paper describing its discovery wherein overexpression of tomosyn-1 led to decreased exocytosis of human growth hormone in response to high K^+ application in PC12 cells (Fujita et al., 1998). The subsequent discovery of an R-SNARE domain in its C-terminus (Masuda et al., 1998), provided a reasonable mechanistic basis for how it might inhibit neurotransmitter release. As discussed above, the formation of fusion competent SNARE complexes between the synaptic vesicle protein synaptobrevin and membrane proteins syntaxin-1 and SNAP25 is necessary for vesicle fusion. Thus, if tomosyn can compete with synaptobrevin in the formation of SNARE complexes (Hatsuzawa et al., 2003) it might interfere with the process. In what follows, we will first review the evidence that shows that tomosyn is a negative regulator of neurotransmitter release. Subsequently, we will discuss studies that try to address how tomosyn might execute this function, which has turned out to be considerably more complicated than initially expected.

Rather surprisingly, the most detailed physiological studies of tomosyn at synapses to date come from the neuromuscular junction of *C. elegans*, a particularly difficult experimental preparation. A mutant of the *C. elegans* tomosyn ortholog was found with a premature stop codon that leads to lower mRNA expression (presumably due to nonsense mediated decay) and a protein truncated halfway through the first β -propeller (Dybbs et al., 2005). This mutant was studied electrophysiologically by two labs, which found that responses to evoked potentials increased (Gracheva et al., 2006; McEwen et al., 2006). There were no changes in synapse numbers, and the enhanced synaptic efficacy was fully explainable by an increased RRP size, as measured with application of a hyperosmotic sucrose solution. Furthermore, the increase in RRP size

correlated well with higher numbers of docked synaptic vesicles (Gracheva et al., 2006). These two studies showed convincingly that tomosyn is a negative regulator of neurotransmitter release. In addition, they established that tomosyn controls RRP size, likely by negatively regulating the number of docked vesicles.

Another study on tomosyn's role in synaptic transmission used cultures of rat superior cervical ganglion cells and assayed the effect of overexpressing tomosyn or knocking it down using siRNA (Baba et al., 2005). As would be expected from a negative regulator, overexpression (4-fold) led to decreases in responses to single APs, yet surprisingly, knockdown (by 80%) gave similar results. This was taken as evidence for both negative and positive roles of tomosyn in neurotransmitter release. However, these results must be interpreted with caution. When using electrophysiological measures of synaptic transmission sensitive to the number of synaptic connections - as in this case - any effects on synapse development need to be studied and if necessary, corrected for appropriately. Given that both tomosyn overexpression and knockdown can interfere with neurite development (Sakisaka et al., 2004) this is a relevant concern. In the Baba et al. paper, there was no attempt to study synapse numbers. Nevertheless, the authors reported that synaptic coupling was significantly reduced between transfected neurons (that either overexpress tomosyn or an siRNA) and wild type counterparts. That is, the probability of finding two neurons connected in a culture was lower if the presynaptic one had modified tomosyn levels. Even though synaptic coupling is not a clean measure of synaptic numbers and might also depend on axon length or trajectory, these results do raise the concern that synaptic connectivity was affected. Therefore, it is possible that the reduction in responses to single APs was not due to a reduced synaptic efficacy, but

rather to a decrease in the number of synapses connecting the pre and postsynaptic neurons. Due to these concerns, it does not seem warranted to extract firm conclusions on the effect of tomosyn levels on neurotransmission from this study.

Regrettably, a study of the tomosyn-1 knockout did not delve into synaptic properties in much detail (Sakisaka et al., 2008). The most informative result was a reduction in paired-pulse facilitation at CA1 to CA3 synapses of the hippocampus (Fig. 1E in Sakisaka et al., 2008), consistent with an increase in P_r . However, there was no follow up to confirm this was the case or to determine if there were changes in P_v or RRP size.

An alternative system in which tomosyn's role has been studied in detail is the adrenal chromaffin cell. This neurosecretory cell has been used successfully as a model to study molecules involved in exocytosis and can be approached using a multitude of biophysical methods including patch-clamp, capacitance, Ca^{2+} uncaging, amperometry and total-internal-reflection fluorescence (TIRF) microscopy (Becherer and Rettig, 2006). When tomosyn is overexpressed (13-fold) Ca^{2+} uncaging elicits a smaller and slower response (Yizhar et al., 2004). This effect was ascribed to a reduced RRP size by fitting the response to a kinetic model. Interestingly, the number of docked vesicles was unchanged when tomosyn levels were increased, illustrating that in chromaffin cells primed vesicles are only a subset of the docked pool (Sorensen, 2004). Despite the differences in morphology between synapses and chromaffin cells, this study also supports a negative role of tomosyn in vesicle priming.

Once the role of tomosyn as a negative regulator of neurotransmission was well established, later studies tried to elucidate its mechanistic basis by taking a structure-

function approach. The initial idea that tomosyn's function would be mainly executed through its C-terminal R-SNARE domain has been thoroughly complicated by a multitude of studies using mutants with various truncations.

In chromaffin cells, overexpression of tomosyn without its C-terminal R-SNARE domain inhibited exocytosis in response to Ca^{2+} uncaging by reducing the RRP size, though this reduction was slightly less than in experiments using full length tomosyn (Yizhar et al., 2007). Conversely, overexpression of only the R-SNARE domain did not affect RRP size. Furthermore, experiments with other truncation mutants showed both β -propeller domains were necessary for inhibition of exocytosis. This suggests that, at least in this cell type, the R-SNARE domain is mostly dispensable and both β -propeller domains are required for tomosyn's function. By contrast, in superior cervical ganglion neurons, injection of either the R-SNARE domain or fragments of the β -propellers inhibited synaptic transmission, indicating both types of domains are necessary for tomosyn's action (Sakisaka et al., 2008).

Biochemical work has provided a few clues as to how parts of tomosyn other than its R-SNARE C-terminal end might negatively regulate neurotransmitter release. Biochemical characterization of the β -propeller domains has shown that they can enhance the formation of SNARE complex oligomers (Sakisaka et al., 2008). This could be a mechanism to inhibit exocytosis if post-fusion *cis*-SNARE complexes are trapped by tomosyn such that they cannot be disassembled by NSF, reducing the availability of SNARE proteins necessary for docking and fusion (Ashery et al., 2009). Another relevant finding is that β -propeller domains can interact with synaptotagmin-1 in a Ca^{2+} dependent manner and inhibit its facilitatory effect on an *in vitro* vesicle fusion assay (Yamamoto et

al., 2011). Additionally, deletion of the first or third unstructured loops in the second β -propeller domain abolishes the inhibitory action of tomosyn on K^+ -induced release of human growth hormone from PC12 cells, despite having normal binding to syntaxin and trafficking to the membrane (Williams et al., 2011). This suggests these loops may be critical for tomosyn's function *in vivo*. Finally, the tail domain has been reported to inhibit the efficacy of the R-SNARE domain's ability to inhibit neurotransmitter release (Yamamoto et al., 2009), though the mechanism underlying this action remains obscure (Yamamoto et al., 2010).

In addition to tomosyn's effects under baseline conditions, its action can be regulated in several ways. First, the phosphorylation of syntaxin by Rho-associated serine/threonine kinase (ROCK) increases its affinity for tomosyn, leading to an inhibition of the formation of fusion competent SNARE complexes (Sakisaka et al., 2004). This layer of regulation has been implicated in tomosyn's effects on neurite extension. Second, tomosyn can be directly phosphorylated by protein kinase A (PKA) in loop two of the second β -propeller domain (Baba et al., 2005). *A priori*, the consequences of this phosphorylation are hard to predict. On the one hand, the phosphorylation reduces tomosyn's affinity for syntaxin, potentially allowing more SNARE complexes to be formed. On the other hand, it leads to enhanced oligomerization of SNARE complexes via the β -propeller domains, presumably with the opposite effect (Sakisaka et al., 2008). Regrettably, physiological experiments on the role of PKA phosphorylation of tomosyn are so far inconclusive due to previously discussed concerns regarding synapse numbers in experiments with transfected superior cervical ganglion neurons in culture. Finally, tomosyn can be SUMOylated in the same loop containing the PKA phosphorylation site

(Williams et al., 2011). Elimination of the SUMOylation site by mutation leads to enhanced inhibition of hGH secretion from PC12 cells, suggesting the covalent attachment of SUMO to tomosyn may inhibit its function.

To summarize, studies on tomosyn indicate clearly that it has a negative influence on synaptic transmission, and that this seems mediated by a reduction in the RRP size. The mechanism of action remains unclear but involves both the β -propellers and the R-SNARE domains of tomosyn. In addition to effects on SNARE complexes and their constituents, interaction with synaptotagmin could be another conduit by which tomosyn regulates synaptic transmission. Furthermore, PKA phosphorylation and SUMOylation sites provide the potential for dynamic regulation. In this thesis, we extend studies of tomosyn's function by using our newly developed techniques to measure effects on P_v and RRP size at hippocampal neurons in culture (Chapter 4).

1.5 Variability between synapses

Having explored the many ways in which P_v and n can be influenced, and after delving in detail into one possible regulator, it is evident that by virtue of any of those mechanisms release properties could vary between presynaptic terminals of the same axon. In fact, there is good evidence that this is the case for many synapses of the central nervous system. In what follows, we will briefly review the evidence for variability between synapses made by the same presynaptic neuron, discuss what little is known about its molecular underpinnings, and finally, consider what the implications of this heterogeneity may be for neural circuit function (Branco and Staras, 2009).

The first reports of variability between presynaptic terminals of the same neuron came from the crustacean neuromuscular junction where different synapses formed by the same axon had varying short-term synaptic plasticity properties depending on the muscle fiber targeted. This variance was shown to be presynaptic in origin and therefore implied the existence of a retrograde signal from target cells to presynaptic varicosities (Frank, 1973). Subsequently, similar results were found in the central nervous system of locusts (Laurent and Sivaramakrishnan, 1992) and crickets (Davis and Murphey, 1993). Regrettably, the lack of molecular tools in these systems did not allow more than a phenomenological characterization.

In the mammalian central nervous system there are several reports of target-specific short-term plasticity in the same axon of neurons in the neocortex (Markram et al., 1998; Reyes et al., 1998). These studies represent some of the most convincing demonstrations of synapse-specific, target-dependent presynaptic properties to date and are therefore worth describing in some detail. Pyramidal cells (P) from layer 2/3 can

contact two types of interneuron targets: bipolar cells (B) and multitufted cells (M). Simultaneous patch clamp of all three cell types in acute slices shows that while $P \rightarrow B$ connections facilitate, $P \rightarrow M$ connections depress (Reyes et al., 1998). This correlates with lower P_r (Koester and Johnston, 2005) and higher failure rates (Rozov et al., 2001) in $P \rightarrow B$ compared to $P \rightarrow M$ synapses. Additionally, $P \rightarrow M$ synapses have larger Ca^{2+} transients during single APs and are less sensitive to Ca^{2+} chelators. This suggests P_v is higher in those terminals due to effects on local Ca^{2+} both through the total amount of Ca^{2+} entry and the coupling between vesicles and channels. At the moment, the molecular players responsible for those differences are unknown. In the hippocampus, presynaptic properties of synapses made by the same axon onto different targets can also differ (Scanziani et al., 1998).

The observation of variable properties between synapses of the same axon has been reproduced in primary neuronal cultures of cortical and hippocampal rodent neurons (both standard and autaptic). There are reports of substantial variation in P_r using a variety of techniques, including application of the use-dependent NMDA receptor blocker MK-801 (Rosenmund et al., 1993), loading and unloading of FM dyes (Murthy et al., 1997; Branco et al., 2008), pHluorin (Granseth and Lagnado, 2008; Matz et al., 2010), and electron microscopy (Branco et al., 2010). In most cases, P_r is an average estimate obtained from low frequency trains of stimulation, as opposed to individual APs. Additionally, few examples attempt to measure P_v or n .

The main reason to use neuronal cultures in studies of P_r variability is to gain mechanistic insights, yet there has been little progress so far beyond a few specific examples. An early study using the activity dependent blocker MK-801 proposed that

Ca^{2+} channel subtypes are differentially distributed across synapses of the same axon, but not according to \mathbf{P}_r (Reid et al., 1997). However, that report must be regarded as preliminary since the method used did not allow direct measurement of \mathbf{P}_r at individual synapses. More recent papers using FM dyes showed that \mathbf{P}_r depends on the activity of the dendritic target (Branco et al., 2008), and is negatively correlated with the activation of presynaptic GABA_B receptors, presumably determined by local GABA levels around each synapse (Laviv et al., 2010). In another example that used pHluorin, the amount of bassoon -a protein enriched at the active zone- was correlated with \mathbf{P}_r at the level of single synapses (Matz et al., 2010). The results were interpreted as an increase in \mathbf{n} , wherein synapses with larger active zones (and thus higher bassoon levels) had more primed vesicles. Finally, in a recent study, the levels of RIM were correlated with the total uptake of an antibody against a synaptic vesicle protein during stimulation (Lazarevic et al., 2011). While this is a very crude measure of synaptic output, the correlation is nevertheless quite interesting. Like bassoon, RIM is a protein enriched at active zones (Mittelstaedt et al., 2010). However, unlike bassoon, which seems to play a structural role, there is good evidence that RIM controls \mathbf{P}_v and \mathbf{n} through specific domains that interact directly with munc13 and Ca^{2+} channels, affecting priming, vesicle to channel coupling and fusion willingness (Deng et al., 2011; Han et al., 2011; Kaeser et al., 2011). Additionally RIM has a relatively short half-life of ~ 1 hour (Yao et al., 2007) which suggests it might act as a dynamic, rate-limiting control variable that sets synaptic strength.

In addition to variable baseline neurotransmission properties, there is also evidence for heterogeneity in how synapses of the same axon can be modulated. An

interesting example is the type III metabotropic glutamate receptor 7 (mGluR7). This G protein-coupled receptor is specifically enriched on presynaptic terminals that contact interneuron targets (Shigemoto et al., 1996; Lujan et al., 1997). Consequently, glutamate release from individual CA3 pyramidal cells is inhibited by type III mGluR agonists at synapses onto interneurons, but not pyramidal cells (Scanziani et al., 1998). Another example is the negative modulation of P_r by GABA_B receptors. In hippocampal neurons in autaptic culture, the agonist baclofen was unable to modify synaptic efficacy at a subset of high P_r synapses, suggesting a differential distribution of the receptors in presynaptic terminals of the same axon (Rosenmund et al., 1993).

The potential role of synapse-specific properties on network function remains unclear in most cases and is likely to depend on the exact circuits in which these connections are involved. A good example of a functional consequence in a circuit is the demonstration of a spatiotemporal shift of recurrent inhibition in pyramidal neurons of the CA1 region of the hippocampus (Pouille and Scanziani, 2004). These principal cells project to two types of inhibitory interneurons using synapses with differing P_r and short-term plasticity properties. Synapses onto one subset of interneurons have high P_r and undergo depression, whereas synapses onto a second subset have low P_r and facilitate during bursts. Additionally, the first set of interneurons project primarily to the somata of CA1 pyramidal cells, whereas the second set of interneurons projects mainly onto apical dendrites. Thus, during a burst of activity in a CA1 pyramidal cell first one and then another subset of interneurons will be preferentially activated. The resulting recurrent inhibition from interneurons back onto CA1 pyramidal cells will therefore shift during the burst, from the soma to the apical dendrites. Whether the wide range of activity

patterns present in CA1 pyramidal cells during exploratory behaviors (Andersen, 2007) are represented by spatially distinct inhibitory patterns using this mechanism is unknown.

The general picture from these studies is that there can be substantial variability in baseline neurotransmission properties between synapses of the same axon, some of it target-dependent. In addition, synaptic strength can be modulated on a synapse by synapse basis. However, so far the underlying mechanisms remain, for the most part, as obscure as the implications for circuit function.

In Chapter 5 of this thesis, we extend the methods developed to study \mathbf{P}_v and \mathbf{n} to individual synapses. We then explore the contributions to synaptic variability of Ca^{2+} channel subtype and the coupling between Ca^{2+} channels and vesicles. Finally, we study the modulation of synaptic strength by the adenylyl cyclase activator forskolin at individual synapses.

2. MATERIALS AND METHODS

2.1 Cell culture and optical setup

Hippocampal CA3-CA1 regions were dissected from 1- to 3-d-old Sprague Dawley rats, dissociated, and plated onto poly-ornithine-coated glass as described previously (Ryan, 1999). A chimera of the pH-sensitive GFP pHluorin and the vesicular glutamate transporter (vG-pH, Voglmaier et al., 2006) was transfected using calcium phosphate precipitation 6-9 days after plating and imaging was performed 13-25 days after plating. Experiments in Chapters 3 and 4 had low transfection efficiencies, such that there were typically only one or a few well separated transfected cell bodies per dish. In cases where we equate single experiments with individual neurons, we confirmed this was the case by staining *post-hoc* for vG-pH (see below) and unambiguously tracing the imaged axons to a single transfected soma. Thus, in those cases the boutons imaged in each experiment belong to a single cell. The coverslips were mounted in a rapid-switching, laminar-flow perfusion and stimulation chamber (volume $\sim 75 \mu\text{l}$) on the stage of a custom-built laser-illuminated epifluorescence microscope. Live-cell images were acquired with an Andor iXon⁺ (model #DU-897E-BV) back-illuminated electron-multiplying charge-coupled device camera. An Ar⁺ ion or solid-state diode pumped 488 nm laser was shuttered using acousto-optic modulation. Fluorescence excitation and collection was through a 40X 1.3 NA Fluar Zeiss objective using 515–560 nm emission and 510 nm dichroic filters (Chroma) and a 1.6X Optivar. Laser power at the back aperture was $\sim 2\text{-}5$ mW. Action potentials were evoked by passing 1 ms current pulses,

yielding fields of ~ 10 V/cm via platinum-iridium electrodes. Experiments in Figures 3.1 and 3.2 were performed at room temperature (~ 28 - 32°C in stimulation chamber), for all others the temperature was clamped at $30.0 \pm 0.1^\circ\text{C}$. Cells were continuously perfused at 0.2-1.0 ml/min. in a saline solution containing (in mM) 119 NaCl, 2.5 KCl, 2 CaCl₂, 2 MgCl₂, 25 HEPES, buffered to pH 7.4, 30 glucose, 10 μM 6-cyano-7-nitroquinoxaline-2,3-dione (CNQX), and 50 μM D,L-2-amino-5-phosphonovaleric acid (AP5). All chemicals were obtained from Sigma except for bafilomycin (Calbiochem), Ca²⁺ channel toxins (Alomone Labs) and Ca²⁺ indicators (Invitrogen). For solutions with different Ca²⁺ concentrations in the 1-4 mM range, we substituted Mg²⁺ to maintain a constant divalent concentration. For 10 mM Ca²⁺ we reduced the concentration of glucose to maintain constant osmolarity. For 18 mM Ca²⁺ we also reduced the concentration of HEPES to the same end. Cells were only exposed to different Ca²⁺ solutions for ~ 15 -30 s necessary to acquire data. For experiments in the presence of 4-aminopyridine (4-AP), we repeatedly stimulated with 1 AP and only analyzed the responses once their amplitude was stable over several trials. A subset of cells showed no effect of 4-AP ($<10\%$ of all experiments) and were excluded from further analysis. For 4-AP experiments with 4mM external Ca²⁺ we incubated the cells in 4-AP continuously with standard external Ca²⁺ (2 mM) and only increased the Ca²⁺ concentration for the ~ 15 -30 s necessary for imaging. To block P/Q-type Ca²⁺ channels we applied ω -agatoxin IVA (400nM) for 2 minutes. To block N-type Ca²⁺ channels we applied ω -conotoxin GVIA (1 μM) for 2 minutes. Neither toxin showed any sign of wash-off during prolonged experiments. Due to the low baseline fluorescence of neurons that express vG-pH (Balaji and Ryan, 2007), we gave brief bursts with 6 APs at 33 Hz every 4 s to find transfected cells in a dish. Cells were allowed to rest 10

minutes after identification with 33 Hz stimuli, at least 30s between 1 AP trials and at least 5 min between 100 Hz AP bursts. Data was acquired at 100 Hz by integrating for 9.74 ms in frame transfer mode and restricting imaging to a subarea of the CCD chip. The maximum width of the imaged field under those conditions was 167 pixels (41.75 μm).

2.2 Image and data analysis of vG-pH experiments

Images were analyzed in ImageJ (<http://rsb.info.nih.gov/ij/>) using a custom-written plugin (<http://rsb.info.nih.gov/ij/plugins/time-series.html>). 2 μm diameter circular ROIs were placed on all varicosities that did not split or merge, were stably in focus throughout all trials and responded to a maximal stimulus at the end of the experiment. To estimate 1 AP ΔF s in Chapters 3 and 4, we took the difference between the average 10 frames before the stimulus and 10 frames after the stimulus. The rise in vG-pH fluorescence in response to a single AP always took 2 frames when acquiring at 100 Hz time resolution. A subset of the data in Figure 3.2A1 was acquired at 2 Hz imaging with 200 ms integration and the 1 AP ΔF was calculated as a point to point difference. In experiments where we obtained information from single synapses (Chapter 5), we used 2 Hz imaging for single AP trials, integrating for 25 ms and then converting the data for comparison with the 100 Hz imaging runs used to estimate RRP size. In those experiments, 1 AP ΔF s were estimated as the point to point difference before and after the stimulus. At the end of each experiment in Chapter 3 we measured the response to 1200 APs at 10 Hz in bafilomycin at 2 Hz temporal resolution. Alternatively, for some experiments in Chapters 4 and 5, we normalized responses to the total number of reporter

molecules in each bouton. This was determined by briefly (<1min) exposing cells to a modified Tyrode's solution containing NH_4Cl buffered at $\text{pH} = 7.40$ instead of HEPES. This solution alkalinizes the interior of all synaptic vesicles and the resulting ΔF is proportional to the total number of vG-pH molecules in the terminal. Given that there is typically one vG-pH molecule per vesicle, and that all vesicles are labeled (Balaji and Ryan, 2007), responses expressed as a percentage of the NH_4Cl ΔF can also be considered equivalent to the same of the total number of vesicles in the synapse (TP).

For experiments where we stimulated at 100 Hz in 4 mM external Ca^{2+} , we calculated the frame at which each AP fired taking into account the 2 frame rise time for the first AP. Independent experiments with varying numbers of APs at 100 Hz confirmed that the each AP took place at the expected frame (not shown). After the end of stimulation, there was an additional slower rise in fluorescence. Operationally, we defined exocytosis that occurred up to and including the last frame of the stimulus period as stimulus-locked and all later rises as delayed. The end of delayed exocytosis was set when the fluorescence stopped rising. Trials with 20 APs at 100 Hz were repeated at least 4 times. To determine objectively from 100 Hz bursts the size of the RRP, in each cell we used an automated method that searched for plateaus in the ΔF response where the fluorescence did not rise significantly. Sliding data windows of increasing size were used to fit a linear model to the cumulative ΔF vs. AP number data. For example, 3 point data windows were used to fit cumulative ΔF vs. AP number between 3 and 5 APs, 4 and 6 APs and so forth up to 18 to 20 APs. Analogously, 4 point data windows were used to fit cumulative ΔF vs. AP number between 3 and 6 APs, 4 and 7 APs and so forth up to 17 to 20 APs. This procedure was repeated up to a 18 point fitting window for the ΔF vs. AP

number data between 3 and 18 APs. For each of the fits, we tested whether the slope was statistically significant (greater than 0) at $\alpha=0.05$ (Sokal and Rohlf, 1994). A plateau representing the RRP size was identified as the largest window where the slope of ΔF vs. AP number was not significant. If there was more than one window of the same size where this condition was met, we picked the one corresponding to the lowest AP numbers. Additionally, we only accepted cases where the slope of ΔF vs. AP number for the points in the plateau was at most 50% of the slope of the ΔF vs. APs 1-3. On average, the ratio of slopes between plateau and the first three points was 0.15 ± 0.02 ($n=24$, range: 0.03-0.50). To determine the RRP size, we averaged the ΔF values within the identified window. On average, these windows where fluorescence did not rise were located between the 8th (range=3-14) and the 14th AP (8-20) in the 100 Hz train.

Individual APs in the presence of 4-AP caused both a stimulus-locked component of exocytosis and the appearance of an additional delayed component. Typically, the latter had much slower kinetics but in some cases it could be further classified into a fast and a slow subcomponent. The fast subcomponent was similar in rate of rise to stimulus-locked exocytosis, while the other subcomponent was noticeably slower (see Fig. 3.2A2 for an example with and Figure 3.4A2 for an example without this fast delayed subcomponent). The end of the fast delayed subcomponent of exocytosis was set at the inflection point where the rate of rise of the fluorescence slowed. Because stimulus-locked exocytosis and the fast subcomponent of delayed release were kinetically similar and distinct from the slow subcomponent of the latter, we took the sum as a measure of fast exocytosis in response to 1 AP.

To estimate the RRP size from single AP data (Fig. 3.2C), we used a generalized Hill model that relates exocytosis (Exo) and the relative increase in intracellular Ca^{2+} (rCa_i):

$$Exo = RRP \frac{rCa_i^n}{rCa_i^n + K^n} \quad (2.1)$$

We estimated Exo from vG-pH ΔF measurements (using the fast exocytosis estimate if applicable) and rCa_i from Magnesium Green (MgGreen) relative $\Delta F/F_0$ measurements (see below). n , K and RRP were fit using a Levenberg-Marquardt optimization procedure with data points weighted inversely by their error bars (Origin 7.0, OriginLab).

2.3 Error analysis

To estimate how precisely we could determine \mathbf{P}_v and RRP size in each cell (Figs. 3.3E and 3.5B), we used a standard formula to propagate the errors arising from fluctuations in our traces (Taylor, 1997):

if $q \equiv q(x, \dots, z)$

then

$$\delta q = \sqrt{\left(\frac{\partial q}{\partial x} \delta x\right)^2 + \dots + \left(\frac{\partial q}{\partial z} \delta z\right)^2}$$

To calculate \mathbf{P}_v and RRP size with their errors, we relied on 3 traces from each cell:

F_1 : response to 1 AP (average of at least 10 trials)

F_{20} : response to 20 APs at 100 Hz (average of at least 4 trials)

F_{Baf} response to 1200 APs at 10 Hz in bafilomycin

To obtain the responses to 1 AP and 1200 APs at 10 Hz in bafilomycin we averaged the last 10 frames before the stimulus and the first 10 frames after the end of the stimulus. This gave us:

$$F_{1pre} \quad , \quad SE_{F_{1pre}}$$

$$F_{1peak} \quad , \quad SE_{F_{1peak}}$$

$$F_{Bafpre} \quad , \quad SE_{F_{Bafpre}}$$

$$F_{Bafpeak} \quad , \quad SE_{F_{Bafpeak}}$$

where the standard error in each case was the standard deviation of the 10 frames divided by the square root of 10. Based on these values, we calculated the responses to 1 AP and 1200 APs at 10 Hz in bafilomycin with their corresponding errors:

$$\Delta F_1 = F_{1peak} - F_{1pre} \quad , \quad SE_{\Delta F_1} = \sqrt{SE^2_{F_{1peak}} + SE^2_{F_{1pre}}}$$

$$\Delta F_{Baf} = F_{Bafpeak} - F_{Bafpre} \quad , \quad SE_{\Delta F_{Baf}} = \sqrt{SE^2_{F_{Bafpeak}} + SE^2_{F_{Bafpre}}}$$

For the 20 AP traces we proceeded similarly, averaging the last 10 frames before the stimulus and the frames included in the plateau to obtain:

$$F_{20\ pre} \quad , \quad SE_{F_{20\ pre}}$$

$$F_{20\ plateau} \quad , \quad SE_{F_{20\ plateau}}$$

where the standard error was the standard deviation divided by the square root of the number of observations in each case (10 for $F_{20\ pre}$ and the number of points included in the plateau for $F_{20\ plateau}$). Thus:

$$\Delta F_{20\ plateau} = F_{20\ plateau} - F_{20\ pre} \quad , \quad SE_{\Delta F_{20\ plateau, inst}} = \sqrt{SE^2_{F_{20\ plateau}} + SE^2_{F_{20\ pre}}}$$

In addition to these instrumental errors, given that we measured the responses to 20 APs at 100 Hz at least 4 times in each experiment we also obtained a statistical estimate of the error in $\Delta F_{20\ plateau}$:

$$SE_{\Delta F_{20\ plateau, stat}} = \frac{SD_{\Delta F_{20\ plateau, stat}}}{\sqrt{n}}$$

where $SD_{\Delta F_{20\ plateau, stat}}$ is the standard deviation of the plateau estimates in different trials (n at least 4). We added the instrumental and statistical contributions to the error in quadrature and combined them to get the total error for $\Delta F_{20\ plateau}$:

$$SE_{\Delta F_{20\ plateau}} = \sqrt{SE^2_{\Delta F_{20\ plateau, inst}} + SE^2_{\Delta F_{20\ plateau, stat}}}$$

Finally, we calculated RRP size and \mathbf{P}_v with their associated errors:

$$RRP = \frac{\Delta F_{20\ plateau}}{\Delta F_{Baf}} \quad , \quad SE_{RRP} = \frac{1}{\Delta F_{Baf}} \sqrt{SE^2_{\Delta F_{20\ plateau}} + RRP^2 SE^2_{\Delta F_{Baf}}}$$

$$P_v = \frac{\Delta F_1}{\Delta F_{20\ plateau}} \quad , \quad SE_{P_v} = \frac{1}{\Delta F_{20\ plateau}} \sqrt{SE^2_{\Delta F_1} + P_v^2 SE^2_{\Delta F_{20\ plateau}}}$$

These calculations provide the error bars for \mathbf{P}_v and RRP size in individual experiments.

To estimate errors involved in the determination of P_v and RRP size at individual synapses, we used the same equations with a few modifications:

- F_1 : response to 1 AP (average of 30 trials)
- F_{20} : response to 20 APs at 100 Hz (average of 12 trials)
- Our responses were normalized to the ΔF resulting from a pulse of 50 mM NH_4Cl , which alkalinizes all cellular compartments.
- F_1 traces were acquired at 2 Hz and we calculated ΔF_1 as the difference between the last point before firing an action potential and the first point after the stimulus. To estimate $SE_{\Delta F_1}$ we took the SE of the response to 1 AP across 30 trials.
- We estimated SE_{NH_4Cl} from the SE of the baseline and peak fluorescence during NH_4Cl application

To estimate the errors of the effects on single action potential responses of Ca^{2+} channel toxins, EGTA we first calculated the error in the ΔF_{1post} (after each pharmacological treatment) using the same formulas as for ΔF_1 and then used:

$$Effect = 1 - \frac{\Delta F_{1post}}{\Delta F_1} \quad , \quad SE_{Effect} = \frac{1}{\Delta F_1} \sqrt{SE^2_{\Delta F_{1post}} + (1 - Effect)^2 SE^2_{\Delta F_1}}$$

For forskolin (a positive modulator of exocytosis), we used:

$$Effect = \frac{\Delta F_{1post}}{\Delta F_1} - 1 \quad , \quad SE_{Effect} = \frac{1}{\Delta F_1} \sqrt{SE^2_{\Delta F_{1post}} + (1 + Effect)^2 SE^2_{\Delta F_1}}$$

2.4 Ca²⁺ indicator measurements and analysis

MgGreen (Figs. 3.2B1, 3.2B3, 3.2B4, 3.3D, 5.3) or Fluo-3 (Fig. 3.2B2) were loaded at 20 μM in their acetoxymethyl ester (AM) form for 10 min and washed off for ~ 30 min before experiments were started. Single AP stimuli led to robust, focal responses distributed over neuritic fields. We analyzed $\Delta F/F_0$ of manually drawn ROIs placed on these punctate responsive regions. F_0 was corrected point to point by subtracting local background from manually drawn ROIs on adjacent non-responsive regions.

The data in Figure 3.2B1 were fit to a single site binding model using a Levenberg-Marquardt optimization procedure with data points weighted inversely by their error bars (Origin 7.0, OriginLab):

$$r \frac{\Delta F}{F_0} = R_{\max} \frac{(Ca^{2+})_e}{(Ca^{2+})_e + K_m} \quad (2.2)$$

For experiments with 100 Hz stimulation in 4 mM external Ca²⁺ (Fig. 3.3D), we calculated the frame at which each AP fired in the same manner as for vG-pH (see above) confirming separately that the each AP took place at the expected frame (not shown).

2.5 shRNA and tomosyn plasmids

We synthesized 60-mer oligonucleotides (Invitrogen) containing the rat tomosyn-1 target sequence (TCTCTTGATAGAGAAGAAC, sequence based on Cheviet et al., 2006) or (GCGGTACTATATTGAGGTAA, sequence based on Sakisaka et al., 2004), annealed them and ligated into pSUPER using *Bgl*III and *Hind*III enzyme sites according to manufacturer's instructions. The second knockdown vector (based on Sakisaka et al., 2004) was only used for preliminary tests of tomosyn knockdown levels; all other data comes from experiments using the first knockdown construct. A plasmid containing the cDNA for mouse tomosyn-1 isoform s was a kind gift from Uri Ashery. We subcloned this cDNA using PCR with appropriate primers into *Eco*RI and *Xho*I sites of a modified pcDNA 3 vector that contained an insert coding for a hemagglutinin (HA) tag immediately upstream of the start codon, cloned between *Kpn*I and *Eco*RI sites (tag sequence is MYPYDVPDYA). Additionally, we subcloned the cDNA into *Eco*RI and *Xho*I sites of pcDNA 3 to generate an untagged expression vector. After cloning, we sequenced the entire cDNA and vector-cDNA junctions to verify no mutations had been introduced during the procedure.

2.6 Immunostaining analysis of tomosyn levels

To quantify the efficiency of shRNA-mediated knockdown, following live cell imaging, neurons were fixed for 10 minutes with 4% paraformaldehyde, permeabilized for 10 minutes with 0.2% Triton X-100, blocked 1 hour at 37°C with 5% BSA, and subsequently incubated for 3 hours with appropriate primary antibodies: chicken monoclonal anti-GFP (Invitrogen) and rabbit polyclonal anti-tomosyn (TC56, a kind gift from Reinhard Jahn), both diluted 1:500. Alexa-488- or Alexa-546-conjugated secondary antibodies were applied in primary antibody incubated samples at 1:1000 dilution for 1 hour at 37°C. At least 3 washes with PBS (phosphate buffered saline) were performed between each solution exchange. Immunofluorescence images of fixed cells were acquired using our microscope under mercury arc lamp illumination.

Neuronal somas were identified by DIC and regions of interest were drawn manually, excluding the nucleus in each case. Multiple background ROIs were drawn in each field, in areas with neither somas nor neurites. These were merged to generate one background ROI for each field which was used to correct all cells in that field. To generate an estimate of tomosyn levels that could be compared across multiple experiments, we normalized to levels in untransfected cells:

$$F_{norm} = \frac{F - F_{background}}{\langle F_{untrans\ cell} - F_{background} \rangle} \quad (2.3)$$

The untransfected cells averaged in each case were from the same field. In some cases there were less than 3 untransfected neurons in a given field, in which case we averaged untransfected cells from multiple nearby fields. Note that with this normalization scheme, untransfected neurons will, by definition, have average tomosyn levels of 100%.

2.7 Statistical analysis and data presentation

All values mentioned in the text are averages \pm standard errors of the mean (SE) unless stated otherwise. All error bars in graphs are SEs unless stated otherwise. Box whisker plots show the median (line), mean (point), 25-75 percentile (box) and 10-90 percentile (whisker) ranges.

To test differences between groups, parametric statistics were used whenever possible (Sokal and Rohlf, 1994). The assumption of homogeneity of variances was assayed with Levene's test, using $\alpha=0.05$ as a cutoff. Normality was assed both visually in a normality q-plot (for cases with more than two groups) and using Lilliefors's test for every group (using $\alpha=0.05$ as a cutoff). If either of the assumptions of parametric tests were not met, we either transformed the data and retested the assumptions or used an equivalent non parametric test. In the latter cases, Mann-Whitney U tests were used in lieu of t-tests or one way ANOVAs with 2 groups, and Kruskal-Wallis tests were used in lieu of one way ANOVAs with more than two groups. For cases with more than two groups and a statistically significant effect of the treatment ($P<0.05$), post hoc comparisons were used to assay differences between groups. Tukey-Kramer tests were used after ANOVAs and multiple comparisons were used after Kruskal-Wallis. All statistical analysis was performed in STATISTICA 8 (StatSoft).

To calculate the P-values of significance tests of correlation coefficients (Chapter 5, Figs. 5.5-8) we used a correction for small numbers of observations (section 15.5 in Sokal and Rohlf, 1994). For each experiment, we calculated the following statistic for the correlation coefficient:

$$t_s = z\sqrt{n-1} \quad (2.4)$$

where

$$z^* = z - \frac{3z+r}{4(n-1)} \quad (2.5) \text{ and } (2.6)$$

$$z = \frac{1}{2} \ln\left(\frac{1+r}{1-r}\right)$$

r = correlation coefficient for each experiment

n = number of synapses per experiment

The value of t_s follows a standardized normal distribution, and comparison to that distribution provides the corresponding P-value. The transformation outlined above is adequate when $n \geq 10$ so in some experiments with fewer synapses our P-values of individual experiments can only be considered imperfect approximations. An alternative test of whether there were correlations between the effect of each treatment and either \mathbf{P}_v or RRP size was to test whether the distribution of correlation coefficients had a mean significantly different from 0. To this end, we used t -tests with null hypothesis $\mu=0$.

3. OPTICAL MAPPING OF RELEASE PROPERTIES IN SYNAPSES

3.1 Exocytosis measured at high time resolution with vG-pH

As described in Chapter 1, there are two key requirements to determine P_v and RRP size (n). The first is a measurement system with a large enough signal-to-noise ratio to estimate precisely the response to a single AP. The second is an appropriate protocol to determine RRP size, where the main consideration is to use stimuli that rapidly deplete this vesicle pool before it refills. We sought to compare and validate different approaches using our optical methods that are, by design, a strictly presynaptic measurement of exocytosis. Using high frequency action potential bursts and single APs under conditions that cause large intracellular Ca^{2+} increases we looked for evidence of pool depletion in each case. To estimate P_v we divided the response to 1 AP in 2 mM external Ca^{2+} (our standard condition) by our estimate of the RRP size (see equation 1.1).

Our exocytosis measurements were based on the sudden rise in pH of synaptic vesicles when they fuse with the plasma membrane. To detect this change optically we used the pH-sensitive GFP pHluorin (Miesenbock et al., 1998) tagged to the lumen of the vesicular glutamate transporter (Voglmaier et al., 2006). The lumen of a synaptic vesicle increases its pH (from approximately 5.6 to 7.4) upon fusing to the membrane and exchanging protons with the extracellular milieu. The pKa of the fluorescent reporter (around 7.1) is such that it dequenches upon that transition, increasing its fluorescence approximately 20-fold (Sankaranarayanan et al., 2000). Previously, it was demonstrated that fluorescence increases in response to a single AP evoked by field stimulation can be

reliably detected in our system using a 100 ms integration window with minimal bleaching or photodamage over several hours in the course of a typical experiment (Balaji and Ryan, 2007).

To faithfully estimate RRP sizes we needed high time resolution to distinguish between stimulus-locked and delayed components of exocytosis expected after large stimuli. Furthermore, since the depression of release during a burst is used as a sign of RRP depletion, we had to image quickly enough to precisely quantify exocytosis in response to each AP within a stimulus train. At the same time, to estimate P_v we required adequate signal-to-noise to detect responses to single action potentials. After some preliminary tests, we selected a ~10 ms integration window, imaging continuously at 100 Hz. Under these conditions, the signal-to-noise ratio (SNR) at individual boutons for single trials is quite low. However, by averaging over many boutons from a single neuron, we measured responses to individual APs with excellent signal-to-noise at high time resolution (SNR>5 for examples shown in Fig. 3.1A). We routinely performed experiments over one hour in length with minimal bleaching or drift in cell responsiveness. To calibrate our signals as a fraction or percentage of the total releasable pool (TRP) we applied a maximally depleting stimulus (1200 APs at 10 Hz) in the presence of the V-ATPase H^+ pump blocker bafilomycin (Baf, Fig. 3.1B). Individual APs led to exocytosis of $0.54 \pm 0.07\%$ of the TRP (n=14 cells).

Importantly, our data acquisition is fast enough that endocytosis is expected to have a negligible effect on the traces of single AP responses. We expect <0.01% decay of the peak amplitude in 100 ms, assuming $\tau_{\text{endo}} \sim 14$ s and $\tau_{\text{reacidification}} \sim 4$ s (Atluri and Ryan, 2006; Granseth et al., 2006; Balaji and Ryan, 2007).

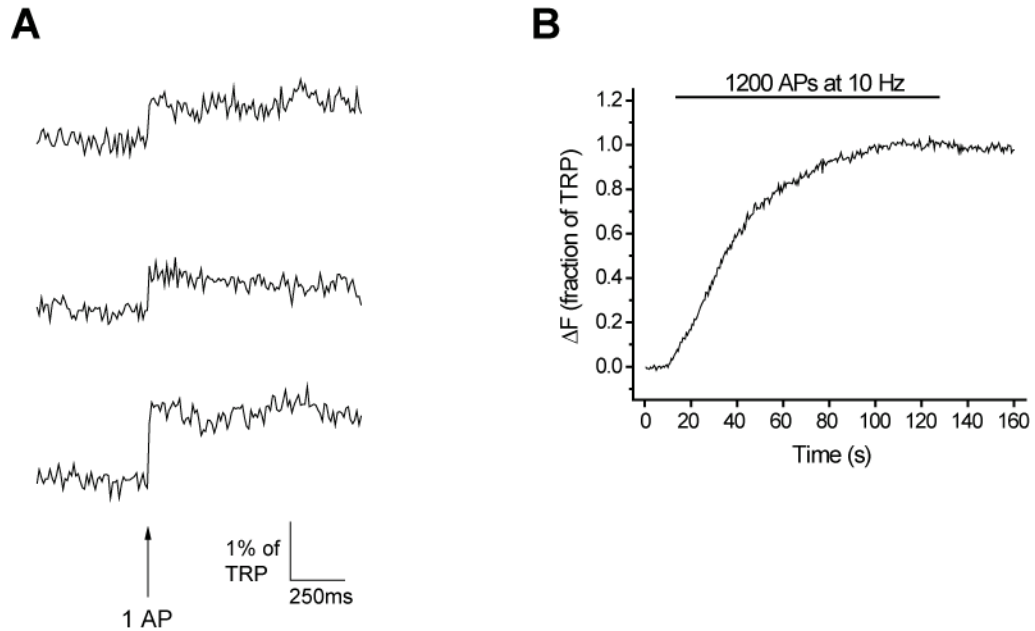


Figure 3.1. Exocytosis in response to 1 AP measured at 10 ms time resolution with vG-pH. **(A)** Representative traces of a neuron's response to 1 AP (n=25 synapses). **(B)** Response to 1200 APs at 10 Hz in the presence of Baf for the same neuron.

3.2 A single AP that causes a large increase in intracellular Ca^{2+} can release the entire RRP

Our first approach to measure the RRP size was to use single APs under conditions where sufficient Ca^{2+} entered the synapse so as to saturate the Ca^{2+} sensors on the vesicles (presumably synaptotagmin-1, see Burgalossi et al., 2010). Under these conditions, all vesicles in the RRP are expected to fuse synchronously. Whether these vesicles fuse separately (Abenavoli et al., 2002; Oertner et al., 2002; Conti and Lisman, 2003) or through compound fusion (Matthews and Sterling, 2008; He et al., 2009) does

not affect our estimate of the RRP size as in both cases the compartments will alkalinize and the fluorescence of vG-pH will increase accordingly.

In order to increase the number of calcium ions that entered the synapse in response to 1 AP, we first chose to elevate extracellular Ca^{2+} in the range from 2 mM to 10 mM. While increasing extracellular Ca^{2+} 2-fold from 2 mM to 4 mM caused a 3-fold increase in exocytosis, the 2.5-fold increase between 4 mM to 10 mM only caused a ~60% increase in exocytosis (Fig. 3.2A1). This suggests that exocytosis as a function of external Ca^{2+} is close to saturation at 10 mM and indeed, increasing external Ca^{2+} concentration to 18 mM yielded only a ~20% additional increase in exocytosis ($\text{exocytosis}_{18\text{mM}}=3.1\pm 0.5\%$ of TRP in 14 cells).

An important point that we wished to address was how changes in extracellular Ca^{2+} concentrations affected relative increases in internal Ca^{2+} concentrations in response to single APs. While the relationship can be assumed to be linear at low Ca^{2+} concentrations, under the conditions used here that is not necessarily the case. In fact, in the calyx of Held giant synapse in the auditory brainstem, the relationship between relative Ca^{2+} entry and extracellular Ca^{2+} is not linear in the 2-10 mM range (Schneggenburger et al., 1999) and conforms to a model reflecting saturation of the flux through the pore of each Ca^{2+} channel. To study this issue directly, we used the low affinity Ca^{2+} indicator MgGreen AM to probe relative changes in intracellular Ca^{2+} concentration in response to 1 AP as a function of extracellular Ca^{2+} . Our results from MgGreen measurements are in good agreement with those from the calyx of Held and show that increases in intracellular Ca^{2+} saturate as extracellular Ca^{2+} is increased (Fig. 3.2B1). This means that the saturation of exocytosis as a function of extracellular Ca^{2+} in

the 2-10 mM range is in large part due to saturation of the flux through the Ca^{2+} channels and not necessarily to saturation of the Ca^{2+} sensors on synaptic vesicles.

The use of an AM loaded Ca^{2+} indicator to determine presynaptic properties can be misleading as the indicator is taken up not only by axons and nerve terminals, but also by dendrites and spines which will be in the same field of view. Thus, it was necessary to determine whether the signals were mainly due to Ca^{2+} entry through the N and P/Q Ca^{2+} channels that drive presynaptic vesicle exocytosis (Meir et al., 1999). To test this we studied the effect of specific blockers of these and other channels on single AP responses. To enhance our signal-to-noise ratio and obtain more precise estimates of the degree of inhibition, we switched to the higher affinity Ca^{2+} indicator Fluo-3 AM and performed experiments with ω -conotoxin MVIIC 10 μM (N, P/Q- blocker), SNX-482 1.2 μM (R-type blocker) or Nimodipine 20 μM (L-type blocker) to test the contribution of different Ca^{2+} channel subtypes to our responses (Fig. 3.2B2). While all three inhibitors decreased responses to 1 AP ($P < 0.05$ in one tailed t-tests with null hypothesis $\mu = 1.0$), the main contribution to the signal was from N and P/Q channels (~80%). This gives us confidence that the response to different stimuli of AM loaded Ca^{2+} indicators can be used to estimate relative increases in intracellular Ca^{2+} in the presynaptic terminal.

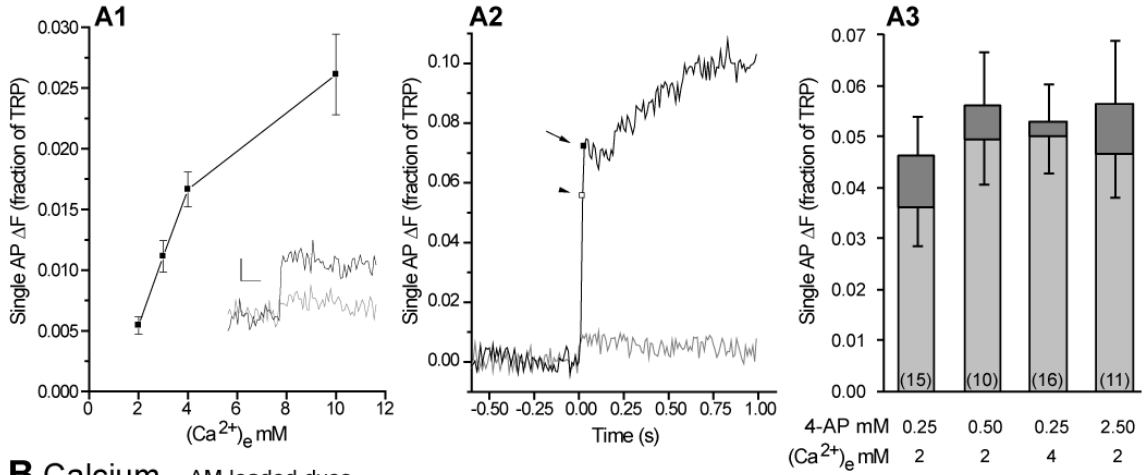
To probe exocytosis in response to single APs under conditions of larger intracellular Ca^{2+} increases we used 4-aminopyridine (4-AP), a K^+ channel blocker that is expected to extend the duration of the action potential and therefore increase the open time of Ca^{2+} channels (Mathie et al., 1998). As predicted, applying 4-AP caused increases in intracellular Ca^{2+} levels in response to one AP larger than those attainable by increasing extracellular Ca^{2+} (Fig. 3.2B3). Importantly, we verified that the response of

the Ca^{2+} indicator itself remained linear in this measurement range (Fig. 3.2B4). In the presence of 4-AP, exocytosis in response to 1 AP also increased beyond what was achieved by increasing the extracellular Ca^{2+} concentration, confirming that the Ca^{2+} sensors on the vesicles were previously not saturated, even at 10 mM external Ca^{2+} (Figs. 3.2A2, 3.2A3). 4-AP caused an increase in the stimulus-locked component of exocytosis and the appearance of delayed component, which could sometimes be further classified into a fast and a slow subcomponent (see Chapter 2 for more details). When there was a fast delayed subcomponent present, we added it to the stimulus-locked response to obtain a measure of fast exocytosis after 1 AP. If there was no fast delayed subcomponent, we simply used the stimulus-locked response for analysis.

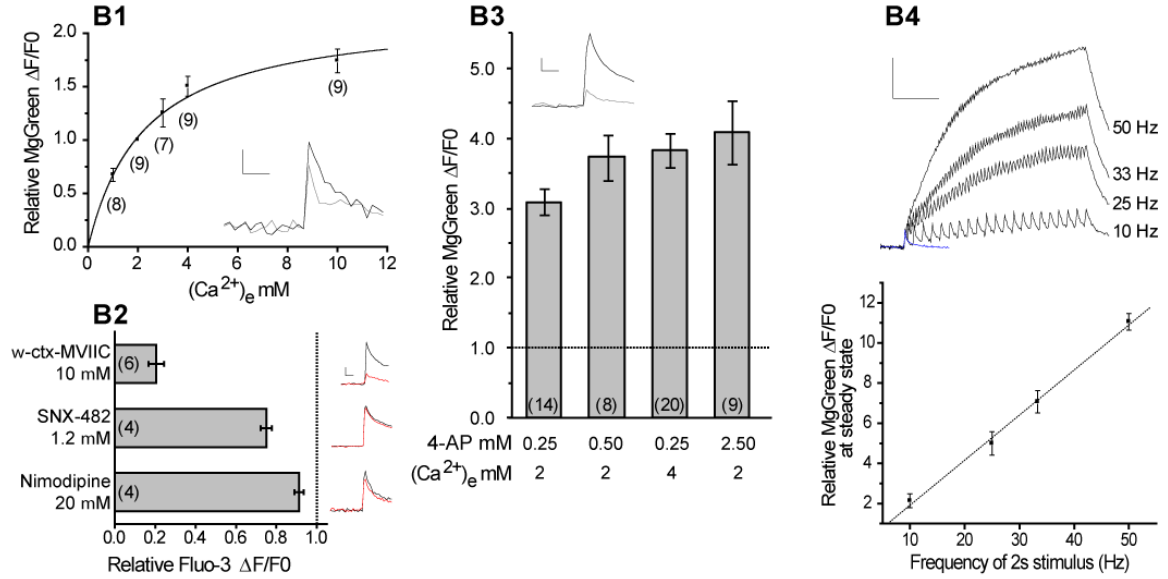
We combined our measurements of exocytosis in response to single action potentials under different conditions (Figs. 3.2A1, 3.2A3) with those of relative increases in intracellular Ca^{2+} under those same conditions (Figs. 3.2B1, 3.2B3) to show how exocytosis varies with increasing internal Ca^{2+} fluxes into the nerve terminal (Fig. 3.2C). The data were well fit by a generalized Hill model -equation (2.1)- where the saturation value corresponds to an estimate of the size of the RRP ($5.9 \pm 0.7\%$). We also analyzed the data using only the stimulus-locked component of exocytosis (excluding the fast subcomponent of delayed release) and found that while the estimate of RRP size was $\sim 20\%$ lower, the difference with the previous estimate was not statistically significant (RRP= $4.9 \pm 0.6\%$ of TRP).

Figure 3.2. Single APs cause exocytosis of the entire RRP in conditions with large intracellular Ca^{2+} increases. **(A1)** Exocytosis in response to 1 AP as a function of extracellular Ca^{2+} ($n=14$ cells). *Inset*: representative individual trials at 2 mM (grey) and 4 mM (black) from one cell. Scale bar= 1% of TRP, 100 ms. **(A2)** Representative experiment showing responses to a single AP under control conditions (2 mM external Ca^{2+} , grey) and with 2.5 mM 4-AP (black). Note the presence of fast (arrow) and slow subcomponents of delayed release after the end of stimulus-locked exocytosis (arrowhead). $n=7$ and 3 trials for control and 4-AP respectively. **(A3)** Average responses to single APs under different 4-AP and extracellular Ca^{2+} conditions. The bars show the stimulus-locked (light grey) and fast delayed (dark grey) components of exocytosis with their SEs. **(B1)** Average relative peak $\Delta F/F_0$ as a function of external Ca^{2+} across several experiments. The line is a fit (to the measurements) by a single site binding model (equation (2.2), $K_m=2.3\pm 0.4$ mM, $R_{\max}=2.2\pm 0.2$). *Inset*: responses to 1 AP at 2 mM (grey) and 4mM (black) in a representative experiment ($n=4$ trials each). **(B2)** Effects of Ca^{2+} channel toxins on single AP responses measured with Fluo-3 AM. Beside each column there is an average control (black) and toxin (red) trace from a representative experiment ($n=3-5$ trials each). Scale bar= 20% $\Delta F/F_0$, 50ms **(B3)** Increases in intracellular Ca^{2+} concentration in response to 1 AP relative to control in different 4-AP and extracellular Ca^{2+} conditions. *Inset*: response to control (grey, $n=5$ trials) and 4-AP (black, $n=13$ trials) from a representative experiment with 2.5 mM 4-AP. Scale bar= 2% $\Delta F/F_0$, 50 ms. **(B4)** *Top*: representative experiment showing responses to 1 AP (blue) and 2 s stimuli at 10, 25, 33 and 50 Hz (black). Scale bar=10% $\Delta F/F_0$, 0.5 s. Traces are averages of 3 trials for 2s stimuli and 13 trials for the 1 AP stimulus. *Bottom*: average steady state $\Delta F/F_0$ at the end of 2 s stimuli of varying frequencies ($n=4$ experiments). Responses are normalized to the single AP peak in each experiment. Line shows fit ($P<0.001$, $R^2=0.995$). **(C)** Exocytosis as a function of the relative increase in internal Ca^{2+} concentration ($n=10-16$ vG-pH experiments, $n=9-20$ MgGreen experiments). The line shows the fit to a generalized Hill model (equation (2.1), $\text{RRP}=5.9\pm 0.7\%$ of TRP, $n=3.4\pm 0.4$, $K=1.9\pm 0.2$).

A Exocytosis - vGlut-pHluorin



B Calcium - AM loaded dyes



C Exocytosis vs Calcium

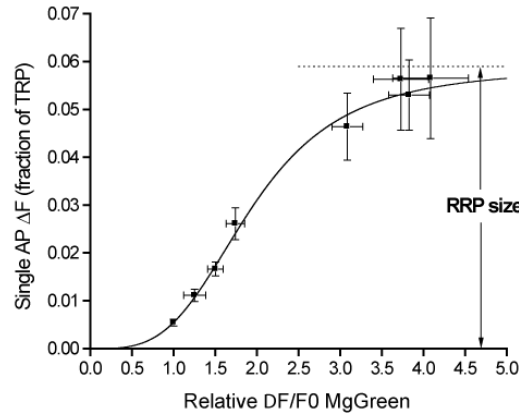


Figure 3.2

3.3 High frequency action potential bursts deplete the RRP

Our second approach to measure the RRP size was to study exocytosis in response to high frequency bursts of APs. In addition to validating our previous results, this type of protocol should be easier to use as it does not require multiple trials until a steady state is reached in the presence of a pharmacological agent (4-AP). We initially tried to measure the RRP by distinguishing a kinetically distinct component of exocytosis using 80 APs at 20 Hz (Fig. 3.3A) or 40 Hz (Fig. 3.3B) at 2 or 4 mM external Ca^{2+} . Under these stimulation conditions we could not observe any obvious kinetic signature of depression expected from a rapid depletion of the RRP in any of the cells we tested (n=10, see Figs 3.3A and 3.3B for a representative example). This was surprising given the widespread use of these protocols in the literature (Murthy and Stevens, 1998; Moulder and Mennerick, 2005; Stevens and Williams, 2007). We explore this apparent discrepancy further in the discussion section of this chapter. While there was some gradual depression of responses during a stimulus train (Figs. 3.3A, 3.3B), any estimate of the RRP size would have required fitting a refilling model to the data. This would introduce additional assumptions regarding both the general kind of model that would be appropriate and its parameters (for example, see Wesseling and Lo, 2002), neither of which we could validate. Due to these complications, we chose instead to increase the strength of the stimulus. We predicted that the larger increase in intracellular Ca^{2+} would lead to a more rapid, clearly noticeable depression of exocytosis as a consequence of RRP depletion. After several tests, we found that increasing our stimulation frequency to 100 Hz and external Ca^{2+} to 4 mM led to responses that showed clear evidence of distinct kinetic phases of exocytosis in all cells tested (see Fig. 3.3C for a representative

example). This protocol led to a rapid rise in fluorescence, followed by a plateau and then an additional increase that continued beyond the end of the stimulus period. We equated the RRP size with the amplitude of the plateau phase for each cell tested (see Chapter 2 for more details). This plateau typically began after 5-10 stimuli and indicated that the rate of exocytosis had dropped to zero. Presumably, under these circumstances all vesicles in the RRP have fused with the membrane and the refilling of that pool becomes the rate limiting step for further exocytosis. The additional rising phase after the plateau proceeded at a lower rate than the original burst (see Figs 3.5A2 and 3.4A1 for smaller and larger magnitudes respectively of this effect) and led to an additional fluorescence increase of $30\pm 4\%$ ($n=24$) over the plateau phase during the remaining stimuli. This rising phase is presumably a consequence of the RRP refilling process catching up and generating primed vesicles that quickly fuse with the membrane due to the elevated Ca^{2+} prevalent inside the nerve terminals. After the end of stimulation, the slower release rate continued, resulting in additional delayed release (amplitude= $1.4\pm 0.1\times$ RRP size, $\tau=360\pm 40$ ms, $n=24$ cells). These kinetics probably reflect the complicated interplay of Ca^{2+} decay, RRP refilling and decreasing exocytosis rates in the synapse after stimulation.

An alternative explanation for the strong depression in exocytosis rates during 100 Hz bursts might be a decrease in Ca^{2+} entry due to progressive inactivation of Ca^{2+} channels (Xu and Wu, 2005). We tested this directly using MgGreen AM and found that the increase in internal Ca^{2+} concentration shows no evidence of significant depression with increasing numbers of APs at 100 Hz in the range where exocytosis rates drop to zero (Fig. 3.3D). Importantly, we applied tetrodotoxin (TTX) to confirm that the Ca^{2+}

signal during 100 Hz stimulation is due to action potentials as opposed to a passive effect of the field stimulation (responses in TTX dropped to $0\pm 1\%$ and could be washed off to $94\pm 2\%$ of the rise before treatment, $n=4$). This strongly suggests that the saturation of stimulus-locked exocytosis during 100 Hz stimulation is due to depletion of vesicles from the RRP.

On average, the RRP size determined from these experiments was $7.3\pm 0.8\%$ of the TRP ($n=24$ cells). Notably, this parameter value was quite variable between cells (Fig. 3.3E, range= 2.2 to 18.7%).

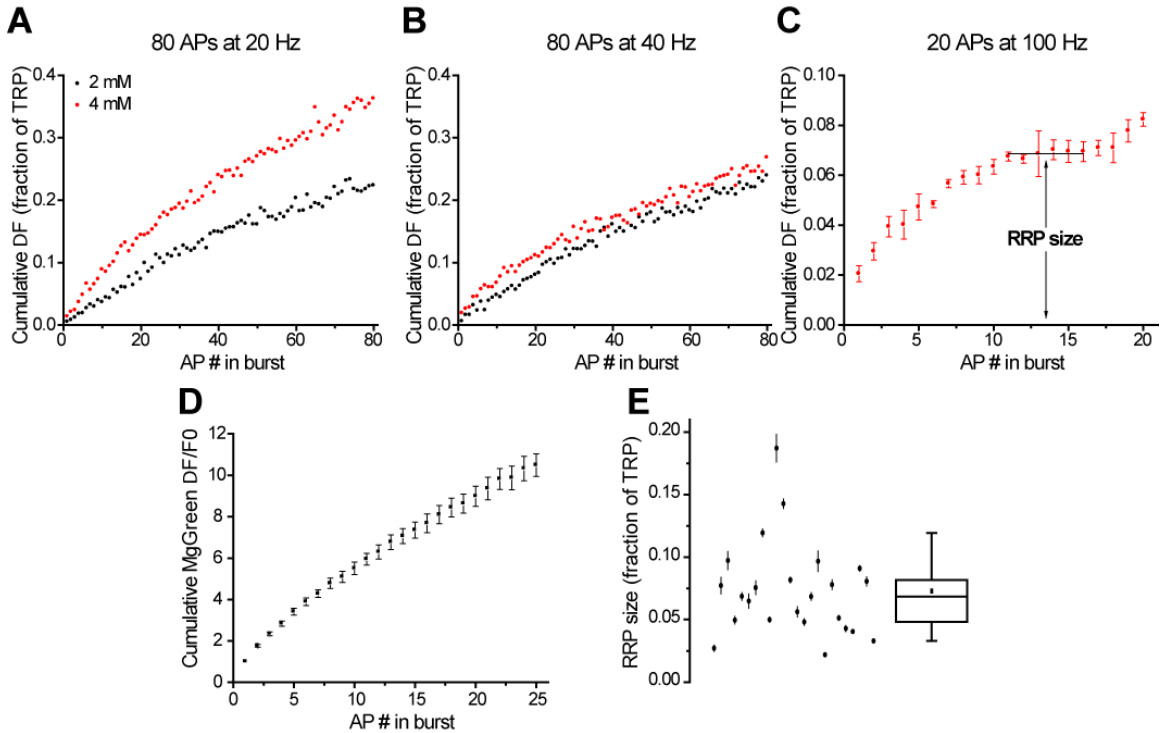


Figure 3.3. Bursts of action potentials at 100 Hz in 4 mM external Ca^{2+} deplete the RRP after exocytosis of approximately 7% of the TRP. (A-C) Responses to different stimuli in the same cell (average of 11 synapses). Responses to 20 (A) and 40 Hz (B) come from individual trials, response to 100 Hz burst (C) is the average of 4 trials. The plateau indicating the depletion of the RRP (C) was detected automatically (see Chapter 2). (D) Ca^{2+} entry at 100 Hz, 4 mM ($n=6$ experiments). Values normalized to first AP. (E) RRP size determined from 100 Hz bursts in 24 cells (see Chapter 2 for explanation of error bars). Box whisker plot shows the median (line), mean (point), 25-75 percentile (box) and 10-90 percentile (whisker) ranges.

3.4 Comparison of methods

Our estimates of RRP size as determined from 100 Hz bursts ($7.3 \pm 0.8\%$ of the TRP) and from single APs under conditions of large intracellular Ca^{2+} rises ($5.9 \pm 0.7\%$ of the TRP) were in reasonable agreement. To confirm that our protocols gave self consistent results, we designed experiments to estimate RRP size using both methods in each cell. From our previous results (Fig. 3.2C) we knew that the response to a single AP in $250 \mu\text{M}$ 4-AP with 4 mM external Ca^{2+} would only be a slight ($\sim 7\%$) underestimate of the RRP size determined by fitting a generalized Hill model to the entire release curve. Therefore, in each of these experiments we began with the 100 Hz protocol and then applied 4-AP to estimate RRP size using single AP responses. Figure 3.4A shows an example of a neuron where we used both protocols and obtained a close correspondence between the different estimates. This observation was true across many cells (Fig. 3.4B) such that the two estimates of RRP size were not significantly different from each other ($5.1 \pm 0.8\%$ vs. $5.5 \pm 0.9\%$ for single AP and 100 Hz burst protocol respectively, $P=0.23$ in two tailed paired t-test, $n=8$). This confirms the validity of our protocols for measuring RRP size.

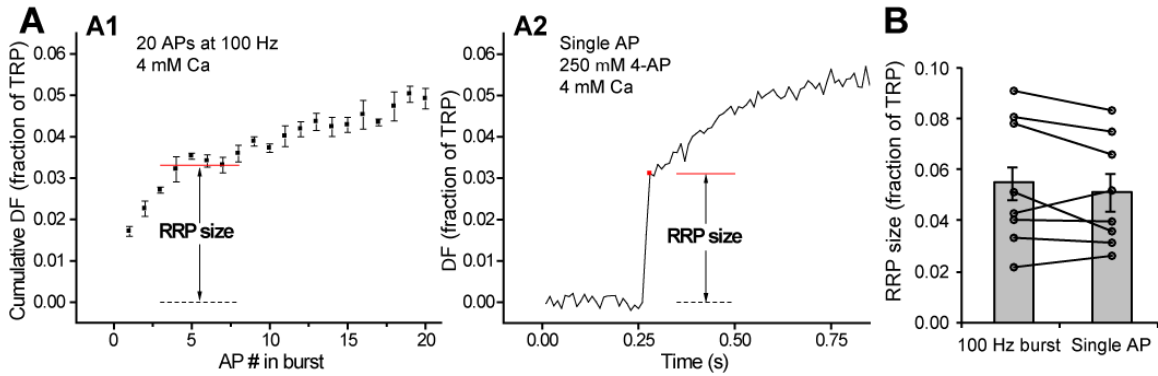


Figure 3.4. Different estimates of RRP size are consistent. **(A)** Example of a neuron (average of 30 synapses) where both methods were used to estimate RRP size (n=4 trials for **(A1)**, n=5 trials for **(A2)**). Note that the vertical scale on both graphs is the same. **(B)** RRP size determined from single APs in the presence of 250 μM 4-AP and 4 mM external Ca^{2+} agrees with estimates from 100 Hz bursts (n=8 cells).

3.5 Estimation of \mathbf{P}_v

Having confirmed that we had reliable methods to estimate RRP size, we could use them to calculate \mathbf{P}_v by measuring responses to 1 AP under standard conditions (2 mM external Ca^{2+}). Figure 3.5A shows results from a single neuron that exemplifies the procedure. By measuring the response to a single AP (Fig. 3.5A1) and then dividing it by the estimate of RRP size obtained with the 100 Hz protocol (Fig.3.5A2), we estimated \mathbf{P}_v for that neuron.

Extending this procedure to many cells, we found $\mathbf{P}_v = 0.10 \pm 0.01$ (n=32 cells). Interestingly, as with RRP size, \mathbf{P}_v was quite variable between cells (Fig. 3.5B, range=0.01 to 0.25).

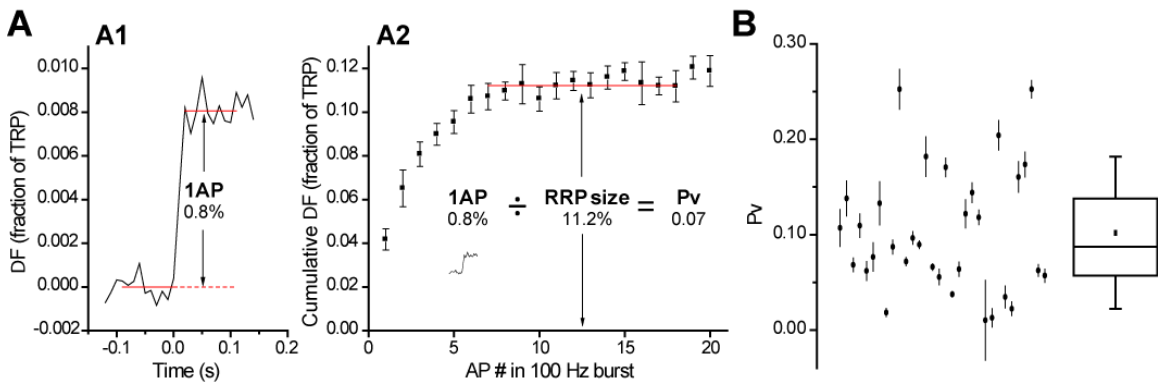


Figure 3.5. P_v varies over a wide range across cells. **(A)** Procedure for determining a neuron's P_v requires a measurement of the response to 1 AP (**A1**, $n=20$ trial average, 12 synapses) and an estimate of the RRP size (**A2**, $n=4$ trial average). Values within each panel are in % of TRP. The trace from **A1** was scaled down 10-fold in the inset in **A2** to be at the same vertical scale as the 100 Hz burst measurement. **(B)** P_v determined with this protocol in 32 cells (see Materials and methods for explanation of error bars). Box whisker plot shows the median (line), mean (point), 25-75 percentile (box) and 10-90 percentile (whisker) ranges

3.6 Discussion

We present here methods to provide optical measures of P_v and RRP size at synapses from neurons expressing vG-pH. Our measurements showed that ~6-7% of all the releasable vesicles in a synapse are in a primed state, ready to fuse in response to an action potential with 0.10 average probability.

An unexpected finding when developing protocols to measure the RRP size was the lack of strong depression in response to 20 or 40 Hz stimulation under both standard (2 mM) and high (4 mM) external Ca^{2+} conditions. We initially tested these protocols due to reports in the literature that use short 20 Hz bursts to deplete the RRP in neurons in culture (Murthy and Stevens, 1998; Stevens and Williams, 2007). These reports are based

on postsynaptic electrophysiological voltage clamp recordings of relatively young (5-15 days after plating) hippocampal neurons grown in culture. Early experiments (Murthy and Stevens, 1998) measured the amplitude of excitatory post synaptic currents (EPSCs) which depressed substantially during 2 s of 20 Hz stimulation. However, the use of EPSC amplitude to study depression during a stimulus will only include release that occurs synchronously, excluding asynchronous exocytosis which occurs between APs in the train, therefore underestimating the total amount of release. It is worth noting that our time resolution is such that the optically measured stimulus-locked exocytosis will include both synchronous and asynchronous components as defined above. A more recent study that takes into account this effect and measures cumulative charge (which will include both the synchronous and asynchronous component) shows much less depression during a 20 Hz, 80 AP train (Figure 5B in Stevens and Williams, 2007). Work from another group using similar methods shows clearer evidence of depression during a 2 s, 20 Hz train (Figure 1 in Moulder and Mennerick, 2005). However, in experiments performed in the presence of the rapidly dissociating AMPA receptor antagonist kynureate (therefore unaffected by AMPA receptor saturation) there was considerably less depression (Figure 6B in same paper), suggesting a postsynaptic contribution to the phenomenon. Due to the comparatively weak depression in both recent papers, the authors had to apply a substantial correction for ongoing refilling of the RRP during stimulation to estimate RRP size. Another consideration is that previous experiments were often performed at a lower temperature (room temperature was $\sim 22^{\circ}\text{C}$ in Stevens and Williams, 2007) than our 20 & 40 Hz experiments (30°C). Higher temperatures have been shown to lower release probability and increase the RRP refilling rate (Pyott and

Rosenmund, 2002) predicting less depression in our experiments. Finally, a recent study measured responses to 40 APs at 20Hz using synaptophysin-pHluorin 2X and the results are similar to those shown here, with little evidence of depression (Supplementary Figure 2E in Matz et al., 2010). In summary, upon closer inspection our lack of clear depression at 20 and 40Hz is not as surprising as it initially seemed to be.

The estimates we present for P_v (0.10) and RRP size (~6-7% of the TRP) are consistent with values reported in the literature for dissociated hippocampal neurons in culture. It was shown previously that there are 64 ± 14 vesicles labeled with vG-pH in the TRP and that most of the vesicles in the synapse are labeled for the transfection conditions and age of cultured neurons used here (Balaji and Ryan, 2007). We therefore estimate that, on average, the RRP corresponds to ~3-5 vesicles, a number similar to the number of docked vesicles observed by electron microscopy in hippocampal synapses in culture (4.6 ± 3.0 in Schikorski and Stevens, 1997). Given this number of vesicles in the RRP, if each has a P_v of 0.1 this indicates that sparse stimulation with single APs causes hippocampal synapses from rat neurons in primary culture to release, on average, 1 vesicle every 3 APs in standard conditions, ($Pr \sim 0.3-0.4$ from equation 1.2) which is consistent with previous estimates (Murthy et al., 1997; Granseth et al., 2006; Branco et al., 2008). The same kind of analysis suggests that under standard conditions multivesicular release is infrequent (probability of releasing 2 or more vesicles ~0.03-0.08). However, if P_v is large enough (for example, in the presence of 4-AP) a single action potential will cause multiple vesicles present in the RRP to exocytose. At the moment, our time resolution is limited to 10 ms so we do not know in detail the temporal

coupling between an action potential firing and the exocytosis of several vesicles under conditions of high P_v .

The sigmoidal relationship between P_v and Ca^{2+} entry, with standard conditions situated quite low on the curve highlights how small changes in Ca^{2+} entry can lead to large effects on baseline P_v . These changes in P_v will cause even greater shifts in P_r (using our estimate of $n=4$ vesicles in equation (1.2), Fig. 3.6) illustrating how forms of modulation that regulate Ca^{2+} entry even slightly can sharply modify synaptic efficacy.

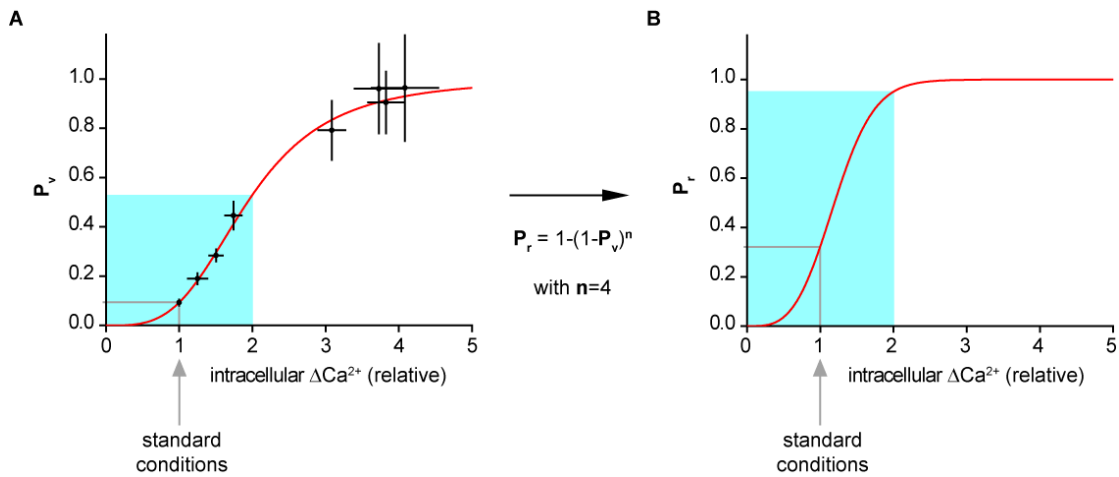


Figure 3.6. Synapses are in range very responsive to changes in Ca^{2+} . **(A)** Estimate of P_v as a function of intracellular Ca^{2+} increases in response to 1 AP (from Fig. 3.2.C). **(B)** Using equation 1.2 and an estimate of the RRP size of 4 vesicles we can calculate the relation of P_r to increases in intracellular Ca^{2+} . Light blue shading in (A) and (B) indicates region where Ca^{2+} entry can be modulated from 0 to 2-fold of normal, with corresponding effects on P_v and P_r . Note the steeper dependence of P_r on Ca^{2+} around the standard conditions region (2 mM extracellular Ca^{2+}).

Interestingly, we noted considerable variability in both P_v and RRP size between cells (Figs. 3.3E, 3.5B). This was somewhat surprising given that we used a relatively homogenous population of neurons cultured from the CA3-CA1 region of the rat hippocampus. It is unknown whether this variability is characteristic of this brain region or a consequence of the *in vitro* growth conditions of the neurons. Measuring P_v and RRP size in cultured neurons prepared from other brain regions and/or cell types might provide some insights into this issue.

Our methods should be widely applicable to study factors that affect P_v and RRP size. By design, they cannot be used to study q and are limited to less temporal resolution and sensitivity than electrophysiological methods. However, because they are restricted to presynaptic properties they avoid complications such as receptor saturation and desensitization inherent in studying presynaptic properties based on a postsynaptic readout (Xu-Friedman and Regehr, 2004). Furthermore, in contrast to electrophysiological studies in culture, they are not affected by changes in the number of synaptic contacts since measurements come from averages -not sums- across synapses. In the chapters that follow we use these methods to examine the role of tomosyn in exocytosis (Chapter 4) and extend the techniques to study properties of exocytosis at the level of single synapses (Chapter 5).

4. TOMOSYN

Having developed methods to measure key presynaptic parameters of synaptic vesicle exocytosis (Chapter 3), we turned our attention to tomosyn, a molecule that might control P_v and/or n . As described in the introduction to this thesis, tomosyn is a particularly interesting candidate for study. It interacts directly with the fusion machinery in synaptic vesicles and, in addition, is one of the few proteins known to exercise a negative control on synaptic efficacy (Ashery et al., 2009). However, the exact mechanisms by which it performs this function are not clear. Thus, we set out to explore this in detail using our new methods.

4.1 Knockdown of tomosyn in hippocampal neurons

To study the effect of tomosyn on exocytosis properties, we used a knockdown approach, cotransfecting primary hippocampal neurons in culture with the vG-pH reporter and an shRNA targeted against tomosyn-1 (based on Cheviet et al., 2006). This reduced tomosyn levels at neuronal somas by an average of 55%, though there was considerable variation in knockdown efficacy between individual cells (Fig. 4.1). The polyclonal antibody we used to detect tomosyn can also recognize tomosyn-2 (Reinhard Jahn, personal communication), yet our shRNA specifically targeted tomosyn-1. Therefore, the remaining tomosyn detected by immunostaining might be tomosyn-2, a poorly characterized isoform that appears to be somatically and postsynaptically localized in CA2 cells of the hippocampus (Barak et al., 2011). Alternatively, we wondered if the

shRNA we used was simply inefficient and whether a different shRNA might lead to more knockdown. However, our attempts using another previously validated knockdown sequence (based on Sakisaka et al., 2004) gave similar results ($46\pm 4\%$ knockdown, $n=38$). In what follows, we characterized neurons where tomosyn levels were reduced using the knockdown sequence developed by Cheviet et al., 2006.

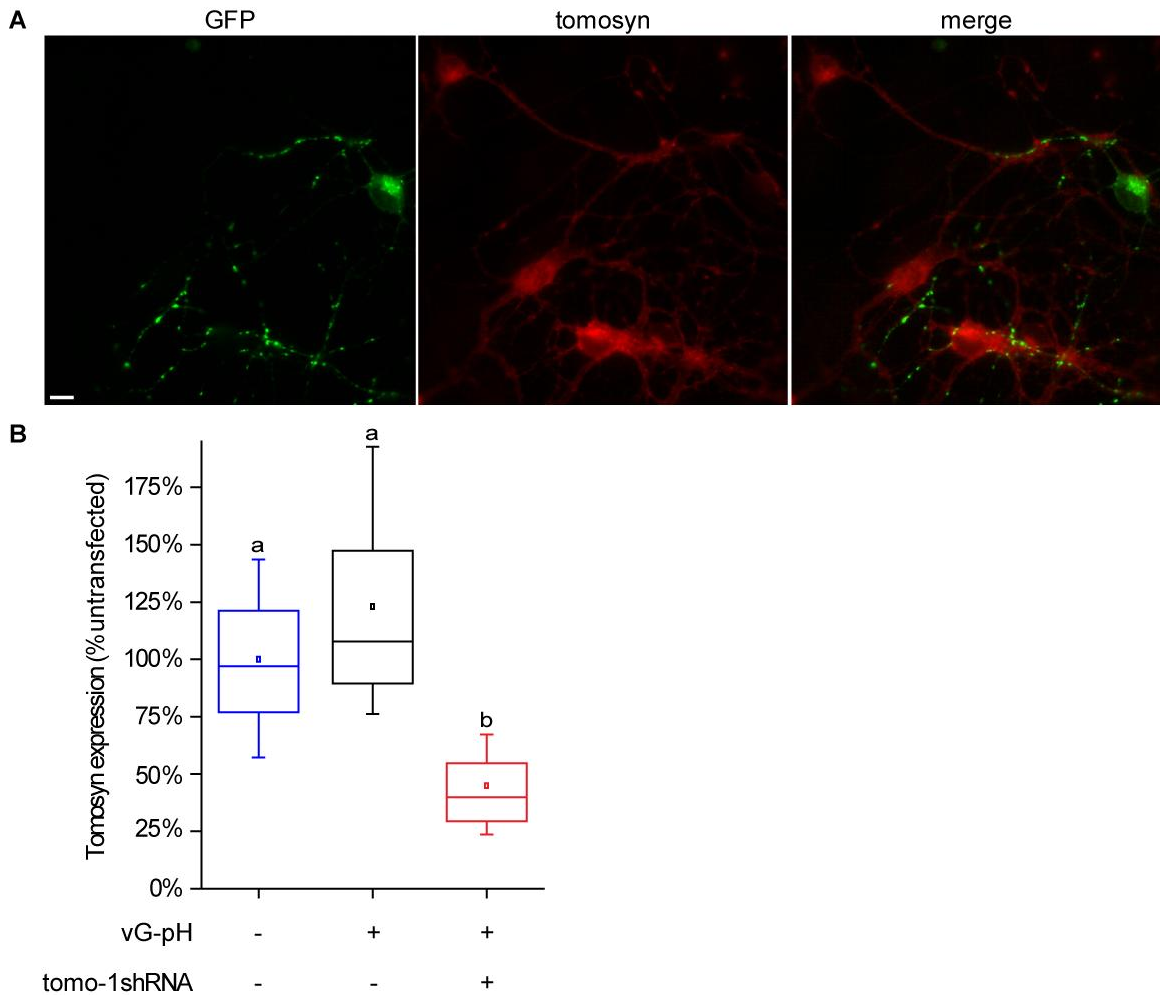


Figure 4.1. shRNA targeting tomosyn-1 leads to partial reduction of tomosyn levels in hippocampal neurons. **(A)** Hippocampal neurons in culture transfected with both vG-pH and tomosyn shRNA. Neurons were stained with anti-GFP (green), which recognizes vG-pH, and anti-tomosyn (red). Note the transfected neuron with a noticeable reduction in somatic tomosyn compared to untransfected cells. Scale bar = 10 μ m. **(B)** Neurons transfected with shRNA targeting tomosyn-1 had reduced levels of tomosyn staining in their cell bodies ($45\pm 2\%$, $n=90$) compared to untransfected neurons ($100\pm 1\%$, $n=528$) or those transfected solely with vG-pH ($123\pm 15\%$, $n=12$). Different letters above whiskers indicate groups that are significantly different ($P<0.05$) from each other using Kruskal-Wallis multiple comparisons.

4.2 Effects of tomosyn knockdown on synaptic efficacy

In spite of reducing tomosyn levels only partially, we studied a subset of these neurons (tomosyn level= $35\pm 6\%$, $n=10$, range: 10-72%) with our protocols and noticed several interesting effects. Neurons with reduced levels of tomosyn showed larger responses to single APs compared to controls (Fig. 4.2A). Using our previously developed protocols, we probed whether this change was due to a modification in n or P_v . Our results showed that, while RRP size was unchanged (Fig 4.2B), P_v rose significantly under both standard (2 mM) and elevated (4 mM) extracellular Ca^{2+} ion concentrations (Figs. 4.2C). We reasoned that if the probability of a primed vesicle fusing in response to 1AP (P_v) had increased, this might affect short term plasticity properties, as a stimuli would lead to a larger depletion of the RRP. Indeed, when we stimulated with 2 APs spaced 250ms apart, the paired pulse ratio (PPR) was smaller when tomosyn levels were reduced, consistent with a larger depletion of the RRP (Fig. 4.2D).

Figure 4.2. Reduction in tomosyn concentration increased P_v and modified short term plasticity. **(A) Top:** Examples of single AP response in individual experiments, averaged over 10 trials (n= 19 and 5 synapses for control and tomo-1 shRNA respectively). Responses are normalized to the total number of labeled synaptic vesicles, determined by NH_4Cl application (see Chapter 2.2). Scale bar: 0.25% of NH_4Cl , 0.1s. **Bottom:** Increase in the response to 1 AP with reduced tomosyn levels (control: $0.4\pm 0.1\%$, n=17; tomo-1 shRNA: $0.55\pm 0.08\%$, n=10; $P=0.04$, Mann-Whitney U test). Responses were normalized to the total pool of vesicles in the terminal, determined with a brief pulse of solution containing NH_4Cl , buffered at pH=7.40 (see Chapter 2). **(B)** No change in the size of the RRP in the presence of tomo-1 shRNA (control: $7.5\pm 0.6\%$, n=38; tomo-1 shRNA: $7.7\pm 0.6\%$, n=10; $P=0.27$, Mann-Whitney U test). **(C)** P_v increases when tomosyn is reduced by shRNA. P_v increased when measured at 2 mM (control: 0.10 ± 0.01 , n=40; tomo-1 shRNA: 0.16 ± 0.02 , n=10; $P=0.009$, ANOVA) or 4 mM (control: 0.34 ± 0.02 , n=38; tomo-1 shRNA: 0.46 ± 0.04 , n=10; $P=0.008$, ANOVA) extracellular Ca^{2+} ion concentration. **(D) Top:** Examples of paired pulse runs in individual experiments, averaged across 10 trials each (n=31 synapses for both control and tomo-1 shRNA). Both traces are normalized to the response to the first AP. Scale bar: 50% of response to first AP, 0.1s. **Bottom:** Change in short term plasticity as a consequence of tomosyn-1 knockdown. The ratio of a 2nd AP response to one delivered 250ms prior was reduced in the presence of the tomo-1 shRNA (control: 0.77 ± 0.07 , n=37; tomo-1 shRNA: 0.45 ± 0.09 , n=9; $P=0.01$, Mann-Whitney U test). * indicates $P<0.05$ in statistical comparison.

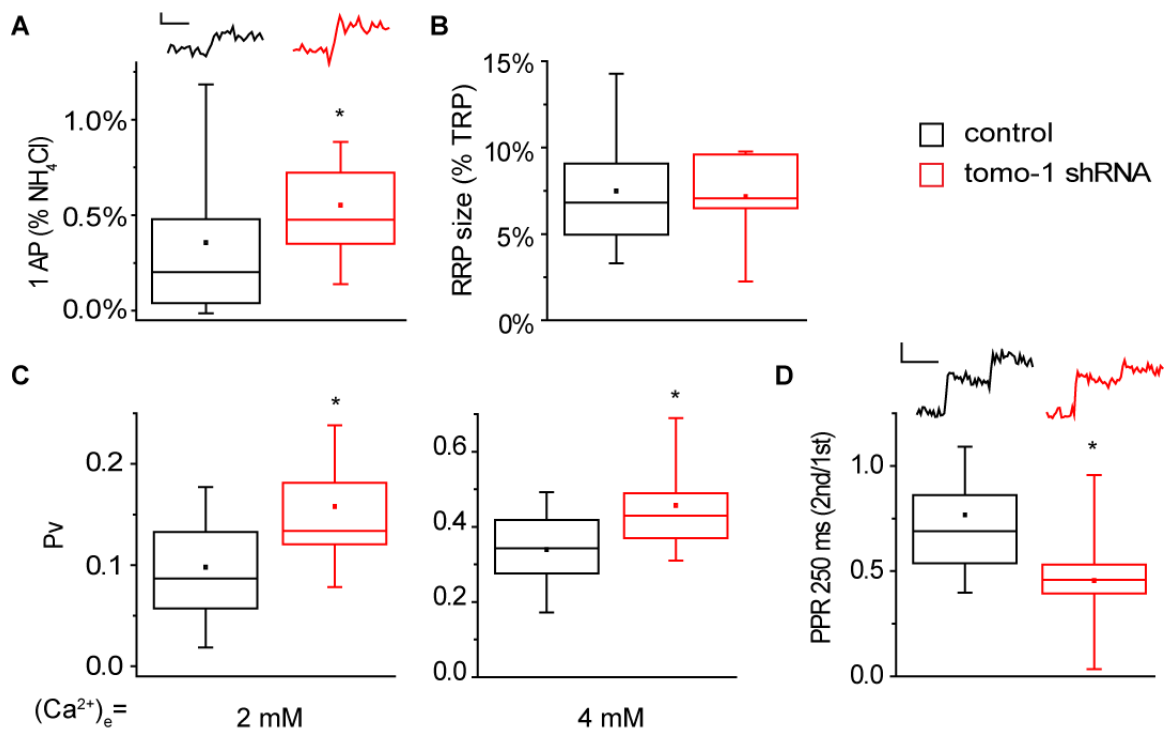


Figure 4.2

Given that responses to single APs were modified when tomosyn was reduced and that short term plasticity was affected, we wondered if there would also be effects on larger stimuli. Strikingly, the amplitude of the response to 100 APs delivered at 10 Hz was not different from control (Fig. 4.3A). If anything, it was *lower* in the knockdown, though the trend was not statistically significant. To further probe the responsiveness to large stimuli, we examined exocytosis in response to 1500 APs at 10 Hz, delivered in the presence of bafilomycin (Baf). Since Baf is a proton pump inhibitor, the alkalinization of a vesicle once it fuses with the membrane will be irreversible and the rise in fluorescence during stimulation will reflect only exocytosis (see Figure 3.1B for an example). Therefore, fitting this rise to a monoexponential process can be used to extract a time constant that will be partially determined by exocytosis properties and partially by vesicle reuse. Consistent with results for a 100 APs stimulus, the time constant in response to 1500 APs at 10 Hz did not differ between knockdown cells and control (Fig. 4.3B). Thus, while a reduction in tomosyn concentration leads to a modification of synaptic efficacy at the level of individual or paired APs, larger stimuli do not seem to be affected.

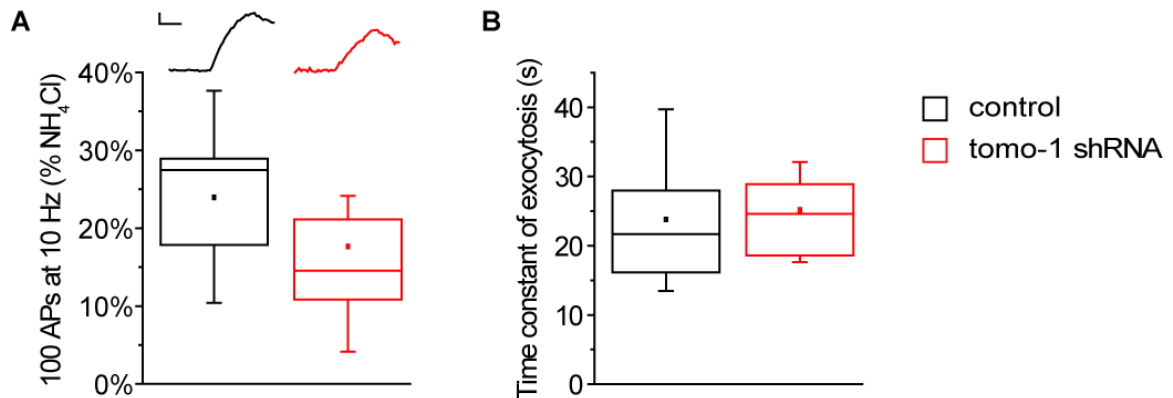


Figure 4.3. Reduction in tomosyn concentration had no effect on exocytosis in response to strong stimuli. **(A)** *Top:* Examples of responses to 100 APs at 10 Hz in individual experiments (n=16 synapses for both control and tomo-1 shRNA). Scale bar: 5% of NH₄Cl, 5s. *Bottom:* Response to 100 APs delivered at 10 Hz. (control: 24±3%, n=13; tomo-1 shRNA: 18±3%, n=10; P=0.18, ANOVA) **(B)** Time constant of exocytosis, measured in the presence of Baf, in response to 1500 APs at 10 Hz. (control: 24±2s, n=27; tomo-1 shRNA: 25±2s, n=8; P=0.19, Mann-Whitney U test).

4.3 Does PKA phosphorylation of tomosyn play a role in synaptic transmission?

Tomosyn contains a phosphorylation site for protein kinase A (PKA) that inhibits its ability to substitute for synaptobrevin in SNARE complexes (Baba et al., 2005) but at the same time may also enhance the β -propeller domains' ability to oligomerize SNARE complexes (Sakisaka et al., 2008). On the basis of these reports, we wondered whether the effect on exocytosis of increasing the amount of cAMP would be modified with reduced levels of tomosyn. In particular, we studied the effects of forskolin, a compound known to increase cAMP concentration through its action on adenyl cyclase (Insel and Ostrom, 2003). As expected from previous reports (Kaneko and Takahashi, 2004; Huang and Hsu, 2006; Gekel and Neher, 2008), incubation of neurons with forskolin led to increased responses to single AP stimuli (Fig. 4.4). However, neurons with reduced levels

of tomosyn (tomosyn level= $44\pm 10\%$, $n=4$, range: 25-62%) did not differ from control in their responsiveness to forskolin application. If anything, there was a trend in the opposite direction, though it did not reach statistical significance, possibly due to the few cells assayed. Thus, the concentration of tomosyn does not seem to be a rate limiting factor for the effects of an elevation in cAMP concentration in nerve terminals.

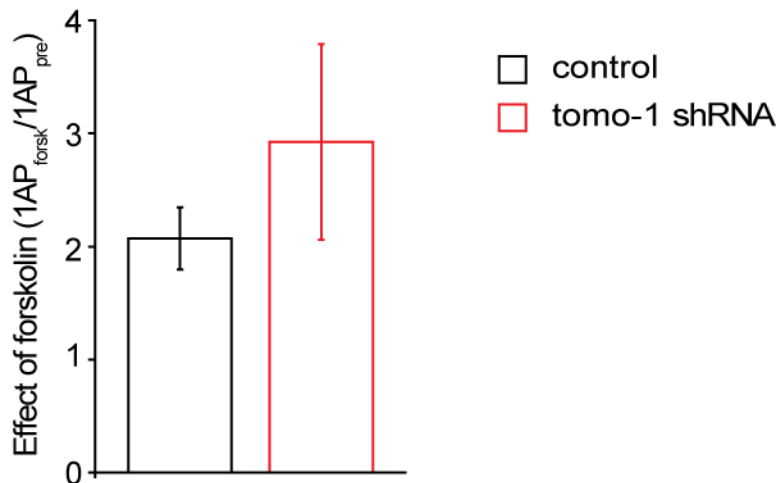


Figure 4.4. The effect of forskolin on responses to single APs was not altered in the presence of tomosyn-1 shRNA. Forskolin effects are calculated as the ratio of the response to 1 AP *after* forskolin treatment (50 mM, 10min preincubation) to the response to 1 AP *before* treatment (control: 2.1 ± 0.3 , $n=11$; tomo-1 shRNA: 2.9 ± 0.9 , $n=4$; $P=0.36$, Mann-Whitney U test).

4.4 Unsuccessful attempt to rescue effects of shRNA

To rule out that the phenotype of the tomosyn knockdown was a consequence of off-target effects of the shRNA (Alvarez et al., 2006) we took a rescue approach. To this end, we generated an N-terminal HA tagged version of mouse tomosyn-1 isoforms (HA-tomo-1) and cotransfected vG-pH, HA-tomo-1 and tomo-1 shRNA. Rat and mouse tomosyn-1 are sufficiently different at the RNA level such that the shRNA, designed against rat tomosyn-1, does not target our rescue construct. Ideally, a neuron with vG-pH, tomo-1 shRNA and HA-tomo-1 should have tomosyn levels indistinguishable from wild type. However, our triple transfection strategy did not always lead to successful rescue of tomosyn levels. This seems to be a technical limitation of our transfection procedure, and has been seen with other rescue constructs in our lab (unpublished observations). To avoid skewing our analysis of exocytosis properties, we only included neurons where tomosyn levels were at least 75% of adjacent untransfected cells, as determined by *post hoc* staining (9/20 cells were excluded). In this subset of neurons, tomosyn levels were near wild type (average =114±11%, n=11, range: 76-193%), and we used these cells as our rescue group.

Surprisingly, none of the single or paired AP exocytosis properties of the rescue differed significantly from the knockdown (Fig. 4.5A-D, knockdown vs. rescue comparisons all had $P>0.1$ in cases with differences between groups). For parameters where the knockdown group differed from controls, the rescue mimicked the knockdown, though control vs. rescue comparisons did not always reach statistical significance at the $\alpha=0.05$ level. In addition, rescue cells were less responsive to both 100 AP and 1500 AP bursts at 10 Hz than controls, though they did not differ significantly from knockdowns

(Fig. 4.5E-F). These results indicate the either the rescue construct used was ineffective or that the phenotypes seen in Figures 4.2 and 4.3 are mediated by non-specific effects of the shRNA. In any case, the absence of a convincing rescue of the tomosyn-1 knockdown renders our conclusions on the effects of tomosyn-1 on exocytosis preliminary.

Figure 4.5. Rescue of tomosyn levels with HA-tagged tomosyn-1 did not revert the effects of tomosyn-1 knockdown. Control and tomo-1 shRNA data taken from Figures 4.2 and 4.3. **(A)** Response to 1 AP (control: $0.4 \pm 0.1\%$, n=17; tomo-1 shRNA: $0.55 \pm 0.08\%$, n=10; rescue: $0.5 \pm 0.2\%$, n=11; P=0.09, Kruskal-Wallis). **(B)** RRP size (control: $7.5 \pm 0.6\%$, n=38; tomo-1 shRNA: $7.7 \pm 0.6\%$, n=10; rescue: $6.3 \pm 0.9\%$, n=10; P=0.58, Kruskal-Wallis). **(C)** P_v at 2 mM (control: 0.10 ± 0.01 , n=40; tomo-1 shRNA: 0.16 ± 0.02 , n=10; rescue: 0.15 ± 0.03 , n=11; P=0.01, ANOVA) and 4 mM (control: 0.34 ± 0.02 , n=38; tomo-1 shRNA: 0.46 ± 0.04 , n=10; rescue: 0.47 ± 0.05 , n=11; P=0.004, ANOVA) extracellular Ca^{2+} ion concentration. **(D)** PPR at 250ms (control: 0.77 ± 0.07 , n=37; tomo-1 shRNA: 0.45 ± 0.09 , n=9; rescue: 0.7 ± 0.2 , n=10; P=0.008, Kruskal-Wallis). **(E)** Response to 10 APs delivered at 10 Hz (control: $24 \pm 3\%$, n=13; tomo-1 shRNA: $18 \pm 3\%$, n=10; rescue: $15 \pm 1\%$, n=10; P=0.06, ANOVA). **(F)** Time constant of exocytosis, measured in the presence of Baf, in response to 1500 APs at 10 Hz (control: $24 \pm 2s$, n=27; tomo-1 shRNA: $25 \pm 2s$, n=8; rescue: $36 \pm 6s$, n=10; P=0.03, Kruskal-Wallis). # and * indicate P<0.1 or <0.05 respectively in statistical comparison with control group.

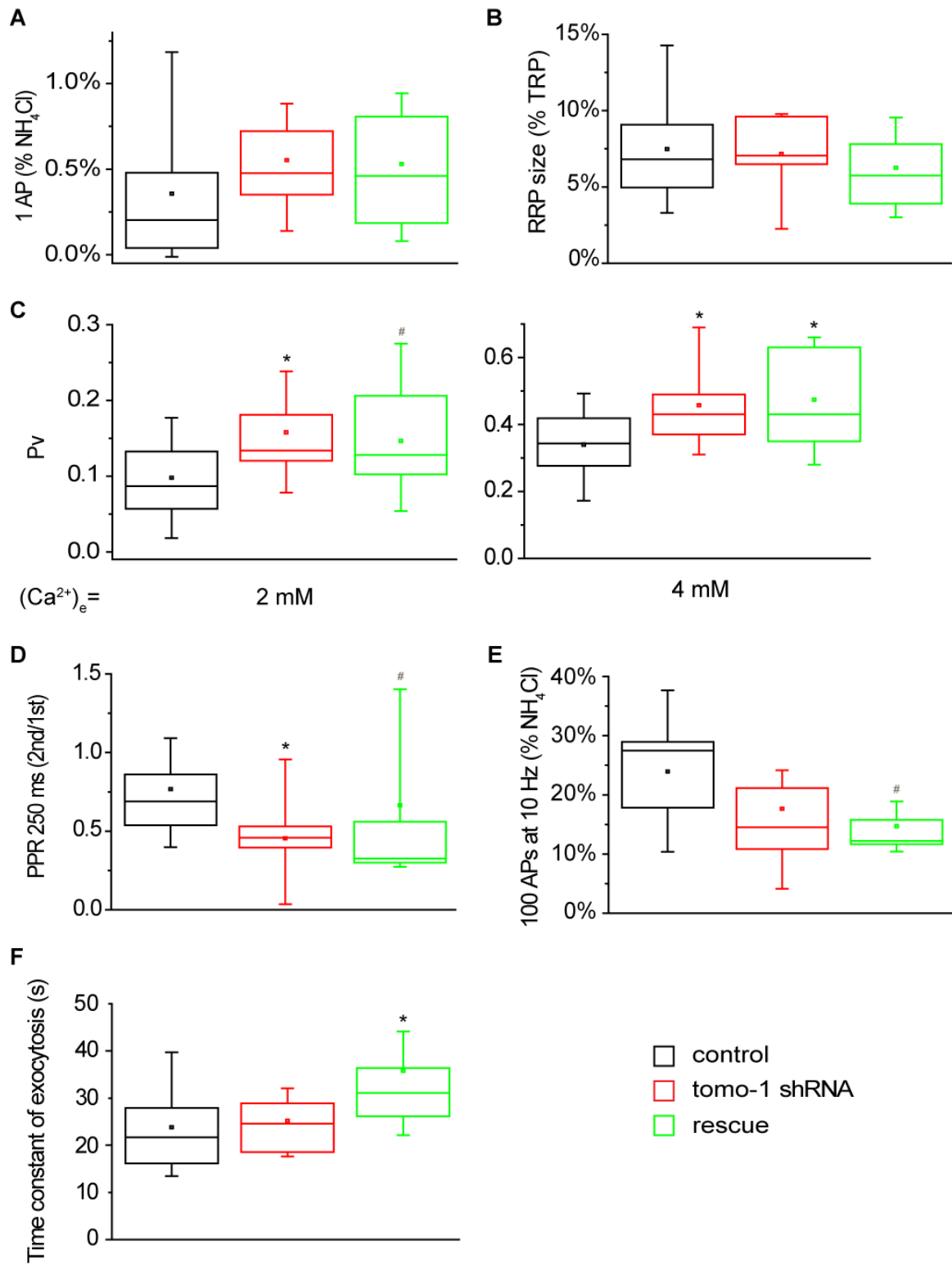


Figure 4.5

4.5 Discussion

Our analysis of the function of tomosyn-1 in exocytosis must be qualified by the fact that our attempt to rescue the effects of the knockdown was unsuccessful.

In the worst case scenario, the failed rescue would imply that the effects of the knockdown construct are actually not a consequence of the reduction in tomosyn-1 concentration (Jackson and Linsley, 2010). However, it is equally possible that the rescue construct was ineffective and it is worth considering a few alternative scenarios in which this is the culprit. We will first discuss why the rescue might have been unsuccessful and then examine the knockdown results assuming they are not a consequence of off-target interactions of the tomo-1 shRNA.

The construct used to rescue the knockdown was an N-terminal, HA tagged mouse tomosyn-1, isoform s. There are several reasons why it might have been ineffective in supplanting the functions of endogenous rat tomosyn-1.

It is possible that the type of tag used and/or its location on the protein led to problems in folding, trafficking or function. The design of our rescue construct was based on previous reports that showed effects on exocytosis in bovine chromaffin cells when overexpressing mouse tomosyn-1 (isoform s) tagged with GFP or CFP (Yizhar et al., 2004; Yizhar et al., 2007) on the N-terminus. To minimize potential disruptions of tomosyn function, we used a smaller tag (HA, 9 amino acids long) instead of a fluorescent protein, though we kept the N-terminal position. Major disruptions in the folding of tagged tomosyn-1 seem unlikely because the rescue protein could still be identified in immunostaining of neuronal somata. Unfortunately, we could not measure clear tomosyn signals at individual presynaptic boutons in control, knockdown or rescue

conditions with our antibody. Thus, we cannot rule out the possibility of a trafficking defect in HA-tomo-1. It is worth noting that the overexpression results in chromaffin cells were obtained under conditions where tomosyn levels were 13-fold above wild type (Yizhar et al., 2004). Even if the tagged tomosyn used therein was less efficient in its trafficking or function, the sheer amount of protein might be sufficient to lead to functional consequences, despite a lower efficacy. To circumvent the potential problems inherent in tagging tomosyn-1 we attempted to develop an untagged version of tomosyn for rescue. Unfortunately, we could not reliably calibrate the transfection procedure to obtain enough cells with tomosyn levels in the wild type range for statistical analysis (only 2/15 cells had tomosyn levels in the 75-200% range).

Another thing to keep in mind is that we attempted to rescue a reduction in rat tomosyn-1 with mouse tomosyn-1 isoform s. It is possible that the few amino acid differences between mouse and rat tomosyn-1 isoform s are responsible for a reduced efficacy of the rescue protein in the context of a rat neuron. This seems unlikely given the 98% sequence identity between the mouse tomosyn-1 isoform s and the equivalent rat tomosyn-1 isoform m. Of the 19 amino acid differences only 7 are non-conservative and these are distributed in unstructured loops or between the blades of the β -propellers' structure. However, while the sequence difference seems unlikely to cause the lack of cross-species rescue, we cannot definitively exclude this possibility. An additional consideration is that we rescued with only one splice isoform but tomosyn-1 has three, all of which were targeted by our shRNA. While the isoform we used is the most abundant one in brain extracts (Yokoyama et al., 1999), that might not be true in the specific subset of cells from the hippocampal CA regions we studied in culture. It could be the case that

the stoichiometry of appropriate isoforms is critical for tomosyn-1 function. While the mouse tomosyn-1 isoform used was able to produce effects when overexpressed in a bovine chromaffin cell (Yizhar et al., 2004), the same caveat regarding the high concentration mentioned above applies to any inferences regarding the cross-species and isoform-specific efficacy.

Despite these possibilities, there is no escaping that any firm conclusions regarding the role of tomosyn in synaptic vesicle exocytosis require a demonstration of successful rescue of the effects of the knockdown. Thus, the discussion of our results that follows is necessarily preliminary and assumes there were no non-specific effects of the knockdown.

An interesting aspect of our results was that reducing tomosyn concentration affected only responses to single or paired AP, but not responses to larger bursts. This indicates that modifications in single AP responses do not always translate to bigger stimuli, highlighting how a neuron could control how it “whispers” independently of how it “shouts,” effectively uncoupling different operating regimes.

As regards the increased responsiveness to single APs, it is worth considering what caused the increase in P_v (Fig. 4.2C). As noted in the introduction to this thesis, effects on P_v could be due to changes in local Ca^{2+} or fusion willingness. The latter seems a particularly attractive possibility on the basis of what is known about tomosyn. Since tomosyn can compete with synaptobrevin to form SNARE complexes, it is possible that the average number of SNARE complexes per primed synaptic vesicle increases when the amount of tomosyn goes down. Given that fusion willingness is proportional to the number of *trans*-SNARE complexes per vesicle (Mohrmann et al., 2010), this would be a

potential mechanism to explain the effects of tomosyn concentration on \mathbf{P}_v . The oligomerization of *cis*-SNARE complexes by the β -propeller domains could also inversely link the availability of SNAREs for fusion-competent complexes and the concentration of tomosyn. Additionally, tomosyn's interaction with synaptotagmin could affect fusion willingness or potentially, local Ca^{2+} through coupling of vesicles to Ca^{2+} channels (Young and Neher, 2009).

In contrast to our results, previous reports from *C. elegans* mutants (Gracheva et al., 2006; McEwen et al., 2006) and bovine chromaffin cells (Yizhar et al., 2004) uncovered only differences in RRP size, but no effects that could be interpreted as modifications in \mathbf{P}_v . There are many differences between these studies and our own including the species, synapse or cell type, concentration range of tomosyn and the assays used. As illustrated above and in the introduction changes of both \mathbf{P}_v and RRP size can be explained in terms of modified SNARE availability. In a simple model, vesicles with at least one *trans*-SNARE complex formed would be fusion competent (van den Bogaart et al., 2010) and therefore primed, whereas any change in the number of *trans*-SNARE complexes per vesicle would affect fusion willingness (Mohrmann et al., 2010). However, it is not clear in this scenario how changes in SNARE availability in a range that affected the number of primed vesicles (those with at least one *trans*-SNARE complex) would not also modify the average number of *trans*-SNARE complexes per vesicles, and thus \mathbf{P}_v . Clearly, more experiments are needed to understand these discrepancies and refine models of tomosyn function.

As regards the potential modulation of tomosyn function by PKA, our results were inconclusive. We found that there was no difference between control and shRNA

transfected neurons, indicating that tomosyn levels in the range explored are not rate-limiting for the expression of the effects of raising cAMP. Perhaps stronger reductions of tomosyn concentrations would uncover an effect. In addition, it is worth pointing out that forskolin-induced rises in cAMP not only stimulate PKA but also the alternative target Epac, a guanine nucleotide exchange factor for the small G protein Rap. It is unclear what fraction of the resulting effects are channeled through the latter pathway in our culture system (for other systems see Kaneko and Takahashi, 2004; Huang and Hsu, 2006; Gekel and Neher, 2008).

In conclusion, our study, while tentative, adds interesting results to a growing body of literature on tomosyn's role in synaptic transmission. Mainly, we see that subtler modifications of tomosyn levels than reported previously can lead to effects on P_v without modifying the RRP size. Furthermore, despite our difficulties with the rescue construct, these results illustrate the utility of the methods we have developed to study the molecular underpinnings of synaptic vesicle exocytosis.

5. EXOCYTOSIS PROPERTIES OF SINGLE SYNAPSES

In the experiments presented so far, we explored average properties across ensembles of synapses. However, synapses can behave very differently, even if they belong to the same axon (Chapter 1.5). Thus, we wished to go beyond ensemble averages and study potential molecular determinants of \mathbf{P}_v and \mathbf{n} at the level of individual synapses. To that end, we set out to expand the applicability of our methods (Chapter 3).

5.1 General measurement considerations

To obtain reliable estimates of \mathbf{P}_v and \mathbf{n} at individual synapses, we had to overcome two main challenges: statistical fluctuations and measurement noise.

The first issue to consider when measuring responses from individual synapses is that potentially large statistical fluctuations are expected from a binomial process with a relatively low \mathbf{P}_v and \mathbf{n} . Our experiments consist of several trials where the stimulus is a single AP. These responses are averaged for each synapse and compared to the corresponding estimate of \mathbf{n} , giving a measure of \mathbf{P}_v . If we assume that a binomial process with parameters \mathbf{P}_v and \mathbf{n} fully describes the behavior of a synapse during this kind of experiment, we can ask how much the *measured* \mathbf{P}_v will fluctuate around the *real* \mathbf{P}_v . The relative size of those fluctuations will depend on \mathbf{P}_v , \mathbf{n} , and the number of trials in the experiment. The expected CV in an estimate of \mathbf{P}_v will be (see Appendix for derivation):

$$CV = \sqrt{\frac{(1 - \mathbf{P}_v)}{k \cdot \mathbf{P}_v \cdot \mathbf{n}}} \quad (5.1)$$

Note that these fluctuations are unavoidable and would be present even if using an idealized detection system without any noise. The only option to minimize their effect is to perform as many trials as possible. For example, an experiment to estimate \mathbf{P}_v in single synapses with an expected CV of 15% would require 100 trials, assuming $\mathbf{P}_v=0.1$ and $\mathbf{n}=4$ (our averages under standard conditions, see Chapter 3). Obtaining such a large number of measurements is problematic because it requires long experiments and total cumulative exposures to laser illumination that tend to be detrimental to cell health. By extension, it is doubly difficult to execute a baseline measurement, follow it with a pharmacological application and measure the effect of that intervention. Furthermore, because our calculation only illustrates the CV of an *average* synapse, we expect many measurements -in lower \mathbf{P}_v synapses- to be subject to larger fluctuations. For all of these reasons, we chose to increase the concentration of extracellular Ca^{2+} ions to 4 mM. Based on Figure 3.2C, this will raise \mathbf{P}_v to 0.35. Using equation 5.1, to measure \mathbf{P}_v with an expected CV of 15% under these conditions requires only 21 trials. This allows shorter experiments where maintaining cell viability is not as challenging. While we are aware that this increase in extracellular Ca^{2+} ion reduces the applicability of our conclusions, we consider it a necessary tradeoff in order to obtain reliable measurements of \mathbf{P}_v at single synapses.

The second challenge when attempting to estimate \mathbf{P}_v and \mathbf{n} at individual boutons was the systematic noise in our measurements. To reduce this noise as much as possible one approach was the same as already mentioned to minimize statistical fluctuations: averaging the results of many trials in each experiment. In addition, we restricted our high temporal resolution imaging only to runs where it was essential. Thus, we only

imaged with 10ms temporal resolution when we used our 100 Hz burst method to estimate RRP size. Conversely, to estimate the size of responses to single APs we used longer integration times (25 ms). This gave us more precision, at the expense of slower imaging rates in those trials. Finally, we minimized illumination of transfected neurons to small temporal windows, with little exposure before and after the stimuli, in an attempt to reduce bleaching and photodamage.

After several preliminary tests, we optimized a protocol which allowed us to measure P_v and n at individual boutons, minimizing experimental noise and statistical fluctuations yet consistently ensuring cell viability. The structure of our experiments was very simple. We started by briefly exposing cells to 50 mM NH_4Cl at pH 7.40. This alkalinized the pH of cellular compartments, unquenched all pHluorin molecules present and allowed us to visualize every transfected bouton in a given field. Following that stimulus, we interleaved 30 single AP runs and 12 trials designed to measure RRP size (20 APs at 100 Hz). These runs served as a baseline to estimate P_v and n . After obtaining these baseline values, we applied one of a few different pharmacological interventions (see below) and measured the resulting effect on single AP responses in 30 independent trials. We ended each experiment with an NH_4Cl application to ensure boutons had not moved, split, merged or fallen out of focus over the course of the experiment. In total, we measured P_v and n at 624 individual synapses in 33 experiments from 10 independent culture sets.

5.2 Data quality and filtering

We used this data set as a starting point and began by applying some basic quality control procedures to ensure synapses had appropriately high signal to noise, were stable throughout the experiment and provided a reliable estimate of n . Each synapse had to fulfill each of the following criteria to be included in any subsequent analysis:

Quality of signal

Signal to noise of 1 AP average response > 4

SE of pharmacological treatment effect < 0.3

Stability of signal

Linear fit of 1 AP responses as a function of time does not show significant slope (at significance level $\alpha=0.01$)

Linear fit of synchronous response to 20 APs (delivered in 100 Hz bursts) as a function of time does not show significant slope (at significance level $\alpha =0.01$)

RRP size determination

We only accepted cases where the slope of ΔF vs. AP number for the points in the RRP plateau was at most 50% the slope of the ΔF vs. APs 1-3, as explained in Chapter 2.

We found that these criteria eliminated synapses with obvious problems (such as instability or poor signal to noise) and left us with a high quality data set. A total of 421 synapses (67%) passed all criteria and formed the basis for further analysis. Figure 5.1 shows data from a representative experiment.

Figure 5.1. P_v and RRP size can be measured precisely at many individual boutons in parallel. **(A)** Field of boutons in a representative experiment. The image is the difference in fluorescence before and after the application of 50 mM NH_4Cl and is smoothed for presentation purposes only. The arrow marks the synapse shown in detail in the rest of the figure. Scale bar = $5\mu\text{m}$. **(B1)** Cumulative exocytosis in response to 20 APs at 100 Hz for the indicated synapse ($n=12$ trials). The orange line indicates the RRP size. The light orange shading indicates the region where a plateau was detected using our methods (see Chapter 3), along with the SE in the RRP size. **(B2)** Exocytosis in response to a single action potential. The thick red line indicates an average over 30 trials. The thin red lines show the SE of this average. The vertical scale is the same as in (B1) and is aligned with that panel for convenience. **(C)** Responses to single APs (red) or 20 APs at 100 Hz (black, stimulus-locked exocytosis only) for the indicated synapse. Note the stability in the response throughout almost 2 hours of imaging. **(D)** and **(E)** RRP size and P_v respectively for 27 synapses in this experiment that passed our filtering criteria. For details on the calculation of the error bars see Chapter 2. Each point corresponds to an individual synapse. Synapses are ordered in both panels according to their single AP responses (as % of TP) from highest (left) to lowest (right). The synapse marked in blue is the one analyzed in (B1), (B2) and (C).

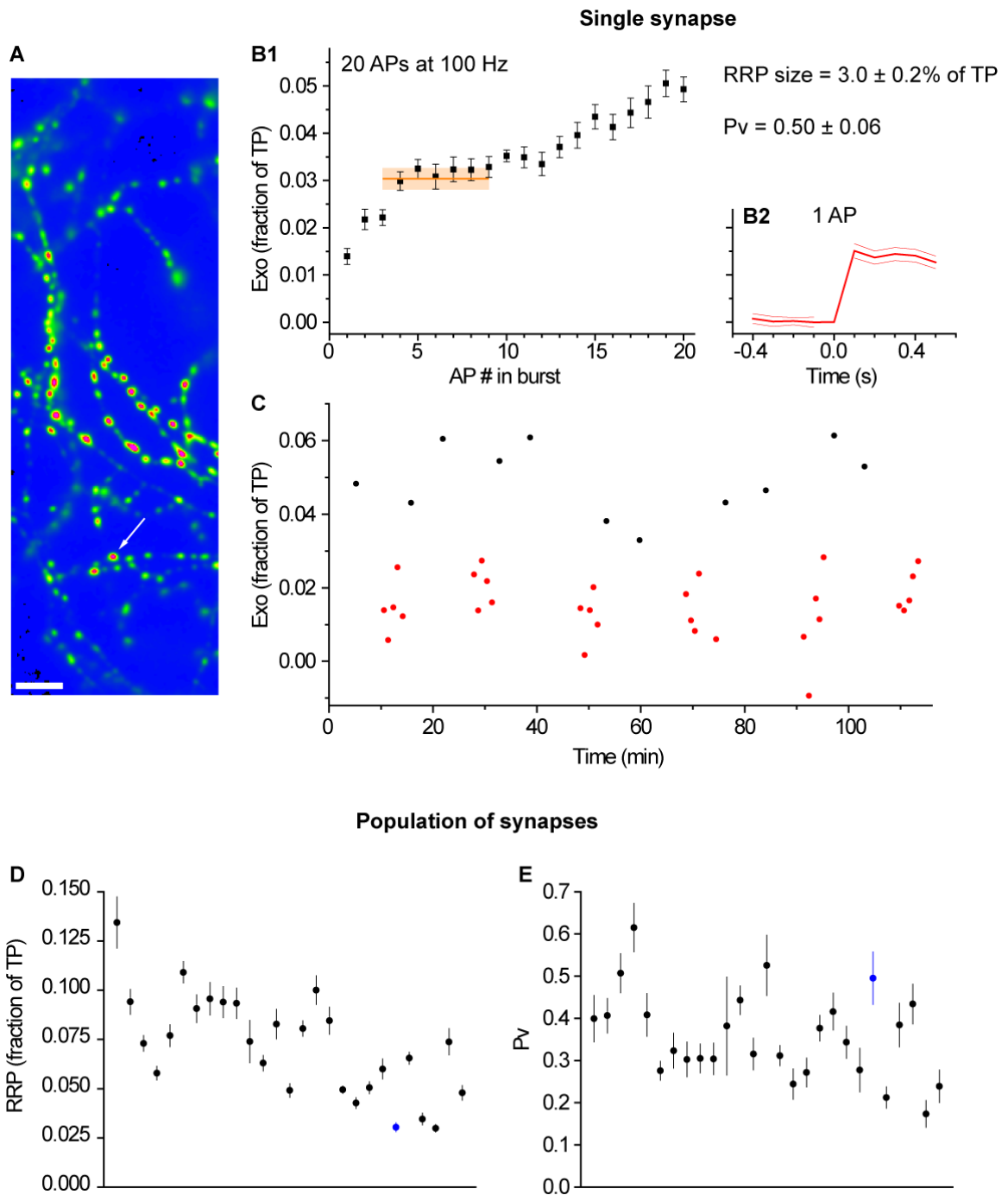


Figure 5.1

For each synapse, we calculated the SEs in the estimates of P_v and RRP size using conventional error propagation techniques (see Chapter 2). The number of trials in our experimental design was sufficient to determine P_v and RRP size with reasonable precision at individual synapses. In the case of RRP size, the median SE -expressed as % of the total number of vesicles- was 0.4% (range=0.1-3.7%). The median %SE -relative to RRP size- was 9% (range=4-18%). In the case of P_v , the median SE was 0.06 (range=0.02-0.19). The median %SE -relative to P_v - was 15% (range=5-40%).

Before proceeding further we examined whether the filtering might bias our data in any way. Even before the filtering criteria were applied, we noted a skew towards more responsive synapses than those included in previous experiments, evidenced by a higher P_v (0.416 ± 0.008) compared to our previous average at 4 mM extracellular Ca^{2+} ion concentration (0.35, from Fig. 3.2C). We speculate this is due to an implicit bias towards selecting more responsive boutons for single synapse experiments. In addition, after filtering we were left with an even more responsive subset of synapses ($P_v = 0.453 \pm 0.008$). This is unsurprising given that the filtering criteria include a signal to noise cutoff, which will be correlated with P_v . We also wondered whether our filtering might select a non-random subset of synapses in terms of responses to the various pharmacological interventions outlined below. This was not the case as the effect of different treatments did not differ between excluded and non-excluded synapses ($P > 0.05$ in Mann Whitney U tests for each intervention). Overall, our experiments to study single synapse properties came from a more responsive population of boutons than those in other chapters of this thesis.

To check whether our results were consistent with those in Chapter 3, we estimated how many vesicles were present in the RRP. To that end we assumed that all synaptic vesicles were labeled and that, on average, there were 64 vesicles in the releasable pool of vesicles (Balaji and Ryan, 2007). Furthermore, we assumed that the releasable pool of vesicles constituted 60% of the total pool of labeled vesicles (Fernandez-Alfonso and Ryan, 2008). Combining these assumptions we estimated that, on average, there would be 106 labeled vesicles in each synapse. Comparing this to the average size of the fluorescence response to a brief alkalinizing pulse of NH_4Cl (see above) we estimated the fluorescence of an individual labeled synaptic vesicle. This parameter allowed us to calculate \mathbf{n} for each synapse (~ 4) which was in excellent agreement with our own results (see Chapter 3) and the number of docked vesicles observed by electron microscopy in hippocampal synapses in culture (Schikorski and Stevens, 1997). Using our estimates of \mathbf{P}_v and \mathbf{n} in equation 5.1 the median expected CV of \mathbf{P}_v measurements -due solely to statistical fluctuations- was 11% (range=3-31%).

5.3 Individual synapses vary considerably in \mathbf{P}_v and \mathbf{n}

Confident that we had robust measures of \mathbf{P}_v and \mathbf{n} at individual boutons, we studied the variability in these basic exocytosis parameters between synapses. Interestingly, we found a large degree of variability in both \mathbf{P}_v and \mathbf{n} (Fig. 5.2). Overall the average CV was 38% for \mathbf{P}_v and 68% for RRP size. Furthermore, a considerable amount of this variability was present in synapses from the same experiment. The average CV of \mathbf{P}_v within each experiment was 29% (range: 14 to 47%) and 44% for RRP size (range: 25 to 81%). The variability in \mathbf{n} was not a consequence of our normalization

to the size of the total pool of vesicles within each synapse as the CVs were still large even when we considered raw ΔF values of RRP size ($CV_{\text{all}}=62\%$; $CV_{\text{within}}=38\%$; range=20-56%). It is important to note that we could not initially rule out that synapses included in our experiments belonged to axons from different somas. Thus, variation between synapses might be due to differences between the neurons that give rise to various subsets of boutons in any given imaged field. To directly obtain estimates of the variability between synapses made by the same axon we took two approaches, detailed below.

First, we used retrospective immunostaining for vG-pH to trace the entire axonal arbor in a subset of our experiments. In most cases (6/9) several transfected somas gave rise to axons that intercrossed in the imaged region such that we could not unambiguously determine that all synapses under study came from just one neuron. However, in three experiments retrospective tracing of processes proved that all imaged synapses were indeed formed by the same axon. The CV of \mathbf{P}_v in those experiments was 18% (n=14 synapses), 21% (10 synapses) and 22% (n=24 synapses). On the other hand, the CV of RRP size was 40%, 49%, and 51% respectively. This analysis suggests that a large amount of variability is present in \mathbf{P}_v and \mathbf{n} , even between synapses made by the same axon. However, the small number of observations warrants some caution in drawing conclusions from these results.

Second, in some cases we were able to determine unambiguously that small groups of adjacent boutons belonged to the same axonal branch. Close inspection of images taken during some experiments clearly showed isolated lengths of axon with groups of three or more boutons, arranged *en passant*. In total, this analysis revealed 72

synapses grouped in 19 axonal branches in 15 experiments. We calculated the CV in \mathbf{P}_v and \mathbf{n} across boutons in each axonal branch (subsequently averaging across branches in experiments with more than one group of boutons that fulfilled the criteria). The average CV in \mathbf{P}_v (across experiments) between boutons of the same axonal branch was 30%. This indicates that variability in \mathbf{P}_v between synapses in an experiment (CV=29%, see above) is present even among boutons on the same axonal branch. Similar conclusions can be drawn from an analysis of the variability in \mathbf{n} . The average CV in \mathbf{n} (across experiments) between boutons of the same axonal branch was 41% (compared to CV=44% between *all* boutons in an experiment). Therefore, there is considerable variability in both \mathbf{P}_v and \mathbf{n} between synapses made by the same axon. We wondered what might explain this large variability in \mathbf{P}_v and \mathbf{n} at the molecular level and explore a few possibilities in the following sections.

Figure 5.2. Large variation in P_v and RRP size between individual synapses. **(A1)** Histogram of P_v across all synapses. **(A2)** Color map of P_v values in all synapses included in our analysis. Each row in this plot represents a single experiment and each dot within that row a single synapse from that experiment. Synapses are colored according to their P_v with cold colors representing low P_v values and warm colors representing high P_v values. The inset shows the P_v color scale. Synapses within each experiment are ranked according to their average response to a single AP (as % of the TP) from left (highest) to right (lowest). Experiments are ordered according to their average synaptic response to a single AP from top (highest) to bottom (lowest). The asterisk highlights the experiment shown in Figure 5.1 and the arrow indicates the synapse shown in more detail in Figures 5.1B-C. **(A3)** The CVs in P_v values for each experiment are shown aligned with the corresponding row in (A2). The average CV in P_v across experiments is shown as a red triangle in the scale bar. Three experiments where all synapses belonged to the same axon are shown in blue. **(B1-3)** Histogram, color map and CVs within each experiment of RRP size, analogous to (A1-3). Synapses in (B2) are ordered identically to (A2) so a dot in the equivalent position on the color maps represents the same synapse, while equivalent rows represent the same experiment. Note that the scaling of colors coding RRP sizes is logarithmic.

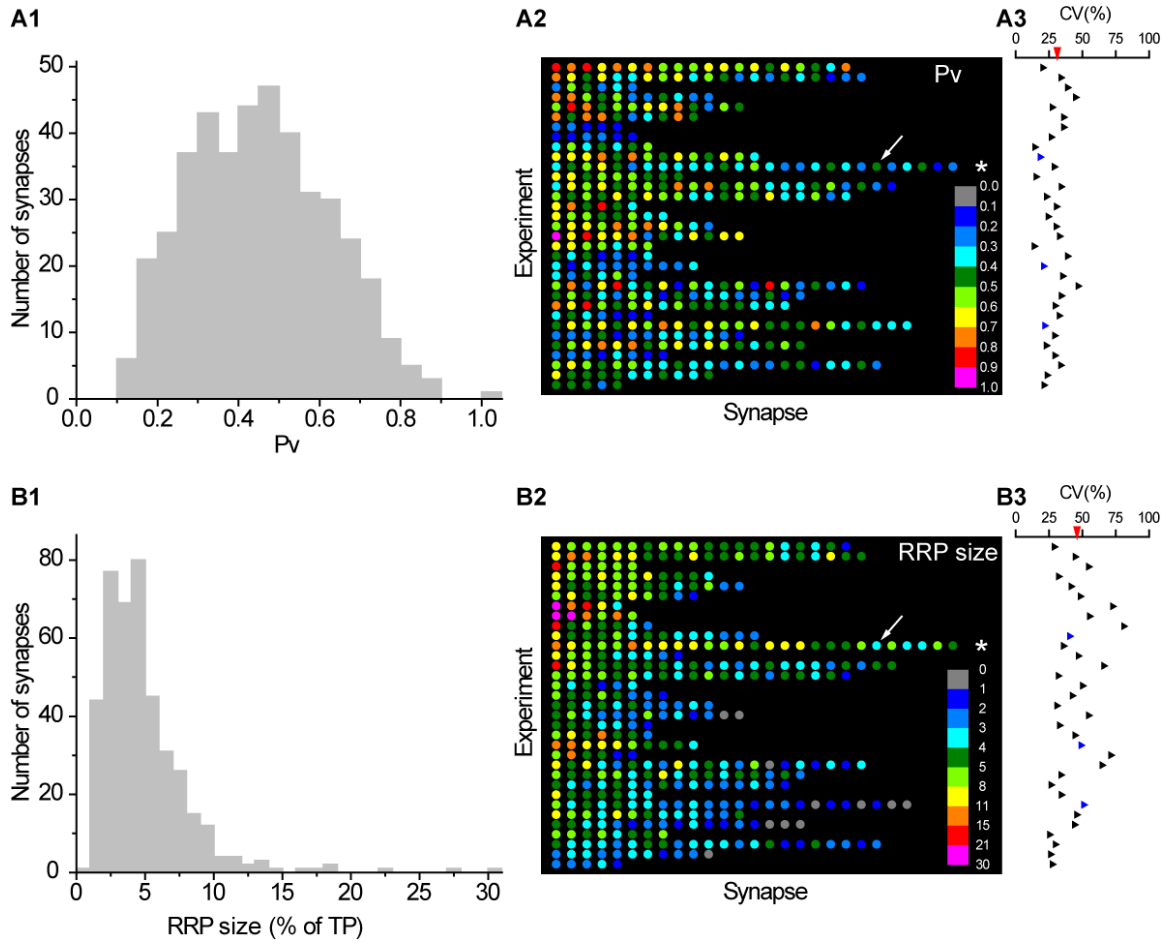


Figure 5.2

5.4 An exploration of molecular determinants of variability in P_v and n

5.4.1 Ca^{2+} channel subtypes

An intriguing hypothesis is that different Ca^{2+} channel subtypes are associated with synapses of different efficacies. A preliminary report attempted to test this in young neurons grown in autaptic cultures and came to the conclusion that there was no correlation between synaptic efficacy and the distribution of P/Q or N type Ca^{2+} channels, despite apparent variation in the contribution of those Ca^{2+} channel subtypes to neurotransmitter release across synapses (Reid et al., 1997). However, that study used a relatively crude measure of P_r , based on the progressive reduction of postsynaptic responses in the presence of the activity dependent blocker MK-801. Critically, P_r was not measured directly at individual synapses. Instead, heterogeneity among synapses was inferred from the need to fit two exponentials to the decay of responses during stimulation in the presence of the blocker. Subsequently, the authors assumed that this reflected the existence of two populations of synapses with high and low responsiveness. Based on our results (Figs. 5.2A1, B1), there is no evidence for two clusters of synapses with clearly separated P_v or n (or P_r , not shown), a key assumption in their analysis. Finally, the study was restricted to young –arguably immature- neurons (one to two weeks old) grown in autaptic cultures. Given the many caveats involved in this report, we do not consider the hypothesis that different Ca^{2+} channel subtypes are associated with synapses of varying efficacy has been tested properly. In what follows, we use our techniques to attack this question directly, by measuring P_v and n at individual synapses and correlating those parameters with the effects of P/Q or N-type Ca^{2+} channel blockers at each bouton.

Before addressing the hypothesis, we wished to determine the relative contributions of N and P/Q type Ca^{2+} channels to exocytosis in response to 1 AP. Using the methods developed in Chapter 3, we found that ω -agatoxin IVA (a specific blocker of P/Q type Ca^{2+} channels) caused a $43\pm 8\%$ decrease in single AP exocytosis ($n=12$ experiments). Conversely, selectively blocking N type Ca^{2+} channels with ω -conotoxin GVIA caused an $82\pm 7\%$ reduction in exocytosis ($n=10$ experiments). The larger effect on exocytosis of blocking N-type Ca^{2+} channels could be due to the presence of more of those channels, a larger current per channel, or to closer coupling between that channel type and primed vesicles. To test the last of these possibilities, we measured the effects of ω -agatoxin IVA and ω -conotoxin GVIA on Ca^{2+} entry in response to a single AP. Blocking P/Q type Ca^{2+} channels reduced Ca^{2+} entry by $19\pm 2\%$ ($n=4$ experiments) whereas blocking N-type Ca^{2+} channels caused a $42\pm 2\%$ decrease ($n=5$ experiments). If the coupling of each Ca^{2+} channel subtype to vesicles were the same, we would expect the reduction in Ca^{2+} entry caused by either toxin to cause a decrease in exocytosis predictable by the curve that relates exocytosis and Ca^{2+} entry under control conditions (Fig. 3.2C). However, if N type channels were closer to vesicles, there should be a larger decrease in exocytosis for a given reduction in Ca^{2+} than expected from the control curve. Thus, plotting the exocytosis and Ca^{2+} entry data in the presence of toxins and comparing it to the control curve is a test of whether the coupling between Ca^{2+} channels and primed vesicles differs according to subtype. In fact, the data obtained in the presence of either toxin agrees well with our control curve relating exocytosis and Ca^{2+} entry (Fig. 5.3). This indicates there is no difference in coupling between P/Q and N Ca^{2+} channel subtypes. Therefore, the larger contribution of N-type Ca^{2+} channels to exocytosis might

be due to larger numbers of active channels in the presynaptic membrane or a higher current per channel.

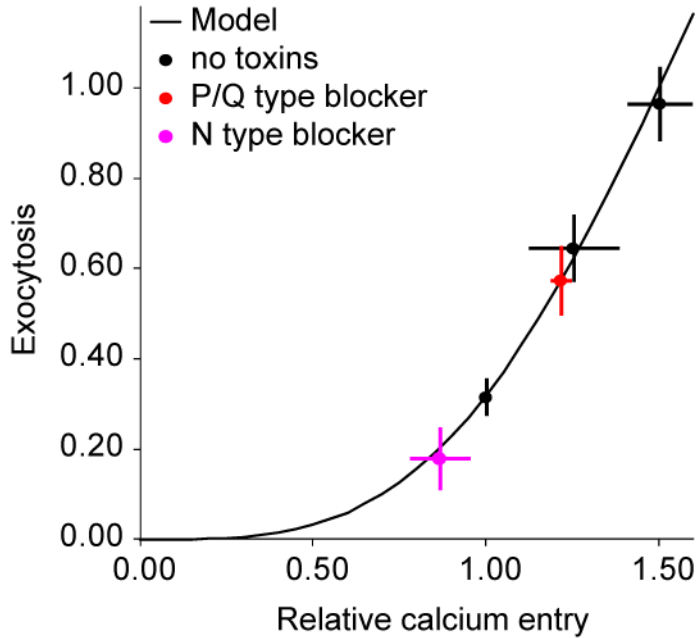


Figure 5.3. P/Q and N-type Ca^{2+} channels do not differ in their coupling to primed synaptic vesicles. Exocytosis as a function of the relative Ca^{2+} entry in response to 1 AP. The model and data without toxins is from the corresponding region in Figure 3.2C. Ca^{2+} entry is normalized to the increase in Ca^{2+} in response to 1 AP with 2 mM extracellular Ca^{2+} , as in Figure 3.2C. For convenience, the exocytosis axis has been normalized to the expected exocytosis for 1 AP at 4 mM extracellular Ca^{2+} . Note the good agreement between the model and the data in the presence of toxins. (*A subset of the toxin experiments were performed by Mike Hoppa*).

Once we had determined the relative importance of N and P/Q-type Ca^{2+} channels for exocytosis, we tested the hypothesis that each Ca^{2+} channel subtype is associated with synapses of different efficacies. To that end, in a subset of the experiments designed to measure properties at single synapses, we applied toxins specific to each Ca^{2+} channel subtype after measuring basal \mathbf{P}_v and \mathbf{n} . We reasoned that if Ca^{2+} channel subtypes were differentially distributed across synapses with different efficacies, there would be a correlation between the effect of the toxins on single AP responses and \mathbf{P}_v . On the other hand, *a priori* we did not expect a correlation between the effect of toxins and RRP size.

Blocking N-type Ca^{2+} channels led to a larger decrease in single AP responses (90 \pm 1%, n=104 synapses in 8 experiments, Figs. 5.4.A.1 and B) than blocking P/Q type Ca^{2+} channels (43 \pm 3% n=104 synapses in 9 experiments, Figs 5.4A2 and B), as expected from the data in Figure 5.3. Interestingly, there was a larger range of effects across synapses when we blocked P/Q type channels (Fig. 5.4B, $\text{CV}_{\text{P/Qeffect}}=64\%$ compared to $\text{CV}_{\text{Neffect}}=15\%$, compare also Figs. 5.5A and 5.6A). We explore possible implications of these observations in the discussion.

As expected, we did not find a clear correlation between the effect of either toxin and RRP size (Figs. 5.5C1-2 and 5.6C1-2). Similarly, we did not find any correlation between the effect of toxin and \mathbf{P}_v (Figs. 5.5B1-2 and 5.6B1-2). Our results indicate that Ca^{2+} channel subtypes are not differentially distributed on boutons with different synaptic efficacies.

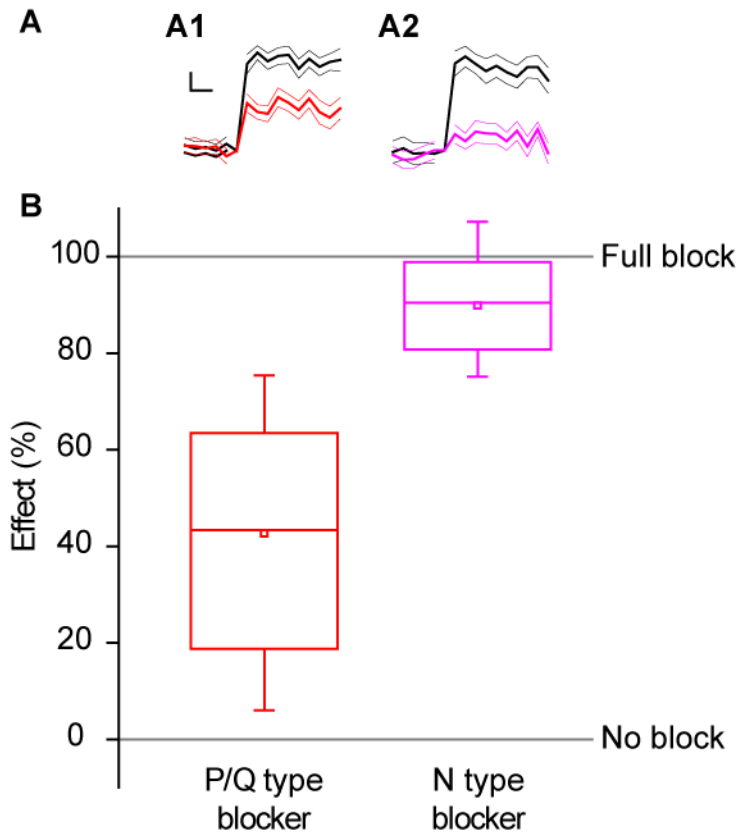


Figure 5.4. Block of P/Q-type Ca^{2+} channels leads to weaker and more variable decrease of exocytosis than block of N type Ca^{2+} channels. **(A)** Representative single synapse responses to 1 AP stimulus before and after the application of toxins that block Ca^{2+} channel subtypes. **(A1)** Response to 1 AP before (black) and after (red) applying ω -agatoxin IVA (effect of toxin= $45\pm 12\%$). **(A2)** Response to 1 AP before (black) and after (magenta) applying of ω -conotoxin GVIA (effect of toxin= $81\pm 11\%$). Each trace in (A1) and (A2) is an average of 30 trials with the thinner lines representing the SEs. Traces are normalized to the size of the response before applying the corresponding toxin and shown on the same scale. Scale bar: 0.2s and 20% of pre-toxin response. **(B)** Effect of P/Q and N-type Ca^{2+} channel blockers across all synapses. The effect of a toxin is defined as the percentage decrease in single AP responses.

Figure 5.5. P/Q-type Ca^{2+} channel distribution is independent of \mathbf{P}_v and \mathbf{n} . **(A)** The effect of ω -agatoxin IVA on exocytosis in response to a single AP. Different colors represent individual experiments, while each dot shows the effect of the blocker on a single synapse (with its SE). Experiments are ordered according to their responses to an individual AP from highest (left) to lowest (right). Within an experiment, synapses are also sorted from most (left) to least responsive (right). **(B1-2)** Effect of a P/Q blocker is independent of \mathbf{P}_v . **(B1)** Each dot is a synapse and the coloring scheme is the same as in (A). Lines represent best fits for each experiment, colored accordingly. **(B2)** Correlation coefficients of the effect of P/Q block with \mathbf{P}_v for each experiment were not significantly different from 0 (two tailed t-test against null hypothesis $\mu=0$, $P=0.27$). Each dot represents the value of the correlation coefficient for 1 experiment, with colors consistent with the rest of the figure. If the correlation coefficient was significantly different from 0 for a given experiment ($P<0.05$), we replaced the dot with a triangle (see Chapter 2 for calculation of the P-value). The gray line represents the average correlation coefficient across experiments. **(C1-2)** Effect of a P/Q blocker is independent of RRP size. Coloring and symbols are analogous to (B1) and (B2). Correlation coefficients of the effect of P/Q block with RRP size for each experiment were not significantly different from 0 (two tailed t-test against null hypothesis $\mu=0$, $P=0.67$).

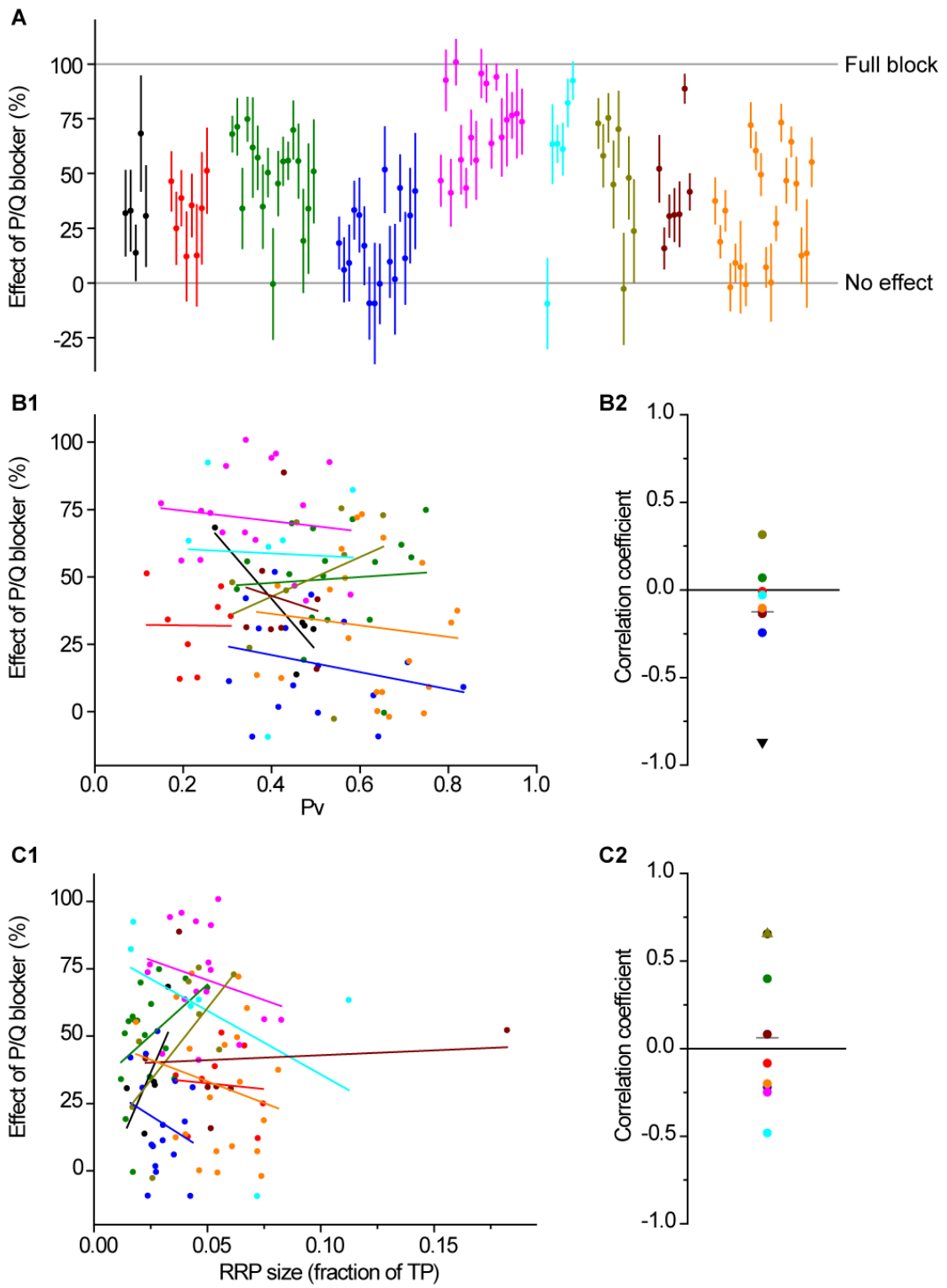


Figure 5.5

Figure 5.6. N-type Ca^{2+} channel distribution is independent of \mathbf{P}_v and \mathbf{n} . **(A)** The effect of ω -conotoxin GVIA on exocytosis in response to a single AP. Different colors represent individual experiments, while each dot shows the effect of the blocker on a single synapse (with its SE). Experiments are ordered according to their responses to an individual AP from highest (left) to lowest (right). Within an experiment, synapses are also sorted from most (left) to least responsive (right). **(B1-2)** Effect of an N blocker is independent of \mathbf{P}_v . **(B1)** Each dot is a synapse and the coloring scheme is the same as in (A). Lines represent best fits for each experiment, colored accordingly. **(B2)** Correlation coefficients of the effect of N block with \mathbf{P}_v for each experiment were not significantly different from 0 (two tailed t-test against null hypothesis $\mu=0$, $P=0.40$). Each dot represents the value of the correlation coefficient for 1 experiment, with colors consistent with the rest of the figure. If the correlation coefficient was significantly different from 0 for a given experiment ($P<0.05$), we replaced the dot with a triangle (see Chapter 2 for calculation of the P-value). The gray line represents the average correlation coefficient across experiments. **(C1-2)** Effect of an N blocker is independent of RRP size. Coloring and symbols are analogous to (B1) and (B2). Correlation coefficients of the effect of N block with RRP size for each experiment were not significantly different from 0 (two tailed t-test against null hypothesis $\mu=0$, $P=0.67$).

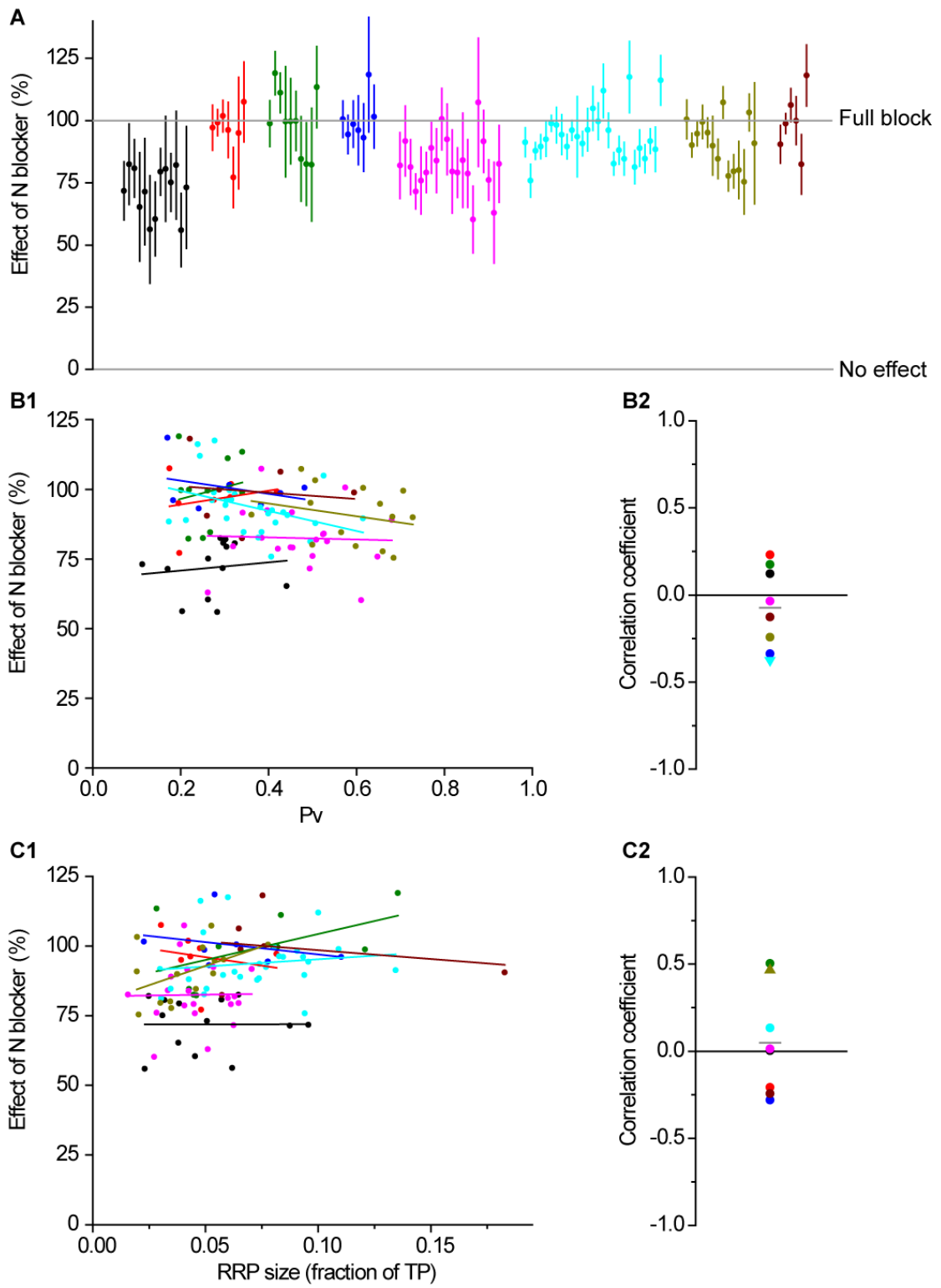


Figure 5.6

5.4.2 Ca^{2+} channel and synaptic vesicle coupling

Another possible source of variability in P_v is the distance between primed synaptic vesicles and the Ca^{2+} channels in the active zone. Given the highly nonlinear dependence of exocytosis on the local intracellular Ca^{2+} concentration, even small differences in positioning are expected to have large effects (Meinrenken et al., 2003).

To probe the distance between Ca^{2+} channels and primed vesicles, we applied EGTA-AM (100 μ M, 90 s pulse), a medium affinity Ca^{2+} buffer. Our reasoning was that EGTA would reduce the size of responses to single APs, and the reduction would be a measure directly correlated with the distance between vesicles and channels (Adler et al., 1991; Borst and Sakmann, 1996). Thus, if this distance is an important variable explaining the differences in P_v across individual synapses, there will be an inverse correlation between P_v and the effect of EGTA. Conversely, there is no reason to expect a correlation between the effect of EGTA and RRP size.

In fact, while there was considerable variation in the effect of EGTA (Fig. 5.7A) we did not find a consistent trend when plotting the effect of EGTA as a function of P_v across many experiments (Fig 5.7B1-2, n=130 synapses in 10 experiments). While some cases did show a negative correlation, this was not consistent over all experiments. As expected, there was no clear correlation between the effect of EGTA and RRP size (Fig 5.7C1-2). This suggests that while distance between synaptic vesicles and Ca^{2+} channels may be an important factor, it is unlikely to account for the differences in P_v among synapses in our experiments.

Figure 5.7. Vesicle to channel distance is not a major determinant of P_v in our experiments **(A)** The effect of EGTA on exocytosis in response to a single AP. Different colors represent individual experiments, while each dot shows the effect of the blocker on a single synapse with its SE. Experiments are ordered according to their responses to an individual AP from highest (left) to lowest (right). Within an experiment, synapses are also sorted from most (left) to least responsive (right). **(B1-2)** Effect of EGTA is independent of P_v . **(B1)** Each dot is a synapse and the coloring scheme is the same as in **(A)**. Lines represent best fits for each experiment, colored accordingly. **(B2)** Correlation coefficients of the effect of EGTA with P_v for each experiment were not significantly different from 0 (one tailed t-test against null hypothesis $\mu=0$, $P=0.19$). Each dot represents the value of the correlation coefficient for 1 experiment, with colors consistent with the rest of the figure. If the correlation coefficient was significantly different from 0 for a given experiment ($P<0.05$), we replaced the dot with a triangle (see Chapter 2 for calculation of the P-value). The gray line represents the average correlation coefficient across experiments. **(C1-2)** Effect of EGTA is independent of RRP size. Coloring and symbols are analogous to **(B1)** and **(B2)**. Correlation coefficients of the effect of EGTA with RRP size for each experiment were not significantly different from 0 (two tailed t-test against null hypothesis $\mu=0$, $P=0.94$).

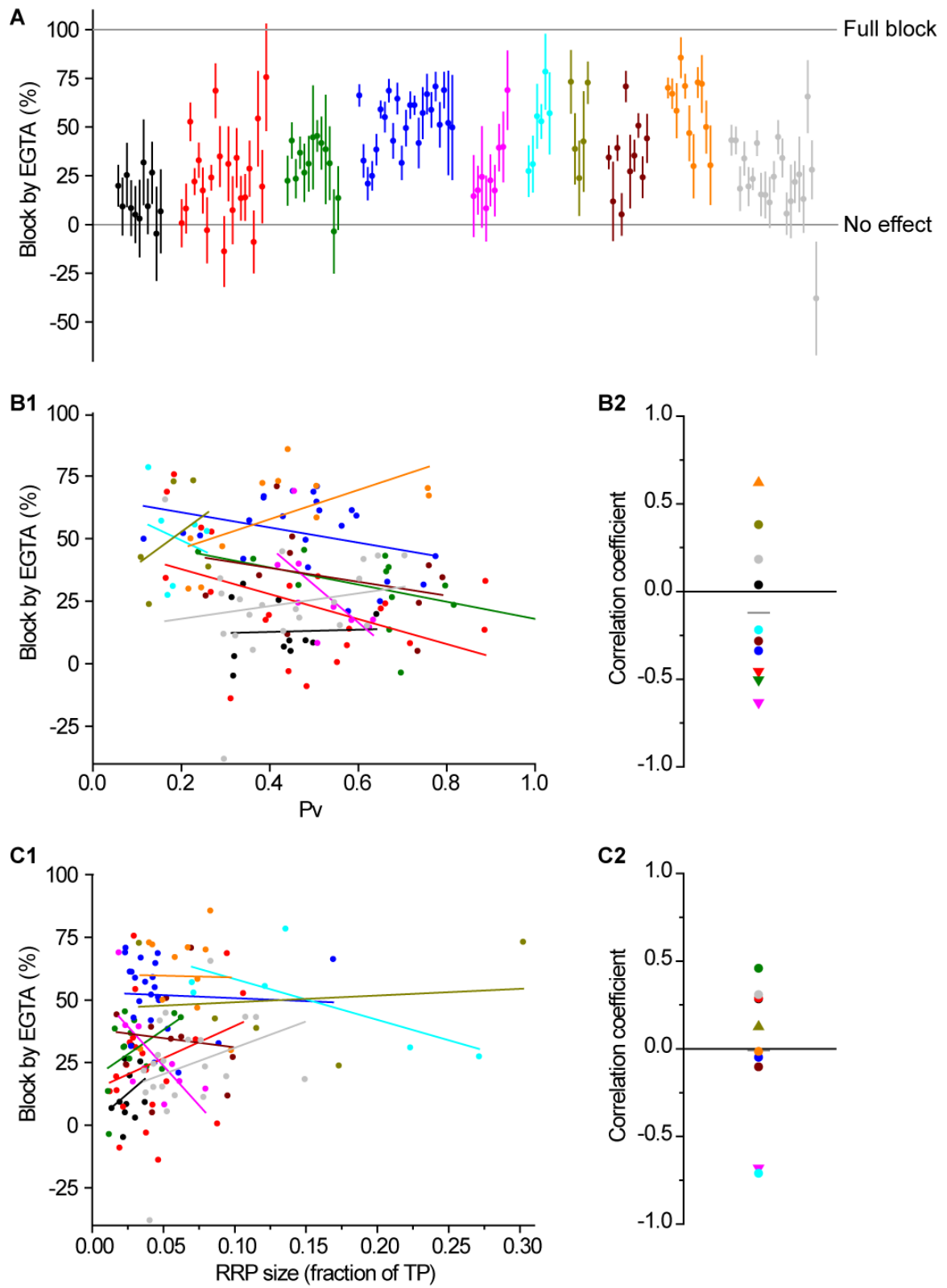


Figure 5.7

5.5 Malleability of synapses – the cAMP pathway

Having explored possible determinants of synaptic properties under basal conditions, we turned our attention to ways in which these properties can be modified. In particular, we wondered whether this malleability might vary across a population of synapses in interesting ways.

One way of altering synaptic strength is to increase intracellular concentrations of cAMP. This activates protein kinase A (PKA) and Epac, the guanine nucleotide exchange factor for the small G protein Rap, leading to increased P_v and/or n in many different neuronal preparations (Trudeau et al., 1996; Chen and Regehr, 1997; Trudeau et al., 1998; Sakaba and Neher, 2001a; Kaneko and Takahashi, 2004; Huang and Hsu, 2006; Gekel and Neher, 2008). To explore this pathway to synaptic potentiation in our system, we used forskolin, a well characterized activator of adenylyl cyclase (Insel and Ostrom, 2003). As expected, applying forskolin (50 μ M) lead to higher single action potential responses. At standard Ca^{2+} concentrations (2 mM), single AP responses increased (+120%, $n=8$ experiments, $P=0.004$, t -test against a null hypothesis of no effect) due to effects on both P_v (+85%) and n (+21%). At the higher external Ca^{2+} concentration used in this chapter (4 mM) there is a smaller rise in single AP responses (35%, $n=12$ experiments, $P=0.02$, t -test against a null hypothesis of no effect), due to increases in both P_v (+19%) and RRP size (+17%).

We wondered whether the responsiveness of individual synapses to forskolin would be negatively correlated with their initial P_v , particularly given that the treatment had smaller effects with higher extracellular Ca^{2+} . To test this, we measured n and P_v at single synapses, subsequently applied forskolin and estimated its effect on single AP

responses. The effect of forskolin was very variable across synapses (Fig. 5.8A) but we consistently observed a negative correlation between the effect of forskolin and initial P_v (Figs. 5.8B1-2). Conversely, there was no correlation between the effect of forskolin and RRP size (Figs. 5.8C1-2). Therefore, synapses with lower basal P_v showed larger responses to the forskolin treatment.

Figure 5.8. The effect of forskolin on exocytosis in response to a single action potential is negatively correlated with P_v **(A)** Effect of forskolin on exocytosis in response to a single AP. Different colors represent individual experiments, while each dot shows the effect of the blocker on a single synapse with its SE. Experiments are ordered according to their responses to an individual AP from highest (left) to lowest (right). Within an experiment, synapses are also sorted from most (left) to least responsive (right). **(B1-2)** Effect of forskolin is negatively correlated with P_v . **(B1)** Each dot is a synapse and the coloring scheme is the same as in (A). Lines represent best fits for each experiment, colored accordingly. **(B2)** There is a negative correlation between the effect of forskolin and P_v (two tailed t-test against null hypothesis $\mu=0$, $P=0.0004$). Each dot represents the value of the correlation coefficient for 1 experiment, with colors consistent with the rest of the figure. If the correlation coefficient was significantly different from 0 for a given experiment ($P<0.05$), we replaced the dot with a triangle (see Chapter 2 for calculation of the P-value). The gray line represents the average correlation coefficient across experiments. **(C1-2)** Effect of forskolin is independent of RRP size. Coloring and symbols are analogous to (B1) and (B2). Correlation coefficients of the effect of forskolin with RRP size for each experiment were not significantly different from 0 (two tailed t-test against null hypothesis $\mu=0$, $P=0.24$).

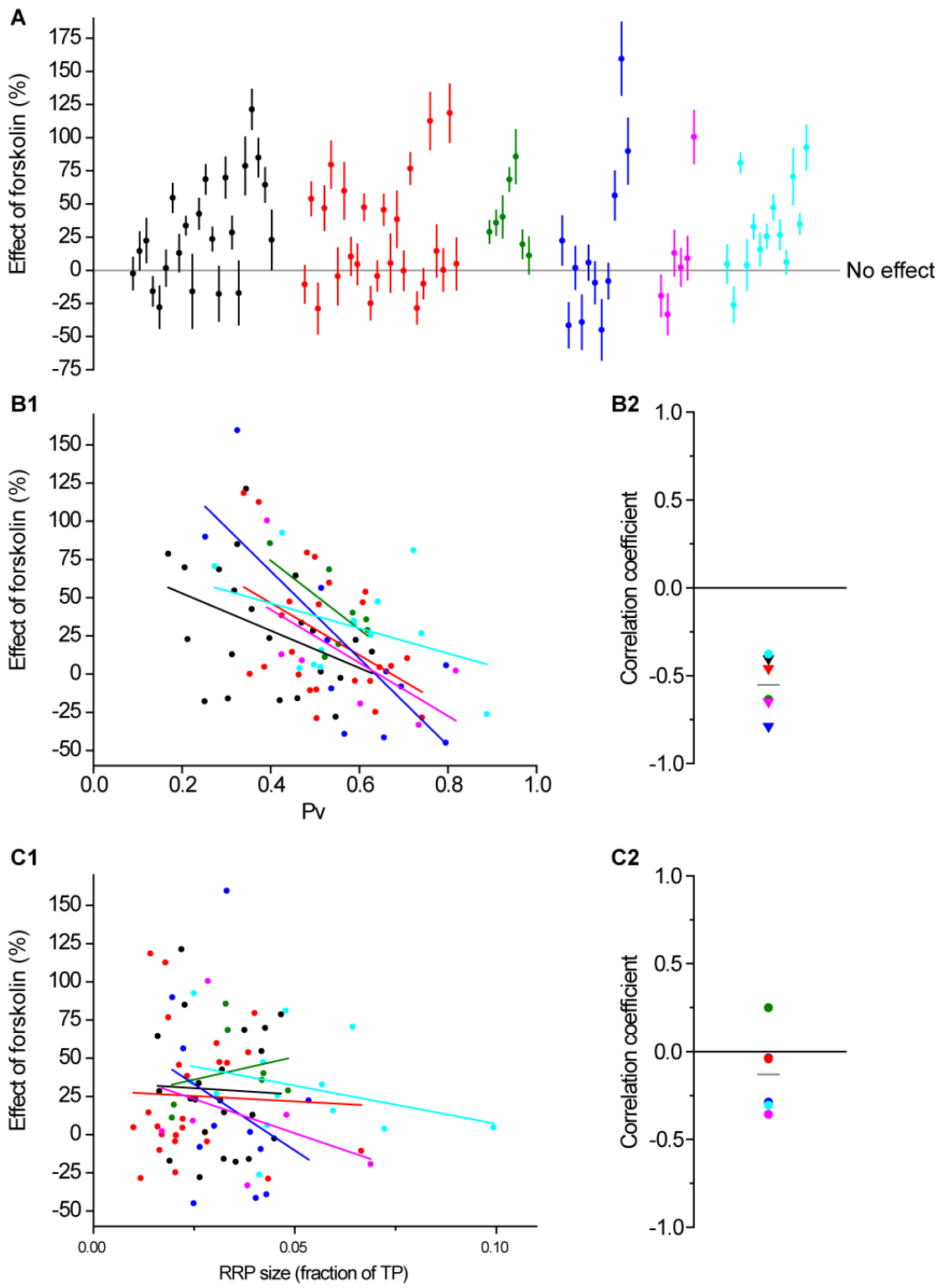


Figure 5.8

To investigate this correlation in more detail we used a few simple models. A first step to study the effect of an activator on boutons with varying initial P_v is a model explaining why those synapses are different in the first place. Recalling the relationship between Ca^{2+} entry and exocytosis (Fig. 3.2C), there are two simple explanations that can account for P_v variation across boutons (Fig. 5.9). The first option is that primed vesicles have different fusogenicities across different synapses (Fig. 5.9A). Alternatively, boutons might vary in the relative entry of Ca^{2+} ions in response to 1 AP (Fig. 5.9B). As regards forskolin, its effect on P_v could similarly be due to an increase in either fusogenicity of primed vesicles, or the amount of Ca^{2+} that enters a synapse in response to an AP.

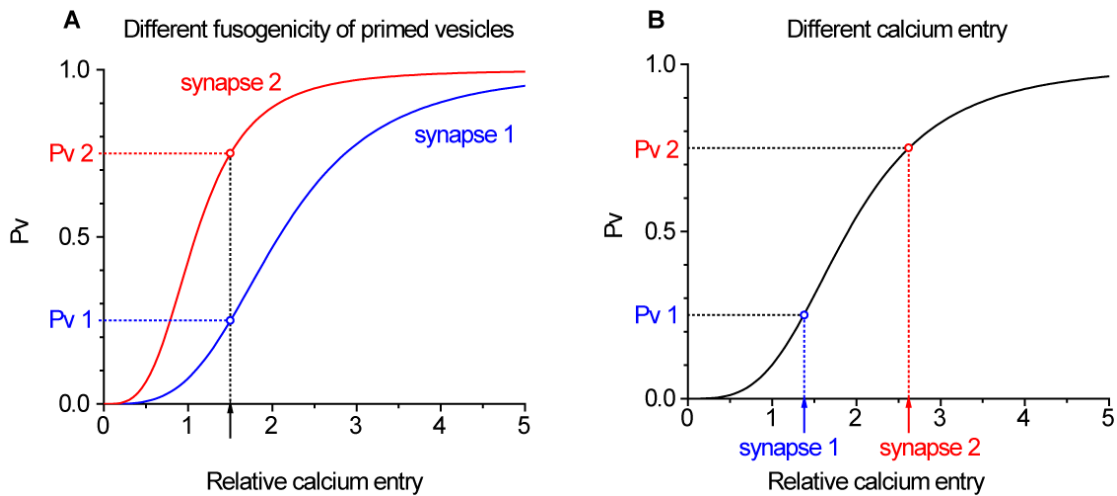


Figure 5.9. Two scenarios that could account for different P_v between synapses. **(A)** Synapses that differ in the average fusogenicity of vesicles in the RRP (parameter K from equation 2.1 is lower in synapse 2). For the same amount of Ca^{2+} entry in response to 1 AP, these synapses have different P_v . **(B)** Synapses whose primed vesicles are equally likely to fuse but that differ in the amount of Ca^{2+} entry in response to 1 AP. This will lead to different P_v between synapses.

To explore these models we took both a graphical and an analytical approach. First, we graphed a hypothetical scenario with two synapses in which initial \mathbf{P}_v varied due to differential fusogenicity of primed vesicles and forskolin caused a uniform increase in Ca^{2+} entry. For simplicity, in this graphical analysis we ignored any effects of forskolin on RRP size. Under these conditions, forskolin will cause a larger increase in the response to an AP in the synapse with lower initial \mathbf{P}_v (Fig. 5.10). We emphasize that in this scenario forskolin causes the *same* increase in Ca^{2+} entry in both boutons. The differential effect on single AP responses arises as a result of the shape of the \mathbf{P}_v vs. Ca^{2+} entry curve and the initial position on that curve of a single AP at 4 mM in both synapses. Other scenarios where variations in \mathbf{P}_v or the effects of forskolin are due to different combinations of fusogenicity and Ca^{2+} entry can also be explored graphically and give similar results (not shown). The addition of effects on RRP size does not modify this basic conclusion.

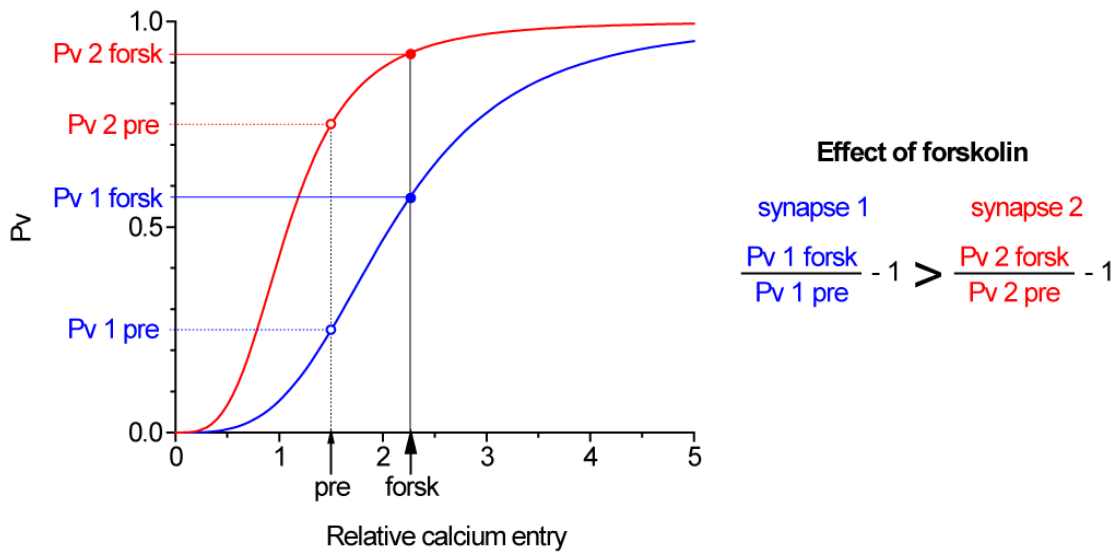


Figure 5.10. Synapses with low initial P_v will potentiate more in the presence of forskolin. We assumed a pair of synapses with differing initial P_v due to different fusogenicities of primed vesicles (as in Fig. 5.9A). We modeled the effect of forskolin as a uniform rise in the relative Ca^{2+} entry in response to 1 AP. This leads to increases in P_v in both synapses. However, the effect is larger in the synapses with lower initial P_v .

Having gained some intuition from a graphical exploration of various scenarios, we explicitly derived analytical models that are based on the same general scheme (see Appendix). The important point gleaned from these models is that even with uniform effects of forskolin on either fusogenicity, Ca^{2+} entry or RRP size across all boutons, the effect on single AP responses will be larger for synapses with lower initial P_v . Thus, the negative correlation between the effect of forskolin and P_v does not necessarily imply that forskolin affects some boutons (e.g., those with low P_v) more than others. So far, we have discussed these models generally, but how well do they actually explain our data?

To test whether our simple models could account for the correlation between the effect of forskolin and P_v we fit them to our data. We illustrate our results with model A (see Appendix), in which forskolin causes a uniform increase in Ca^{2+} entry during a

single action potential across synapses. Fits to model B, in which forskolin causes a uniform increase in fusogenicity of primed vesicles across synapses gave equivalent results (not shown). While model A predicts a negative correlation between the effect of forskolin and initial \mathbf{P}_v , it does not capture the central trend of the data very well (Fig. 5.11, compare the binned data points and the model curve). Furthermore, most of the data from single synapses resides considerably outside the boundaries of what the model predicts, and these differences are not due to systematic errors in \mathbf{P}_v or our estimates of the effect of forskolin. Further highlighting the heterogeneity, even groups of synapses with initially similar \mathbf{P}_v responded very differently to forskolin. This suggests that individual synapses are differentially malleable by activation of the cAMP pathway.

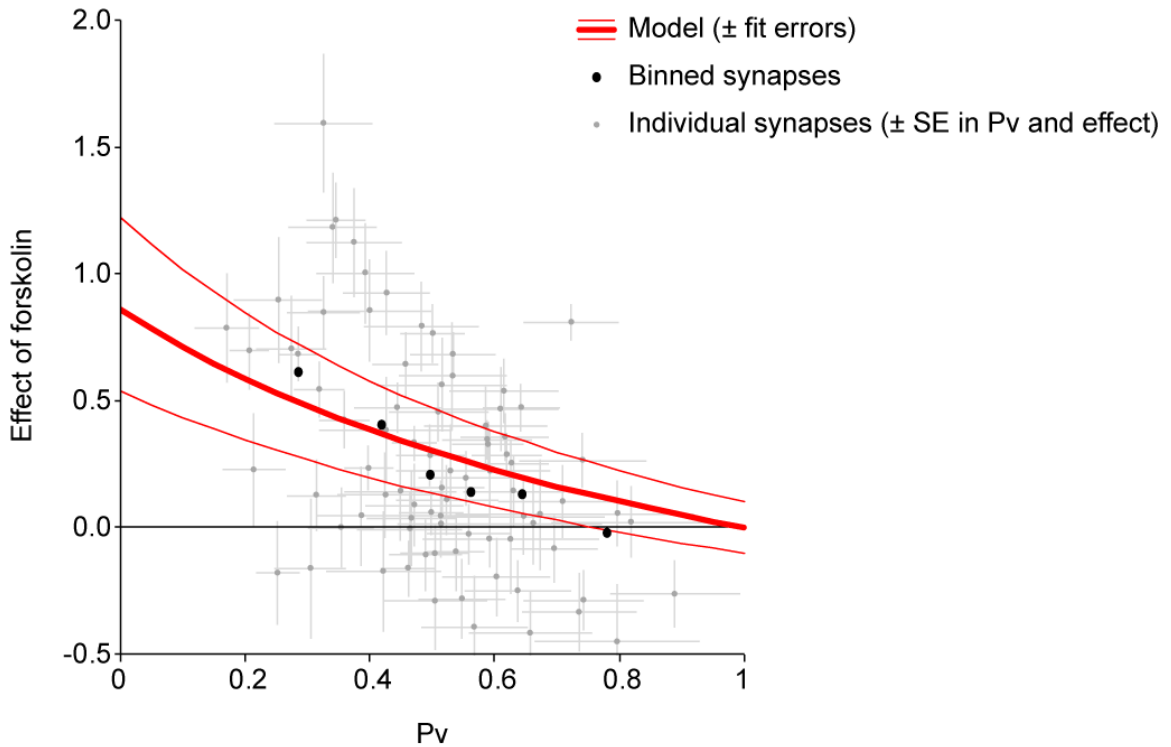


Figure 5.11. Forskolin effects are more variable than expected from model. Effect of forskolin as a function of initial P_v . Data are the same as in Figure 5.8B1, but with the corresponding error bars for P_v and the effect of forskolin. The best fit to Model A (see Appendix) indicates a uniform Ca^{2+} rise ($\alpha=0.20\pm0.03$) and no effect on RRP size ($\rho=1.0\pm0.1$). For a clearer representation of the central trend of the data, individual synapses were binned (15 synapses per bin). Note that while the model correctly predicts a negative correlation, it neither fits the central trend in detail nor accounts for the large variability between synapses with similar P_v .

5.6 Discussion

In this chapter, we extended the techniques developed in Chapter 3 to study P_v and n to the level of individual presynaptic terminals. Our method is robust, and allows precise estimates of both parameters in individual synapses. An interesting result from our measurements is that there is great variability between synapses in their baseline P_v and n , even when comparing synapses made by the same axonal branch. This variability could not be explained by the differential distribution of Ca^{2+} channel subtypes or the varying distances between those channels and primed synaptic vesicles. Additionally, modulation of synapses by activation of cAMP-dependent pathways is highly variable between individual presynaptic terminals.

The large amount of variability in both P_v and n between synapses made by the same axonal branch suggests that each synapse's microenvironment - not its axonal origin - is critical in determining its exocytosis properties. Critical players in determining that microenvironment might be local dendritic activity (Branco et al., 2008) and GABA levels (Laviv et al., 2010).

The synapses in our study were more sensitive to block of N than P/Q-type Ca^{2+} channels. In principle, there are several potential explanations for this differential sensitivity. P/Q-type channels might be fewer, have lower unitary currents or reside farther away from primed synaptic vesicles compared to N-type channels. We can rule out the last possibility on the basis of the data in Figure 5.3. The lack of difference in coupling between Ca^{2+} channel subtypes agrees with previous reports in hippocampal neurons (Wu and Saggau, 1995; Reid et al., 1998). This leaves differing numbers of channels or currents per channel as possible explanations of our results. Regrettably,

there are currently no methods available to directly count the number of active Ca^{2+} channels at a small hippocampal synapse or to measure the current of an individual channel in that context. To our knowledge, there are no studies that have disentangled these two effects to estimate the relative numbers of N and P/Q-type channels in hippocampal synapses where both subtypes are present. On the other hand, unitary Ca^{2+} channel currents have been measured outside the context of the synapse and do not seem to differ significantly between N and P/Q-type channels (Meir et al., 1999).

An intriguing observation was the lower variance across synapses in the effect of an N-type inhibitor on single AP exocytosis, compared to a P/Q-type inhibitor. It is possible that some of this might be due to a ceiling effect, given that reductions in single AP responses by blocking N-type channels are close to the 100% bound. If this accounted for the entire difference in variance across synapses in the effects of P/Q and N-type blockers, we would expect experiments with similar average effects of the channel blocker to have similar CVs in that effect among their synapses. By chance, there were two experiments (one with either blocker) where the average reduction in single action potential responses was the same (72%). Interestingly, the CV of the toxin effect across synapses was higher in the experiment with the P/Q compared to the N-type blocker ($\text{CV}_{\text{P/Q}}=27\%$, 17 synapses vs. $\text{CV}_{\text{N}}=13\%$, 13 synapses). While this does not rule out the possibility of a ceiling effect, it suggests that it cannot account fully explain the difference in variance between the effects of a P/Q and N-type blocker. In what follows we speculate that this difference would be expected under certain scenarios where synapses have more active N than P/Q-type Ca^{2+} channels.

What would the effects of a lower number of P/Q than N-type Ca^{2+} channels be on the variance across synapses of the effect of specific toxins? There are two relevant points to consider. The first is how channels are trafficked to the active zone. The second is how those channels distribute within the active zone with respect to primed synaptic vesicles.

If we assume that the trafficking of Ca^{2+} channels to synapses is a random process with a lower mean number of channels per synapse for subtype P/Q compared to N we can use the Poisson distribution to estimate the variance in the number of channels between synapses. The coefficient of variation in the number of channels per synapse will be

$$CV_i = \frac{1}{\sqrt{N_i}} \quad (5.2)$$

with N_i =mean number of Ca^{2+} channel subtype i per synapse

This implies a higher coefficient of variation in the number of P/Q type channels across synapses, since $N_{P/Q} < N_N$. Note that the effect is more pronounced for smaller numbers of Ca^{2+} channels (~ 10 or less, Fig. 5.12). Thus, assuming we are within the relevant range of Ca^{2+} channel numbers, this could explain why the effect on exocytosis of a P/Q type blocker is both smaller and more variable than that of an N type blocker.

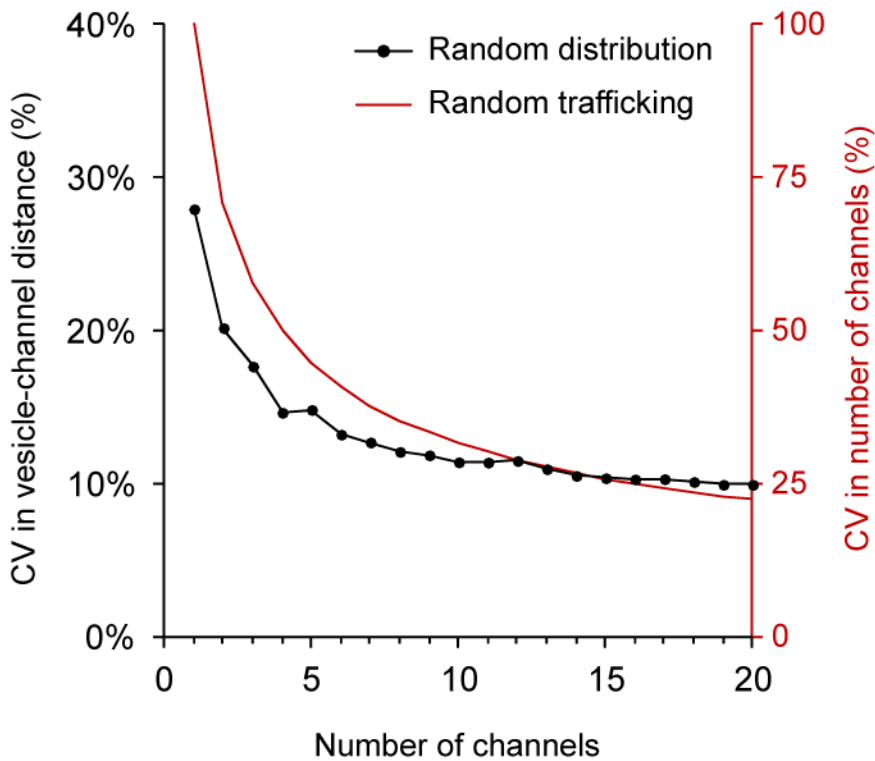


Figure 5.12. Modeling the effects of Ca^{2+} channel numbers. Left axis: the effect of channel numbers on the CV in vesicle-channel distance, assuming random distribution of channels in the active zone. Right axis: the CV in channel number assuming trafficking of channels to active zones is a random process.

As regards the placement of channels within the active zone, we attempted to gain some insights by assuming they are distributed randomly and that there are fewer P/Q than N-type channels. Distributing a small number of channels at random within an active zone will lead to larger variability across synapses in the distances between those channels and vesicles than if there were more channels (see Figure 5.12 and Appendix for details on modeling). The effect of increased variance in the coupling is particularly strong if the number of P/Q-type channels is low (~ 5 or less). While the distance between vesicles and channels has a complicated relation with \mathbf{P}_v , this could still explain why the

effect of a P/Q-type blocker is both smaller and more variable than that of an N-type blocker.

There are several caveats with the analysis presented above. First, we do not have a quantitative model for how much a ceiling effect in N-type block would reduce the variance in the effect of ω -conotoxin GVIA on single AP exocytosis across synapses. Furthermore, we do not know whether a Poisson process can be used to describe trafficking or whether the channels are distributed randomly in the active zone. Additionally, it is unclear whether the number of channels is in the range where the previous assumptions lead to larger variances across synapses of the effect on exocytosis of blocking P/Q-type channels. As regards the issue of channel numbers, a recent study on synapses between inhibitory basket cells and granule cells (which exclusively use P/Q-type channels) in the dentate gyrus of hippocampal slices came to the conclusion that there were 3-5 channels in the vicinity of each primed vesicle (Bucurenciu et al., 2010). If we assume the total number of channels per vesicle in our preparation is similar, this would suggest, on average, between 12-20 channels per active zone. If we additionally assume that there are no differences in unitary currents between the subtypes, we can use the average effects on Ca^{2+} entry of blocking P/Q (19%) and N-type (42%) channels to estimate the number of channels. To that end, we need to make one additional assumption regarding the total accounting of Ca^{2+} channels present in the synapse. As the summed block in Ca^{2+} entry for N and P/Q-type channels is not 100%, there are two possibilities. Either other channel subtypes are present and contribute to exocytosis or part of the Ca^{2+} entry measured with our methods is too far from primed vesicles to influence release. In the first case, that would mean there are 5-8 N-type, 2-4 P/Q-type and 5-8 undefined

Ca²⁺ channels in the active zone. In the second case, that would mean there are 8-14 N-type and 4-6 P/Q type Ca²⁺ channels in an active zone (with 8-13 channels farther away, not influencing exocytosis). This would place the number of channels close to or within the range where the effects of random trafficking and distribution are most relevant to the variance in exocytosis block. However, we highlight again that the assumptions involved in reaching that conclusion are currently very speculative. A final point regarding our models is that while both scenarios could account for our results, neither explains why there are more N-type Ca²⁺ channels in the first place or what would limit the number of channels to relatively low absolute numbers.

In contrast to the preceding discussion, we do not know of any scenario where a smaller unitary current for P/Q-type channels would lead directly to a higher variance from synapse to synapse in the effect of a toxin that blocks those channels. While it is certainly possible that this is occurring, there would have to be an independent explanation for why the variance in the effect of a P/Q-type blocker on exocytosis is larger than for an N-type blocker.

Our results ruled out the hypothesis that different Ca²⁺ channel subtypes are associated with synapses of different efficacies. There was no clear relation between a synapse's initial \mathbf{P}_v and the type of Ca²⁺ channels present. Thus, the relative mix of N and P/Q-type Ca²⁺ channels present at a presynaptic terminal does not affect synaptic strength.

We did not find convincing evidence that the distance between synaptic vesicles and Ca²⁺ channels contributed to the variance in \mathbf{P}_v . This conclusion must be taken with some caution as the effect of EGTA is an indirect measure of vesicle-channel distance.

Small differences in loading times (across experiments), the concentration of intracellular esterases (across synapses) or intracellular Ca^{2+} buffer concentrations (across synapses) make it a crude way to compare vesicle-channel distances between individual presynaptic terminals. In fact, several experiments showed a slight negative correlation between the effect of EGTA and \mathbf{P}_v (Figs 5.7B1-2). However, overall this trend did not reach statistical significance. Alternatively, it is possible that this parameter does not vary greatly across synapses or that with high levels of extracellular Ca^{2+} it is not as influential in determining local Ca^{2+} at primed synaptic vesicles.

As discussed above, neither the type of Ca^{2+} channels present nor their distance to primed vesicles explained the variance in exocytosis parameters between synapses. This leaves open the key question of what the molecular determinants of that variance might be. In the future, it will be interesting to test other potential explanations for this heterogeneity. As detailed in Chapter 1, in principle there are several ways to influence \mathbf{P}_v and \mathbf{n} but it is unclear which are used under normal conditions and whether there are a few dominant mechanisms to set these important parameters. One possibility that can be assayed with tools that are currently available is to what extent there is variability in the relative amount of Ca^{2+} entry on a synapse per synapse basis and whether it might be enough, in principle, to account for the variability in \mathbf{P}_v . Note that if there are 12-20 Ca^{2+} channels per active zone and they are trafficked randomly we expect a CV in channel number of around 25% (Fig. 5.12). If we put this together with the basic relationship between exocytosis and Ca^{2+} (Fig. 3.2C) we expect that 25% CV in channel numbers to translate to considerable variability in \mathbf{P}_v (see Fig. 3.6 for a graphical version of this argument). Of course, an ideal experiment would be to measure Ca^{2+} entry and

exocytosis properties in the same set of synapses. Regrettably, useful reporters of Ca^{2+} entry at the single action potential level have spectra that overlap with that of vG-pH. However, the lab has recently developed a red shifted pH-sensitive fluorescent protein (Sung-Hyun Kim, personal communication). With appropriate optimization, a combination of Ca^{2+} and exocytosis reporters might allow the simultaneous measurement of \mathbf{P}_v , \mathbf{n} , and Ca^{2+} entry at individual synapses.

Our experiments with forskolin led to interesting insights into the effects of positive modulation of synapses. Our simple models suggest that any intervention that raises \mathbf{P}_v uniformly across synapses will lead to a negative correlation between the potentiation of single action potential exocytosis and initial \mathbf{P}_v . Interestingly, while the model explained the general trend in the data, there was a great deal of variability that was unexplained. The most likely explanation is that the effects of forskolin are not homogenous across boutons. Single synapses could vary in the concentration of adenylyl cyclase, in the extent to which this enzyme can be activated, in the coupling to downstream effectors or the potency of those downstream pathways in modulating \mathbf{P}_v or \mathbf{n} . Whether any of these variables is, in turn, correlated with or determined by \mathbf{P}_v is an interesting question that remains open.

Overall, our study of individual synapse properties highlights the large amount of variability present in both basal exocytosis parameters and the degree to which those parameters can be modulated, even for synapses that belong to the same axon. While we cannot rule out that this variability is an artifact of our culture conditions, several examples in more intact preparations suggest it is representative of what actually occurs in vivo (see Chapter 1). If this variability is indeed a defining feature of hippocampal

neurons -or neurons in general- it is interesting to speculate whether it is simply a byproduct of cellular processes that use relatively few molecules (Ribault et al., 2011) or whether, in addition, it has some adaptive value for neural circuit function (Branco and Staras, 2009).

6. FINAL DISCUSSION

In this thesis we have developed methods to study two basic properties of synaptic vesicle exocytosis (Chapter 3). First, we were able to measure the size of the primed pool of synaptic vesicles (\mathbf{n}), a subset of all vesicles in a presynaptic terminal that are immediately available for neurotransmitter release upon arrival of an action potential. Second, we estimated the probability that each vesicle in that privileged pool would fuse with the membrane in response to an action potential (\mathbf{P}_v). Our optical method is, by design, exclusively presynaptic. This provides a new way to study these parameters that is not affected by postsynaptic complications present in electrophysiological studies such as neurotransmitter receptor desensitization, saturation or diffusion. Furthermore, it is not affected by changes in the number of synaptic contacts since measurements come from averages -not sums- across synapses. Our estimates of \mathbf{P}_v (0.1) and \mathbf{n} (4 vesicles) across different cells agree well with previous measures and suggest synapses are in a range where modulations of Ca^{2+} entry can have dramatic effects. In addition, there is considerable variation in these properties between cells. The significance of this finding is unknown.

The techniques we have developed are compatible with a wide array of standard molecular biology tools available for cultured neurons and thus represent a simple way to investigate the molecular underpinnings of synaptic vesicle exocytosis. Our study of tomosyn's role in this process is merely one example of the potential of the method (Chapter 4). While our attempts to determine this molecule's function in exocytosis were hampered by the lack of a successful rescue construct, we were still able to obtain

potentially interesting insights. Whereas large changes in the levels of tomosyn have been reported to lead to modifications in \mathbf{n} , the subtler modulations of concentration we tested herein altered only \mathbf{P}_v , leaving \mathbf{n} unperturbed. Thus, variations in tomosyn levels might contribute to setting \mathbf{P}_v across neurons and perhaps even synapses.

Taking advantage of the fact that imaging can be performed across many synapses in parallel, our technique was extended to study the properties of single presynaptic terminals (Chapter 5). Interestingly, we found a striking degree of variability in \mathbf{P}_v and \mathbf{n} among individual synapses, even if those synapses were on the same axonal branch. We tested whether the complement of Ca^{2+} channel subtypes present at each synapse might differentiate them, but neither the fraction of P/Q nor N-type Ca^{2+} channels was correlated with \mathbf{P}_v or \mathbf{n} . Furthermore, we did not find evidence that synapses with higher \mathbf{P}_v had primed synaptic vesicles closer to Ca^{2+} channels. Thus, our results rule out two possible explanations for the molecular underpinnings of the variability in \mathbf{P}_v and \mathbf{n} among synapses. Many other hypotheses remain to be tested. Our results from individual synapses also tentatively suggest few Ca^{2+} channels (~ 10) are present in the active zone.

In addition to varying in parameters that determine their baseline efficiency, synapses also differ in the extent to which those properties can be modified. In particular, we found that activation of the cAMP pathway led to larger response increases in synapses with lower initial \mathbf{P}_v . Simple modeling suggested this inverse correlation is to be expected of any positive modulator of Ca^{2+} entry or vesicle fusogenicity. This general trend was overlaid on a great degree of synapse to synapse heterogeneity suggesting the cAMP pathway and its effectors are differentially coupled to the exocytosis machinery across synapses.

Overall, our experiments found a large degree of variability among individual synapses, highlighting two open questions in neuroscience. First, what determines synapse to synapse variability at the molecular level? Second, what are the consequences of this variability for neural network function? We hope the techniques we have developed will aid in the search for answers to those questions.

A. APPENDIX

A.1 Derivation of equation 5.1

We define:

X_i = number of vesicles that fuse in response to 1 AP in trial i ,

where X_i is binomially distributed for every i , with parameters \mathbf{P}_v and \mathbf{n} .

Therefore:

$$\text{Avg}(X_i) = \mathbf{P}_v \cdot \mathbf{n}$$

$$\text{Var}(X_i) = \mathbf{P}_v \cdot \mathbf{n} \cdot (1 - \mathbf{P}_v)$$

for every i .

Additionally:

Y = average number of vesicles that fuse in response to a single AP in k trials

$$Y = k^{-1} \cdot (X_1 + X_2 + \dots + X_k)$$

To get an idea of the fluctuation in estimates of \mathbf{P}_v , we will study the coefficient of variation (CV) of Y , as a function of k , \mathbf{P}_v and \mathbf{n} :

$$\text{Avg}(Y) = \mathbf{P}_v \cdot \mathbf{n}$$

$$\text{Var}(Y) = k^{-1} \cdot \mathbf{P}_v \cdot \mathbf{n} \cdot (1 - \mathbf{P}_v)$$

Therefore:

$$\text{CV}(Y) = \sqrt{\frac{(1 - \mathbf{P}_v)}{k \cdot \mathbf{P}_v \cdot \mathbf{n}}} \quad (5.A.1)$$

A.2 Models of forskolin effects on P_v and n

Our models are based on equation 2.1, which is reproduced below with a more convenient notation:

$$Q = n \cdot \frac{d^a}{d^a + K^a} \quad (5.A.2)$$

where

Q = exocytosis in response to a single AP

n = RRP size

d = Ca^{2+} entry in response to a single AP

K = parameter inversely related to fusogenicity

a = cooperativity

We define

f = effect of forskolin

with

$$f = \frac{Q_{forsk}}{Q_{pre}} - 1 \quad (5.A.3)$$

We wish to find

$$f \equiv f(P_{v_{pre}}) \quad (5.A.4)$$

In all models we assume forskolin has an effect $(\rho-1)$ on RRP size, therefore:

$$\rho = \frac{n_{forsk}}{n_{pre}} \quad \text{with } \rho > 1 \quad (5.A.5)$$

We also assume that the cooperativity parameter is constant, and not affected by forskolin ($a = 3.4$, see Fig. 3.2C).

Thus:

$$f = \rho \frac{d_{forsk}^a \cdot (d_{pre}^a + K_{pre}^a)}{d_{pre}^a \cdot (d_{forsk}^a + K_{forsk}^a)} - 1 \quad (5.A.6)$$

Using (5.A.6) as a starting point, we consider four models which have different assumptions with respect to the underlying causes of initial \mathbf{P}_v variation and the effect of forskolin on \mathbf{P}_v .

A.2.1 Model A.1

We assume initial \mathbf{P}_v differences between synapses are due to differences in fusogenicity (K). In that case, we can estimate K from the \mathbf{P}_v of each synapse. From (5.A.2):

$$K = d \cdot \left(\frac{1 - P_v}{P_v} \right)^{\frac{1}{a}} \quad (5.A.7)$$

In addition, we assume forskolin raises \mathbf{P}_v by increasing Ca^{2+} entry (by α) and does not affect fusogenicity:

$$d_{forsk} = d_{pre} \cdot (1 + \alpha), \text{ with } \alpha > 0 \quad (5.A.8)$$

$$\text{and } K_{forsk} = K_{pre} = K \quad (5.A.9)$$

Combining (5.A.6), (5.A.7), (5.A.8) and (5.A.9):

$$f = \rho \frac{(1 + \alpha)^a}{P_{v_{pre}} \cdot ((1 + \alpha)^a - 1) + 1} - 1 \quad (5.A.10)$$

This equation predicts the effect of forskolin on single action potential responses (f) as a function of initial \mathbf{P}_v . We fit it to our data to find the best estimates of forskolin's effects on Ca^{2+} entry (α) and RRP size (ρ) in Figure 5.11.

A.2.2 Model A.2

We assume initial \mathbf{P}_v differences between synapses are due to differences in Ca^{2+} entry

(d). In that case, we can estimate d from the \mathbf{P}_v of each synapse. From (5.A.2):

$$d = K \left(\frac{P_v}{1 - P_v} \right)^{\frac{1}{a}} \quad (5.A.11)$$

In addition, as in model A.1, we assume forskolin raises \mathbf{P}_v by increasing Ca^{2+} entry and does not affect fusogenicity.

Combining (5.A.6), (5.A.8), (5.A.9) and (5.A.11):

$$f = \rho \frac{(1 + \alpha)^a}{P_{v_{pre}} ((1 + \alpha)^a - 1) + 1} - 1 \quad (5.A.12)$$

Thus, the relation between the effect of forskolin on single action potential responses and \mathbf{P}_v is identical to model A.1. This indicates that the important point in determining the relation is the effect of forskolin, and not the mechanism underlying the initial variation in \mathbf{P}_v values.

A.2.3 Model B.1

We assume initial \mathbf{P}_v differences between synapses are due to differences in fusogenicity, as in model A.1. As for the effects of forskolin on \mathbf{P}_v , we assume it decreases K (by β) and does not affect Ca^{2+} entry:

$$K_{\text{forsk}} = K_{\text{pre}} \cdot (1 + \beta), \text{ with } \beta < 0 \quad (5.A.13)$$

$$\text{and } d_{\text{forsk}} = d_{\text{pre}} = d \quad (5.A.14)$$

Combining (5.A.6), (5.A.7), (5.A.13) and (5.A.14):

$$f = \rho \frac{1}{P_{v_{\text{pre}}} (1 - (1 + \beta)^a) + (1 + \beta)^a} - 1 \quad (5.A.15)$$

This equation predicts the effect of forskolin on single action potential responses as a function of initial \mathbf{P}_v . We fit it to our data to find the best estimates of forskolin's effects on fusogenicity and RRP size and found a very similar curve to that shown in Figure 5.11 ($\beta = -0.29 \pm 0.02$; $\rho = 1 \pm 0.1$).

A.2.4 Model B.2

We assume initial \mathbf{P}_v differences between synapses are due to differences in Ca^{2+} entry, as in model A.2. For forskolin, we assume it decreases K (by β) and does not affect Ca^{2+} entry, as in model B.1.

Combining (5.A.6), (5.A.11), (5.A.13) and (5.A.14):

$$f = \rho \frac{1}{P_{v_{pre}} (1 - (1 + \beta)^a) + (1 + \beta)^a} - 1 \quad (5.A.16)$$

As expected from the fact that the effects of forskolin were modeled identically to model B.1, the relation between the effect of forskolin on single action potential responses and \mathbf{P}_v is identical to that model.

A.3 Model of random distribution of Ca^{2+} channels in the active zone

We assume that each active zone is a two-dimensional 1 by 1 square. Therefore, the position of any object in that region is determined by 2 numbers between 0 and 1 representing the horizontal and vertical position respectively. To randomly place an object within an active zone, we assign two random numbers between 0 and 1, and this pair will represent the position of that object. We treat both channels and vesicles as point objects that do not crowd each other out and insert both randomly in the active zone in all our simulations. For simplicity, we assume there are 4 synaptic vesicles in the RRP (the average across our experiments) and do not vary this number across synapses. In different simulations, we vary the number of Ca^{2+} channels present.

Once Ca^{2+} channels and vesicles are placed in the active zone, for each Ca^{2+} channel we calculate its distance to each synaptic vesicle as:

$$\sqrt{(x_i - x_j)^2 + (y_i - y_j)^2}$$

$(i \neq j)$

Where (x_i, y_i) and (x_j, y_j) represent the position of channel i and vesicle j in the active zone.

We average these distances for every channel-vesicle combination to obtain the average distance of that channel to a synaptic vesicle. For active zones with more than one Ca^{2+} channel we average these distances across channels to obtain the average channel to vesicle distance for that active zone. Thus, once we have defined the number of Ca^{2+} channels in an active zone, placed synaptic vesicles and channels at random, we obtain the average vesicle to channel distance within that synapse. This constitutes one run of our model. We ran this model 1000 times for each number of Ca^{2+} channels we were interested in (1-20). For each number of Ca^{2+} channels explored, we calculated the average vesicle-channel distance and the standard deviation of that distance across the 1000 simulated synapses. Finally, we obtained the coefficient of variation of that distance across simulated synapses. This was plotted as a function of the number of Ca^{2+} channels (Fig. 5.12).

REFERENCES

- Abbott LF, Regehr WG (2004) Synaptic computation. *Nature* 431:796-803.
- Abenavoli A, Forti L, Bossi M, Bergamaschi A, Villa A, Malgaroli A (2002) Multimodal quantal release at individual hippocampal synapses: evidence for no lateral inhibition. *J Neurosci* 22:6336-6346.
- Adler EM, Augustine GJ, Duffy SN, Charlton MP (1991) Alien intracellular calcium chelators attenuate neurotransmitter release at the squid giant synapse. *J Neurosci* 11:1496-1507.
- Alvarez VA, Ridenour DA, Sabatini BL (2006) Retraction of synapses and dendritic spines induced by off-target effects of RNA interference. *J Neurosci* 26:7820-7825.
- Andersen P (2007) *The hippocampus book*. Oxford ; New York: Oxford University Press.
- Ariel P, Ryan TA (2010) Optical mapping of release properties in synapses. *Front Neural Circuits* 4.
- Ashery U, Bielopolski N, Barak B, Yizhar O (2009) Friends and foes in synaptic transmission: the role of tomosyn in vesicle priming. *Trends Neurosci* 32:275-282.
- Atluri PP, Ryan TA (2006) The kinetics of synaptic vesicle reacidification at hippocampal nerve terminals. *J Neurosci* 26:2313-2320.
- Baba T, Sakisaka T, Mochida S, Takai Y (2005) PKA-catalyzed phosphorylation of tomosyn and its implication in Ca²⁺-dependent exocytosis of neurotransmitter. *J Cell Biol* 170:1113-1125.
- Balaji J, Ryan TA (2007) Single-vesicle imaging reveals that synaptic vesicle exocytosis and endocytosis are coupled by a single stochastic mode. *Proc Natl Acad Sci U S A* 104:20576-20581.
- Barak B, Williams A, Bielopolski N, Gottfried I, Okun E, Brown MA, Matti U, Rettig J, Stuenkel EL, Ashery U (2011) Tomosyn expression pattern in the mouse hippocampus suggests both presynaptic and postsynaptic functions. *Front Neuroanat* 4:149.
- Becherer U, Rettig J (2006) Vesicle pools, docking, priming, and release. *Cell Tissue Res* 326:393-407.
- Bennett MR (1999) The concept of a calcium sensor in transmitter release. *Prog Neurobiol* 59:243-277.
- Blatow M, Caputi A, Burnashev N, Monyer H, Rozov A (2003) Ca²⁺ buffer saturation underlies paired pulse facilitation in calbindin-D28k-containing terminals. *Neuron* 38:79-88.
- Bollmann JH, Sakmann B, Borst JG (2000) Calcium sensitivity of glutamate release in a calyx-type terminal. *Science* 289:953-957.
- Borst JG, Sakmann B (1996) Calcium influx and transmitter release in a fast CNS synapse. *Nature* 383:431-434.
- Borst JG, Sakmann B (1999) Depletion of calcium in the synaptic cleft of a calyx-type synapse in the rat brainstem. *J Physiol* 521 Pt 1:123-133.
- Branco T, Staras K (2009) The probability of neurotransmitter release: variability and feedback control at single synapses. *Nat Rev Neurosci* 10:373-383.
- Branco T, Marra V, Staras K (2010) Examining size-strength relationships at hippocampal synapses using an ultrastructural measurement of synaptic release probability. *J Struct Biol* 172:203-210.

- Branco T, Staras K, Darcy KJ, Goda Y (2008) Local dendritic activity sets release probability at hippocampal synapses. *Neuron* 59:475-485.
- Brose N, Hofmann K, Hata Y, Sudhof TC (1995) Mammalian homologues of *Caenorhabditis elegans* unc-13 gene define novel family of C2-domain proteins. *J Biol Chem* 270:25273-25280.
- Bucurenciu I, Bischofberger J, Jonas P (2010) A small number of open Ca²⁺ channels trigger transmitter release at a central GABAergic synapse. *Nat Neurosci* 13:19-21.
- Burgalossi A, Jung S, Meyer G, Jockusch WJ, Jahn O, Taschenberger H, O'Connor VM, Nishiki T, Takahashi M, Brose N, Rhee JS (2010) SNARE protein recycling by alphaSNAP and betaSNAP supports synaptic vesicle priming. *Neuron* 68:473-487.
- Chapman ER (2008) How does synaptotagmin trigger neurotransmitter release? *Annu Rev Biochem* 77:615-641.
- Chen C, Regehr WG (1997) The mechanism of cAMP-mediated enhancement at a cerebellar synapse. *J Neurosci* 17:8687-8694.
- Cheviet S, Bezzi P, Ivarsson R, Renstrom E, Viertl D, Kasas S, Catsicas S, Regazzi R (2006) Tomosyn-1 is involved in a post-docking event required for pancreatic beta-cell exocytosis. *J Cell Sci* 119:2912-2920.
- Conti R, Lisman J (2003) The high variance of AMPA receptor- and NMDA receptor-mediated responses at single hippocampal synapses: evidence for multiquantal release. *Proc Natl Acad Sci U S A* 100:4885-4890.
- Davis GW, Murphey RK (1993) A role for postsynaptic neurons in determining presynaptic release properties in the cricket CNS: evidence for retrograde control of facilitation. *J Neurosci* 13:3827-3838.
- de Wit H (2010) Morphological docking of secretory vesicles. *Histochem Cell Biol* 134:103-113.
- de Wit H, Walter AM, Milosevic I, Gulyas-Kovacs A, Riedel D, Sorensen JB, Verhage M (2009) Synaptotagmin-1 docks secretory vesicles to syntaxin-1/SNAP-25 acceptor complexes. *Cell* 138:935-946.
- Deng L, Kaeser PS, Xu W, Sudhof TC (2011) RIM proteins activate vesicle priming by reversing autoinhibitory homodimerization of Munc13. *Neuron* 69:317-331.
- Dittman J, Ryan TA (2009) Molecular circuitry of endocytosis at nerve terminals. *Annu Rev Cell Dev Biol* 25:133-160.
- Dittman JS, Regehr WG (1998) Calcium dependence and recovery kinetics of presynaptic depression at the climbing fiber to Purkinje cell synapse. *J Neurosci* 18:6147-6162.
- Dybbs M, Ngai J, Kaplan JM (2005) Using microarrays to facilitate positional cloning: identification of tomosyn as an inhibitor of neurosecretion. *PLoS Genet* 1:6-16.
- Fernandez-Alfonso T, Ryan TA (2008) A heterogeneous "resting" pool of synaptic vesicles that is dynamically interchanged across boutons in mammalian CNS synapses. *Brain Cell Biol* 36:87-100.
- Fioravante D, Regehr WG (2011) Short-term forms of presynaptic plasticity. *Curr Opin Neurobiol* 21:269-274.
- Frank E (1973) Matching of facilitation at the neuromuscular junction of the lobster: a possible case for influence of muscle on nerve. *J Physiol* 233:635-658.
- Fredj NB, Burrone J (2009) A resting pool of vesicles is responsible for spontaneous vesicle fusion at the synapse. *Nat Neurosci* 12:751-758.
- Fujita Y, Shirataki H, Sakisaka T, Asakura T, Ohya T, Kotani H, Yokoyama S, Nishioka H, Matsuura Y, Mizoguchi A, Scheller RH, Takai Y (1998) Tomosyn: a syntaxin-1-binding

- protein that forms a novel complex in the neurotransmitter release process. *Neuron* 20:905-915.
- Gekel I, Neher E (2008) Application of an Epac activator enhances neurotransmitter release at excitatory central synapses. *J Neurosci* 28:7991-8002.
- Gracheva EO, Burdina AO, Holgado AM, Berthelot-Grosjean M, Ackley BD, Hadwiger G, Nonet ML, Weimer RM, Richmond JE (2006) Tomosyn inhibits synaptic vesicle priming in *Caenorhabditis elegans*. *PLoS Biol* 4:e261.
- Granseth B, Lagnado L (2008) The role of endocytosis in regulating the strength of hippocampal synapses. *J Physiol* 586:5969-5982.
- Granseth B, Odermatt B, Royle SJ, Lagnado L (2006) Clathrin-mediated endocytosis is the dominant mechanism of vesicle retrieval at hippocampal synapses. *Neuron* 51:773-786.
- Granseth B, Odermatt B, Royle SJ, Lagnado L (2009) Comment on "The dynamic control of kiss-and-run and vesicular reuse probed with single nanoparticles". *Science* 325:1499; author reply 1499.
- Groffen AJ, Jacobsen L, Schut D, Verhage M (2005) Two distinct genes drive expression of seven tomosyn isoforms in the mammalian brain, sharing a conserved structure with a unique variable domain. *J Neurochem* 92:554-568.
- Hammarlund M, Palfreyman MT, Watanabe S, Olsen S, Jorgensen EM (2007) Open syntaxin docks synaptic vesicles. *PLoS Biol* 5:e198.
- Han Y, Kaeser PS, Sudhof TC, Schneggenburger R (2011) RIM determines Ca(2)+ channel density and vesicle docking at the presynaptic active zone. *Neuron* 69:304-316.
- Hatsuzawa K, Lang T, Fasshauer D, Bruns D, Jahn R (2003) The R-SNARE motif of tomosyn forms SNARE core complexes with syntaxin 1 and SNAP-25 and down-regulates exocytosis. *J Biol Chem* 278:31159-31166.
- Hattendorf DA, Andreeva A, Gangar A, Brennwald PJ, Weis WI (2007) Structure of the yeast polarity protein Sro7 reveals a SNARE regulatory mechanism. *Nature* 446:567-571.
- He L, Wu LG (2007) The debate on the kiss-and-run fusion at synapses. *Trends Neurosci* 30:447-455.
- He L, Xue L, Xu J, McNeil BD, Bai L, Melicoff E, Adachi R, Wu LG (2009) Compound vesicle fusion increases quantal size and potentiates synaptic transmission. *Nature* 459:93-97.
- Heine M, Groc L, Frischknecht R, Beique JC, Lounis B, Rumbaugh G, Huganir RL, Cognet L, Choquet D (2008) Surface mobility of postsynaptic AMPARs tunes synaptic transmission. *Science* 320:201-205.
- Hosoi N, Holt M, Sakaba T (2009) Calcium dependence of exo- and endocytotic coupling at a glutamatergic synapse. *Neuron* 63:216-229.
- Hua Y, Sinha R, Martineau M, Kahms M, Klingauf J (2010) A common origin of synaptic vesicles undergoing evoked and spontaneous fusion. *Nat Neurosci* 13:1451-1453.
- Huang CC, Hsu KS (2006) Presynaptic mechanism underlying cAMP-induced synaptic potentiation in medial prefrontal cortex pyramidal neurons. *Mol Pharmacol* 69:846-856.
- Insel PA, Ostrom RS (2003) Forskolin as a tool for examining adenylyl cyclase expression, regulation, and G protein signaling. *Cell Mol Neurobiol* 23:305-314.
- Ishikawa T, Kaneko M, Shin HS, Takahashi T (2005) Presynaptic N-type and P/Q-type Ca²⁺ channels mediating synaptic transmission at the calyx of Held of mice. *J Physiol* 568:199-209.
- Jackson AL, Linsley PS (2010) Recognizing and avoiding siRNA off-target effects for target identification and therapeutic application. *Nat Rev Drug Discov* 9:57-67.

- Jahn R, Scheller RH (2006) SNAREs--engines for membrane fusion. *Nat Rev Mol Cell Biol* 7:631-643.
- Kaesler PS, Deng L, Wang Y, Dulubova I, Liu X, Rizo J, Sudhof TC (2011) RIM proteins tether Ca^{2+} channels to presynaptic active zones via a direct PDZ-domain interaction. *Cell* 144:282-295.
- Kaneko M, Takahashi T (2004) Presynaptic mechanism underlying cAMP-dependent synaptic potentiation. *J Neurosci* 24:5202-5208.
- Kochubey O, Schneggenburger R (2011) Synaptotagmin increases the dynamic range of synapses by driving Ca^{2+} -evoked release and by clamping a near-linear remaining Ca^{2+} sensor. *Neuron* 69:736-748.
- Kochubey O, Lou X, Schneggenburger R (2011) Regulation of transmitter release by Ca^{2+} and synaptotagmin: insights from a large CNS synapse. *Trends Neurosci* 34:237-246.
- Koester HJ, Johnston D (2005) Target cell-dependent normalization of transmitter release at neocortical synapses. *Science* 308:863-866.
- Laurent G, Sivaramakrishnan A (1992) Single local interneurons in the locust make central synapses with different properties of transmitter release on distinct postsynaptic neurons. *J Neurosci* 12:2370-2380.
- Laviv T, Riven I, Dolev I, Vertkin I, Balana B, Slesinger PA, Slutsky I (2010) Basal GABA regulates GABA(B)R conformation and release probability at single hippocampal synapses. *Neuron* 67:253-267.
- Lazarevic V, Schone C, Heine M, Gundelfinger ED, Fejtova A (2011) Extensive Remodeling of the Presynaptic Cytomatrix upon Homeostatic Adaptation to Network Activity Silencing. *J Neurosci* 31:10189-10200.
- Lujan R, Roberts JD, Shigemoto R, Ohishi H, Somogyi P (1997) Differential plasma membrane distribution of metabotropic glutamate receptors mGluR1 alpha, mGluR2 and mGluR5, relative to neurotransmitter release sites. *J Chem Neuroanat* 13:219-241.
- Markram H, Wang Y, Tsodyks M (1998) Differential signaling via the same axon of neocortical pyramidal neurons. *Proc Natl Acad Sci U S A* 95:5323-5328.
- Masuda ES, Huang BC, Fisher JM, Luo Y, Scheller RH (1998) Tomosyn binds t-SNARE proteins via a VAMP-like coiled coil. *Neuron* 21:479-480.
- Mathie A, Wooltorton JR, Watkins CS (1998) Voltage-activated potassium channels in mammalian neurons and their block by novel pharmacological agents. *Gen Pharmacol* 30:13-24.
- Matthews G, Sterling P (2008) Evidence that vesicles undergo compound fusion on the synaptic ribbon. *J Neurosci* 28:5403-5411.
- Matz J, Gilyan A, Kolar A, McCarvill T, Krueger SR (2010) Rapid structural alterations of the active zone lead to sustained changes in neurotransmitter release. *Proc Natl Acad Sci U S A* 107:8836-8841.
- McBain CJ, Kauer JA (2009) Presynaptic plasticity: targeted control of inhibitory networks. *Curr Opin Neurobiol* 19:254-262.
- McEwen JM, Madison JM, Dybbs M, Kaplan JM (2006) Antagonistic regulation of synaptic vesicle priming by Tomosyn and UNC-13. *Neuron* 51:303-315.
- Meinrenken CJ, Borst JG, Sakmann B (2003) Local routes revisited: the space and time dependence of the Ca^{2+} signal for phasic transmitter release at the rat calyx of Held. *J Physiol* 547:665-689.

- Meir A, Ginsburg S, Butkevich A, Kachalsky SG, Kaiserman I, Ahdut R, Demirgoren S, Rahamimoff R (1999) Ion channels in presynaptic nerve terminals and control of transmitter release. *Physiol Rev* 79:1019-1088.
- Miesenbock G, De Angelis DA, Rothman JE (1998) Visualizing secretion and synaptic transmission with pH-sensitive green fluorescent proteins. *Nature* 394:192-195.
- Mittelstaedt T, Alvarez-Baron E, Schoch S (2010) RIM proteins and their role in synapse function. *Biol Chem* 391:599-606.
- Mochida S, Few AP, Scheuer T, Catterall WA (2008) Regulation of presynaptic Ca(V)2.1 channels by Ca²⁺ sensor proteins mediates short-term synaptic plasticity. *Neuron* 57:210-216.
- Mohrmann R, de Wit H, Verhage M, Neher E, Sorensen JB (2010) Fast vesicle fusion in living cells requires at least three SNARE complexes. *Science* 330:502-505.
- Moulder KL, Mennerick S (2005) Reluctant vesicles contribute to the total readily releasable pool in glutamatergic hippocampal neurons. *J Neurosci* 25:3842-3850.
- Murthy VN, Stevens CF (1998) Synaptic vesicles retain their identity through the endocytic cycle. *Nature* 392:497-501.
- Murthy VN, Sejnowski TJ, Stevens CF (1997) Heterogeneous release properties of visualized individual hippocampal synapses. *Neuron* 18:599-612.
- Neher E (2010) What is Rate-Limiting during Sustained Synaptic Activity: Vesicle Supply or the Availability of Release Sites. *Front Synaptic Neurosci* 2:144.
- Neher E, Sakaba T (2008) Multiple roles of calcium ions in the regulation of neurotransmitter release. *Neuron* 59:861-872.
- Oertner TG, Sabatini BL, Nimchinsky EA, Svoboda K (2002) Facilitation at single synapses probed with optical quantal analysis. *Nat Neurosci* 5:657-664.
- Pang ZP, Sudhof TC (2010) Cell biology of Ca²⁺-triggered exocytosis. *Curr Opin Cell Biol* 22:496-505.
- Pobbati AV, Razeto A, Boddener M, Becker S, Fasshauer D (2004) Structural basis for the inhibitory role of tomosyn in exocytosis. *J Biol Chem* 279:47192-47200.
- Pouille F, Scanziani M (2004) Routing of spike series by dynamic circuits in the hippocampus. *Nature* 429:717-723.
- Pyott SJ, Rosenmund C (2002) The effects of temperature on vesicular supply and release in autaptic cultures of rat and mouse hippocampal neurons. *J Physiol* 539:523-535.
- Reid CA, Clements JD, Bekkers JM (1997) Nonuniform distribution of Ca²⁺ channel subtypes on presynaptic terminals of excitatory synapses in hippocampal cultures. *J Neurosci* 17:2738-2745.
- Reid CA, Bekkers JM, Clements JD (1998) N- and P/Q-type Ca²⁺ channels mediate transmitter release with a similar cooperativity at rat hippocampal autapses. *J Neurosci* 18:2849-2855.
- Reyes A, Lujan R, Rozov A, Burnashev N, Somogyi P, Sakmann B (1998) Target-cell-specific facilitation and depression in neocortical circuits. *Nat Neurosci* 1:279-285.
- Ribrault C, Sekimoto K, Triller A (2011) From the stochasticity of molecular processes to the variability of synaptic transmission. *Nat Rev Neurosci* 12:375-387.
- Rizo J, Rosenmund C (2008) Synaptic vesicle fusion. *Nat Struct Mol Biol* 15:665-674.
- Rosenmund C, Stevens CF (1996) Definition of the readily releasable pool of vesicles at hippocampal synapses. *Neuron* 16:1197-1207.

- Rosenmund C, Clements JD, Westbrook GL (1993) Nonuniform probability of glutamate release at a hippocampal synapse. *Science* 262:754-757.
- Rozov A, Burnashev N, Sakmann B, Neher E (2001) Transmitter release modulation by intracellular Ca²⁺ buffers in facilitating and depressing nerve terminals of pyramidal cells in layer 2/3 of the rat neocortex indicates a target cell-specific difference in presynaptic calcium dynamics. *J Physiol* 531:807-826.
- Rusakov DA, Fine A (2003) Extracellular Ca²⁺ depletion contributes to fast activity-dependent modulation of synaptic transmission in the brain. *Neuron* 37:287-297.
- Ryan TA (1999) Inhibitors of myosin light chain kinase block synaptic vesicle pool mobilization during action potential firing. *J Neurosci* 19:1317-1323.
- Sakaba T, Neher E (2001a) Preferential potentiation of fast-releasing synaptic vesicles by cAMP at the calyx of Held. *Proc Natl Acad Sci U S A* 98:331-336.
- Sakaba T, Neher E (2001b) Quantitative Relationship between Transmitter Release and Calcium Current at the Calyx of Held Synapse. *J Neurosci* 21:462-476.
- Sakaba T, Schneggenburger R, Neher E (2002) Estimation of quantal parameters at the calyx of Held synapse. *Neurosci Res* 44:343-356.
- Sakisaka T, Baba T, Tanaka S, Izumi G, Yasumi M, Takai Y (2004) Regulation of SNAREs by tomosyn and ROCK: implication in extension and retraction of neurites. *J Cell Biol* 166:17-25.
- Sakisaka T, Yamamoto Y, Mochida S, Nakamura M, Nishikawa K, Ishizaki H, Okamoto-Tanaka M, Miyoshi J, Fujiyoshi Y, Manabe T, Takai Y (2008) Dual inhibition of SNARE complex formation by tomosyn ensures controlled neurotransmitter release. *J Cell Biol* 183:323-337.
- Sankaranarayanan S, De Angelis D, Rothman JE, Ryan TA (2000) The use of pHluorins for optical measurements of presynaptic activity. *Biophys J* 79:2199-2208.
- Scanziani M, Gahwiler BH, Charpak S (1998) Target cell-specific modulation of transmitter release at terminals from a single axon. *Proc Natl Acad Sci U S A* 95:12004-12009.
- Schikorski T, Stevens CF (1997) Quantitative Ultrastructural Analysis of Hippocampal Excitatory Synapses. *J Neurosci* 17:5858-5867.
- Schneggenburger R, Neher E (2000) Intracellular calcium dependence of transmitter release rates at a fast central synapse. *Nature* 406:889-893.
- Schneggenburger R, Neher E (2005) Presynaptic calcium and control of vesicle fusion. *Curr Opin Neurobiol* 15:266-274.
- Schneggenburger R, Forsythe ID (2006) The calyx of Held. *Cell Tissue Res* 326:311-337.
- Schneggenburger R, Meyer AC, Neher E (1999) Released Fraction and Total Size of a Pool of Immediately Available Transmitter Quanta at a Calyx Synapse. *Neuron* 23:399-409.
- Schneggenburger R, Sakaba T, Neher E (2002) Vesicle pools and short-term synaptic depression: lessons from a large synapse. *Trends Neurosci* 25:206-212.
- Schoch S, Gundelfinger ED (2006) Molecular organization of the presynaptic active zone. *Cell Tissue Res* 326:379-391.
- Schwaller B (2010) Cytosolic Ca²⁺ buffers. *Cold Spring Harb Perspect Biol* 2:a004051.
- Scullin CS, Wilson MC, Partridge LD (2010) Developmental changes in presynaptic Ca²⁺ clearance kinetics and synaptic plasticity in mouse Schaffer collateral terminals. *Eur J Neurosci* 31:817-826.

- Shigemoto R, Kulik A, Roberts JD, Ohishi H, Nusser Z, Kaneko T, Somogyi P (1996) Target-cell-specific concentration of a metabotropic glutamate receptor in the presynaptic active zone. *Nature* 381:523-525.
- Siksou L, Varoqueaux F, Pascual O, Triller A, Brose N, Marty S (2009) A common molecular basis for membrane docking and functional priming of synaptic vesicles. *Eur J Neurosci* 30:49-56.
- Sokal RR, Rohlf FJ (1994) *Biometry : the principles and practice of statistics in biological research*, 3rd Edition. New York: Freeman.
- Sorensen JB (2004) Formation, stabilisation and fusion of the readily releasable pool of secretory vesicles. *Pflugers Arch* 448:347-362.
- Stevens CF, Wesseling JF (1998) Activity-dependent modulation of the rate at which synaptic vesicles become available to undergo exocytosis. *Neuron* 21:415-424.
- Stevens CF, Williams JH (2007) Discharge of the readily releasable pool with action potentials at hippocampal synapses. *J Neurophysiol* 98:3221-3229.
- Sun J, Pang ZP, Qin D, Fahim AT, Adachi R, Sudhof TC (2007) A dual-Ca²⁺-sensor model for neurotransmitter release in a central synapse. *Nature* 450:676-682.
- Takamori S, Holt M, Stenius K, Lemke EA, Grønborg M, Riedel D, Urlaub H, Schenck S, Brügger B, Ringler P, Müller SA, Rammner B, Gräter F, Hub JS, De Groot BL, Mieskes G, Moriyama Y, Klingauf J, Grubmüller H, Heuser J, Wieland F, Jahn R (2006) Molecular anatomy of a trafficking organelle. *Cell* 127:831-846.
- Taylor JR (1997) *An introduction to error analysis : the study of uncertainties in physical measurements*, 2nd Edition. Sausalito, Calif.: University Science Books.
- Trudeau LE, Emery DG, Haydon PG (1996) Direct modulation of the secretory machinery underlies PKA-dependent synaptic facilitation in hippocampal neurons. *Neuron* 17:789-797.
- Trudeau LE, Fang Y, Haydon PG (1998) Modulation of an early step in the secretory machinery in hippocampal nerve terminals. *Proc Natl Acad Sci U S A* 95:7163-7168.
- van den Bogaart G, Holt MG, Bunt G, Riedel D, Wouters FS, Jahn R (2010) One SNARE complex is sufficient for membrane fusion. *Nat Struct Mol Biol* 17:358-364.
- Varoqueaux F, Sigler A, Rhee JS, Brose N, Enk C, Reim K, Rosenmund C (2002) Total arrest of spontaneous and evoked synaptic transmission but normal synaptogenesis in the absence of Munc13-mediated vesicle priming. *Proc Natl Acad Sci U S A* 99:9037-9042.
- Verhage M, Sorensen JB (2008) Vesicle docking in regulated exocytosis. *Traffic* 9:1414-1424.
- Voglmaier SM, Kam K, Yang H, Fortin DL, Hua Z, Nicoll RA, Edwards RH (2006) Distinct endocytic pathways control the rate and extent of synaptic vesicle protein recycling. *Neuron* 51:71-84.
- Wang LY, Kaczmarek LK (1998) High-frequency firing helps replenish the readily releasable pool of synaptic vesicles. *Nature* 394:384-388.
- Wesseling JF, Lo DC (2002) Limit on the role of activity in controlling the release-ready supply of synaptic vesicles. *J Neurosci* 22:9708-9720.
- Wilhelm BG, Groemer TW, Rizzoli SO (2010) The same synaptic vesicles drive active and spontaneous release. *Nat Neurosci* 13:1454-1456.
- Williams AL, Bielopolski N, Meroz D, Lam AD, Passmore DR, Ben-Tal N, Ernst SA, Ashery U, Stuenkel EL (2011) Structural and functional analysis of tomosyn identifies domains important in exocytotic regulation. *J Biol Chem* 286:14542-14553.

- Wojcik SM, Brose N (2007) Regulation of membrane fusion in synaptic excitation-secretion coupling: speed and accuracy matter. *Neuron* 55:11-24.
- Wu LG, Saggau P (1995) Block of multiple presynaptic calcium channel types by omega-conotoxin-MVIIIC at hippocampal CA3 to CA1 synapses. *J Neurophysiol* 73:1965-1972.
- Xu-Friedman MA, Regehr WG (2004) Structural contributions to short-term synaptic plasticity. *Physiol Rev* 84:69-85.
- Xu J, Wu LG (2005) The decrease in the presynaptic calcium current is a major cause of short-term depression at a calyx-type synapse. *Neuron* 46:633-645.
- Yamamoto Y, Mochida S, Kurooka T, Sakisaka T (2009) Reciprocal intramolecular interactions of tomosyn control its inhibitory activity on SNARE complex formation. *J Biol Chem* 284:12480-12490.
- Yamamoto Y, Fujikura K, Sakaue M, Okimura K, Kobayashi Y, Nakamura T, Sakisaka T (2010) The tail domain of tomosyn controls membrane fusion through tomosyn displacement by VAMP2. *Biochem Biophys Res Commun* 399:24-30.
- Yamamoto Y, Mochida S, Miyazaki N, Kawai K, Fujikura K, Kurooka T, Iwasaki K, Sakisaka T (2011) Tomosyn inhibits synaptotagmin-1-mediated step of Ca²⁺-dependent neurotransmitter release through its N-terminal WD40 repeats. *J Biol Chem* 285:40943-40955.
- Yao I, Takagi H, Ageta H, Kahyo T, Sato S, Hatanaka K, Fukuda Y, Chiba T, Morone N, Yuasa S, Inokuchi K, Ohtsuka T, Macgregor GR, Tanaka K, Setou M (2007) SCRAPER-dependent ubiquitination of active zone protein RIM1 regulates synaptic vesicle release. *Cell* 130:943-957.
- Yizhar O, Matti U, Melamed R, Hagalili Y, Bruns D, Rettig J, Ashery U (2004) Tomosyn inhibits priming of large dense-core vesicles in a calcium-dependent manner. *Proc Natl Acad Sci U S A* 101:2578-2583.
- Yizhar O, Lipstein N, Gladysheva SE, Matti U, Ernst SA, Rettig J, Stuenkel EL, Ashery U (2007) Multiple functional domains are involved in tomosyn regulation of exocytosis. *J Neurochem* 103:604-616.
- Yokoyama S, Shirataki H, Sakisaka T, Takai Y (1999) Three splicing variants of tomosyn and identification of their syntaxin-binding region. *Biochem Biophys Res Commun* 256:218-222.
- Young SM, Jr., Neher E (2009) Synaptotagmin has an essential function in synaptic vesicle positioning for synchronous release in addition to its role as a calcium sensor. *Neuron* 63:482-496.
- Zhang Q, Li Y, Tsien RW (2009) The dynamic control of kiss-and-run and vesicular reuse probed with single nanoparticles. *Science* 323:1448-1453.